Adsorption of Perfluoroalkyl Substances from Groundwater Using

Pilot and Lab Scale Columns

by

Krishishvar Venkatesh

A Thesis Presented in Partial Fulfillment
of the Requirements for the Degree
Master of Science

Approved April 2020 by the
Graduate Supervisory Committee:

Paul Westerhoff, Chair
Shahnawaz Sinha
Marylaura Lind

ARIZONA STATE UNIVERSITY

May 2020

ABSTRACT

Per- and polyfluoroalkyl substances (PFAS) are a group of man-made chemicals that are detected ubiquitously in the aquatic environment, biota, and humans. Human exposure and adverse health of PFAS through consuming impacted drinking water is getting regulatory attention. Adsorption using granular activated carbon (GAC) and ion exchange resin (IX) has proved to be efficient in removing PFAS from water. There is a need to study the effectiveness of commercially available sorbents in PFAS removal at the pilot-scale with real PFAS contaminated water, which would aid in efficient full-scale plant design. Additionally, there is also a need to have validated bench-scale testing techniques to aid municipalities and researchers in selecting or comparing adsorbents to remove PFAS. Rapid Small-Scale Column Tests (RSSCTs) are bench-scale testing to assess media performance and operational life to remove trace organics but have not been validated for PFAS. Different design considerations exist for RSSCTs, which rely upon either proportional diffusivity (PD) or constant diffusivity (CD) dimensionless scaling relationships.

This thesis aims to validate the use of RSSCTs to simulate PFAS breakthrough in pilot columns. First, a pilot-scale study using two GACs and an IX was conducted for five months at a wellsite in central Arizona. PFAS adsorption capacity was greatest for a commercial IX, and then two GAC sources exhibited similar performance. Second, RSSCTs scaled using PD or CD relationships, simulated the pilot columns, were designed and performed. For IX and the two types of GAC, the CD–RSSCTs simulated the PFAS breakthrough concentration, shape, and order of C8 to C4 compounds observed pilot columns better than the PD-RSSCTs. Finally, PFAS breakthrough and adsorption

capacities for PD- and CD-RSSCTs were performed on multiple groundwaters (GWs) from across Arizona to assess the treatability of PFAS chain length and functional head-group moieties. PFAS breakthrough in GAC and IX was dictated by chain length (C4>C6>C8) and functional group (PFCAs>PFSAs) of the compound. Shorter-chain PFAS broke through earlier than the longer chain, and removal trends were related to the hydrophobicity of PFAS. Overall, single-use IX performed superior to any of the evaluated GACs across a range of water chemistries in Arizona GWs.

DEDICATION

I dedicate this thesis to my loving parents Shanthi Chinnappa and Venkatesh Krishnan,

and my doting little sister Trrisha Venkat. None of this would have been possible without

them.

ACKNOWLEDGMENTS

TABLE OF CONTENTS

LIST OF TABLES

LIST OF FIGURES

x

CHAPTER 1

INTRODUCTION

1.1 Introduction and Goals

Per- and Poly-fluoroalkyl substances (PFAS), are ubiquitous man-made chemicals which are used because of their surfactant and thermally resistant properties in a wide variety of applications such as cookware (e.g., Teflon coating), firefighting foams, water repellent clothes, stain repellent carpets, cosmetics. PFAS compounds are highly stable due to the C-F bond, which also makes this compound recalcitrant to degradation and persist in the environment (Du et al. 2014). There has been contamination of PFAS in drinking water sources across the U.S., and studies show PFAS may pose serious health concerns including elevated levels of cholesterol, cancer, thyroid disease, immunosuppression in early childhood. (Granum et al. 2013; Sunderland et al. 2019; Rappazzo, Coffman, and Hines 2017; Zhang et al. 2016)

PFAS occurrence in various water sources such as lakes, river water, wastewater, groundwater, are widely studied (Ateia et al. 2019; Hölzer et al. 2009; Arvaniti and Stasinakis 2015; Lapworth et al. 2012; Appleman et al. 2014; Rahman, Peldszus, and Anderson 2014; Ahrens 2011). Due to recent regulations on PFOS and PFOA, manufacturers stopped using these chemicals and switched to smaller chain compounds like PFHxS and PFBS. Even though the bioaccumulation of these smaller chain compounds is smaller than the longer chain compounds, their persistence in the environment is still the same (Li et al. 2020). Therefore, the total amount of PFAS influx to the environment has not changed.

Thus, US EPA has a health advisory limit (HAL) of 70 ng/L for PFOA and PFOS in drinking water. Six perfluorinated compounds namely, perfluorooctanesulfonic acid (PFOS), perfluorooctanoic acid (PFOA), perfluorononanoic acid (PFNA), perfluorohexanesulfonic acid (PFHxS), perfluoroheptanoic acid (PFHpA) and perfluorobutanesulfonic acid (PFBS), are in the third Unregulated Contaminant Monitoring Rule (UCMR 3) (U.S. EPA 2016). UCMR 3 will provide the basis for future federal regulations at the end of monitoring. Additionally, many states like California, Vermont, Massachusetts, New York, New Jersey, New Hampshire, and Minnesota have their PFAS regulatory limits much stringent compared to EPA's limits, for example, California has a notification limit of 6.5 ng/L for PFOS and 5.1 ng/L for PFOA.

In Arizona, the Arizona Department of Environmental Quality (ADEQ) identified sixty-eight public water systems out of one thousand five hundred to be in the vicinity of potential PFAS contamination sources. One hundred nine wells were selected for sampling, out of which eighty-nine wells were non detect, fourteen wells were under EPA health advisory limit, and six wells above EPA HAL (ADEQ 2019). These results confirm PFAS contamination in Arizona, and with increasing attention towards PFAS and alarming health concerns, there could be stricter regulatory limits imposed on PFAS shortly and not just on PFOS and PFOA.

Various treatment options, like advanced oxidation and reduction processes, reverse osmosis, nanofiltration, are studied for PFAS removal. However, for a full-scale system, only adsorption using granular activated carbon (GAC) and ion exchange (IX) resins have been widely considered for drinking water systems. Most of the adsorption studies with GAC and IX have been performed in synthetic water with very high PFAS

concentration. Limited literature is available on PFAS adsorption studies in real groundwaters and at environmentally relevant concentrations and/or ratios (Xiao et al. 2017; Woodard, Berry, and Newman 2017; Park et al. 2020; C. J. Liu, Werner, and Bellona 2019).

Therefore, there is a need to study the effectiveness of commercially available sorbents in PFAS removal at the pilot-scale with real water contaminated with PFAS, which would aid in efficient full-scale plant design. Additionally, there is also a need to have a quick, valid bench-scale testing method to aid municipalities and researchers in choosing the right sorbent types. Rapid Small-Scale Column Tests (RSSCTs), are accepted as a quick and valuable bench-scale testing methodology for the assessment of media performance and operational life to remove trace organics. There are primarily two scaling relations used in designing the RSSCTs: (1) constant diffusivity (CD) and (2) proportional diffusivity (PD). In this thesis, RSSCTs were performed with real groundwaters (GWs) to validate the selection of appropriate RSSCT scaling equations for designing pilot or full-scale columns.

1.2 Objectives:

The goal of this thesis is to validate the RSSCT approach to simulate PFAS breakthrough in pilot-scale columns and to understand the nature of PFAS breakthrough in GAC and IX columns. Specific objectives include the following:

(1) Compare adsorbent capacity of commercial granular activated carbon (GAC) vs. anion exchange resin (IX) materials to adsorb PFAS from groundwater, in a field pilot-scale study.

(2) Compare CD vs. PD-RSSCT breakthrough curves of GAC and IX to each other and against pilot-scale performance.

(3) Document trends in PFAS removal by GAC and IX based upon chain length and functional head-group moieties.

This thesis contains six chapters. PFAS were detected at local drinking water well, a GW wellsite. Due to the increased attention of PFAS and its rising health concerns, utility operating this drinking water well decided to act on it and planned to perform an investigative pilot-scale study to choose the right PFAS mitigation strategy. Further, the study also focuses on validating bench-scale methodology to simulate pilot column performance of PFAS breakthrough, which would aid in selecting appropriate adsorbent media for PFAS removal in groundwater in a fraction of time taken by pilot columns. Finally, RSSCTs performed on multiple GWs impacted with PFAS, would help in understanding the role of chain length and functional head group moieties in PFAS removal by GAC and IX. Chapter 2 provides a background summary of PFAS and adsorption materials. Chapter 3 is a description of the GW site, where the pilot study was performed. Chapter 3 also summarizes the pilot and RSSCT design and setup, along with a brief description of analytical methods. Chapter 4 provides brief results of the pilot study and the RSSCTs simulating pilot columns; key findings were instrumental in answering objectives 1 & 2 stated above. Chapter 5 is a research paper, I was a co-author on and involved in 60% of the research; it provides brief results on trends of PFAS breakthrough by GAC and IX in multiple GWs with varying PFAS concentration. Key results from both Chapters 4 & 5 answers objective 3 of this thesis.

CHAPTER 2

BACKGROUND ON ADSORPTION OF PFAS

Current strategies to remove PFAS have been widely based on nondestructive or physical separation technologies (e.g., adsorption, reverse osmosis, ion exchange). Few technologies cleave the C-C bond, which could breakdown the long-chain carbon compounds to shorter-chain compounds (Butt, Muir, and Mabury 2014; J. Liu et al. 2017; Vecitis et al. 2009). The shorter chain compounds are more mobile, soluble, and as environmentally persistent as compared to the longer-chain compounds. Therefore, breaking down the long-chain compounds to shorter-chain compounds does not help much. Furthermore, only very few technologies are out there, like thermolysis, photolysis, electrolysis, which have shown promising results in cleaving the C-F bond (Gole et al. 2018; Fernandez et al. 2016; Chaplin 2014). Thus, transforming the PFAS to neutral compounds would minimize the risk and would be beneficial. However, the scalability of technology is critical for full-scale implementation. In this regard, only adsorption using IX and GACs and, to some extent, reverse osmosis (RO), are successful at large and full-scale implementation. Since this study focuses on adsorption, approaches to adsorb organic pollutants are further discussed.

2.1 Adsorption

Adsorption is a physical separation process where pollutants in the liquid phase (adsorbate) are transferred to the solid phase (adsorbent), thus removed from the liquid phase. Adsorbates are transferred to the solid-phase through transport by diffusion (surface, pore), and onto the deeper pores inside the sorbent surface, where these constituents are

adsorbed. If the adsorption happens only through a chemical reaction on a solid surface, it is known as chemisorption. Whereas, when it occurs through weak bonding forces, such as Van der Waals forces, then it is known as physisorption. Physical adsorption is one of the most widely used processes in drinking water treatment.

Granular activated carbon (GAC) and powdered activated carbon (PAC) are commonly used in the packed bed columns and slurry tank operational mode, respectively, at full-scale water treatment plants (J. Crittenden et al. 2014). The activated carbon has widely been used in adsorption of synthetic organic compounds (SOCs) or taste and odor compounds (T&O), or oxyanions (J. Crittenden et al. 2014). Using GACs to remove PFAS compounds have been studied in recent years (C. J. Liu, Werner, and Bellona 2019; Xiao et al. 2017; McCleaf et al. 2017; Park et al. 2020; Woodard, Berry, and Newman 2017). PFAS compounds can also be removed by anion exchange resins (AER), as PFAS compounds are generally anionic in ambient pH due to their low pKa values (Gagliano et al. 2020), they are adsorbed by the functionalized surface charge on the resin.

The PFAS compounds have a hydrophobic tail attached to an ionic head. PFAS adsorption occurs through the electrostatic attraction of the PFAS functional charge or hydrophobic interaction with the tail of the compound on graphite surfaces (Du et al. 2014). These mechanisms work independently or in combination and are the dominant transport and adsorption mechanisms of PFAS onto the sorbent. Adsorbents are usually studied in packed-bed columns setup to remove PFAS. Adsorbents are packed inside the column, and the water is passed through the media. Therefore, water would have contact time with the adsorbent defined as the empty bed contact time (EBCT) at a specified hydraulic loading rate (HLR). The EBCT and HLR are two important design parameters of the packed bed

column. Generally, for full-scale systems, EBCTs will be in the range (10-15 minutes), whereas the HLR can vary in the range (10-15 gpm/ft^2).

Pilot-scale studies using full-sized media (i.e., uncrushed, as-is) are generally performed to aid full-scale adsorption column design. However, pilot studies are conducted in a smaller column (compared to the full-scale system) to predict the full-scale system's performance. Sometimes, these media are crushed to maintain a certain minimum ratio of particle diameter to column diameter to minimize channeling effect or to avoid short-circuiting. Pilot studies are dynamic, where the feed water quality most probably vary during the operation of the study (i.e., dynamic), this is due to pumping patterns or recharge events, similar to the full-scale system. This dynamic or the varying water quality could play an important role in PFAS removal, as the adsorption could also be affected by varying incoming PFAS concentration or variation in dissolved organic matter (DOM) or dissolved ions concentration (due to competition of co-occurring ions). Additionally, when the columns are run for a longer time, even the biological activities can promote contaminant degradation that also could be factored in such operation (only if chlorine or disinfection is not applied). Thus, pilot-scale studies have excellent reliability as they can predict the full-scale behavior more closely than the bench-scale column study.

2.1.1 Rapid Small-Scale Column Tests (RSSCTs)

The RSSCTs are a scaled-down version of the full-scale system, using mathematical models. The dispersed flow pore and surface diffusion model (DFPSDM) is assumed to be the most appropriate model to represent a full-scale adsorption system. The mass transfer similitude between the RSSCT – small columns (SC) to the full-scale system – large columns (LC) is maintained by equating dimensionless groups in the model

7

between these two systems. DFPSDM considers the mass transfer mechanisms like intraparticle diffusion, advection, dispersion, liquid diffusivity. There are several assumptions made between these two scales. Three assumptions are made while developing the scaling equations to obtain such closer agreement (J. C. Crittenden, Berrigan, and Hand 1986; J. C. Crittenden et al. 1991; Westerhoff et al. 2005). Boundary conditions for the LC and SC should occur at the same dimensionless conditions in the dimensionless differential equations. In the dimensionless differential equations, dimensionless parameters (such as Reynolds (R) and Schmidt (S) numbers) for both the scales should be similar. Also, the mass transfer mechanism is assumed to remain the same for different particle sizes (Westerhoff et al. 2005). No modeling was done in this study, and the scaling equations obtained from a previous study (Westerhoff et al. 2005) were used to scale down the full-scale column to the RSSCT column.

Accordingly, the RSSCTs can be designed under two design approaches (1) Constant Diffusivity (CD) and (2) Proportional Diffusivity (PD). The CD design assumes that intraparticle diffusion (surface and pore diffusion) is independent of the particle size (i.e., contaminant removal is unaffected by the particle size of the adsorbent). For CD, the perfect similarity is assumed in the intraparticle diffusion between the full-sized and crushed particles, and the external mass transfer is the rate-limiting step here. Trace concentration of organics with a low molecular weight (MW) and no potential sorption competition (e.g., organic matter or other co-occurring ions) in the background water matrix is predicted well by CD design (J. C. Crittenden, Berrigan, and Hand 1986; Cummings and Summers 1994)

On the other hand, the PD design assumes the intraparticle diffusion linearly increases with the particle size of sorbent and is the rate-limiting step. The CD takes a short amount of time and water to predict the breakthrough, whereas the PD takes a longer time. However, the PD is usually assumed to be a better performance predictor of a full-scale adsorption system for bulk organics (Westerhoff et al. 2005).

Equations 1 through 5 are used to design RSSCTs,

$$\frac{EBCT_{SC}}{EBCT_{LC}} = \left[\frac{d_{p,SC}}{d_{p,LC}}\right]^{2-X} = \frac{t_{SC}}{t_{LC}} \tag{1}$$

$$\frac{V_{SC}}{V_{LC}} = \left[\frac{d_{p,LC}}{d_{p,SC}}\right] \tag{2}$$

$$\frac{V_{SC}}{V_{LC}} = \left[\frac{d_{p,LC}}{d_{p,SC}}\right] \times \frac{R_{SC} \times s}{R_{LC} \times s} \tag{3}$$

$$R = \frac{V \times \rho_L \times d_p}{\mu} \tag{4}$$

$$S = \frac{\mu}{D_L \times \rho_L} \tag{5}$$

where X defines the dependence of intraparticle diffusivity on particle size: $X=0$ when diffusivity is constant (CD); $X=1$ when diffusivity is linearly proportional to sorbent particle size (PD). SC= small column (RSSCT); LC = large column (pilot-scale); EBCT = Empty bed contact time; V = hydraulic loading rate; t is run duration; d_p is the diameter of the particle. Reynolds number (R) and Schmidt number (S) can be calculated from the liquid diffusivity (D_L), dynamic viscosity (μ), and density (ρ_L).

The constant diffusivity (CD) RSSCTs are designed using Equations 1 and 2, with X =0. However, using Equation 1 generally leads to very high loading rates in the small columns, which is practically impossible to have, due to increased pressure drops across the crushed media. Operation at such loading rates would also crush the media even more

9

and thus increasing the head losses even more. Therefore, to have reasonable loading rates in small columns, Equation 3 is used. The product of Reynolds and Schmidt gives an idea about the dispersion effects; the idea is to set Reynolds number such that dispersion effects are negligible. When the product of Reynolds and Schmidt number is in the range 200 – 200,000, dispersion effects are negligible (Westerhoff et al. 2005). Similarly, PD-RSSCTs are designed using Equations 1 and 3.

Although RSSCTs have been validated for trace organics removal, the applicability for PFAS removal in GACs and IX resin is yet to be validated by comparing the results with field pilot-scale testing. This study is aimed at filling that knowledge gap by performing a pilot-scale study and comparing those results to CD and PD based RSSCTs. Commercial sorbents (Calgon F 400 - GAC1, Norit GAC 400 – GAC2 and Purolite PFA694E – IX) were chosen for these testing.

CHAPTER 3

FACILITIES AND METHODS

3.1 Groundwater Site

A pilot-scale study was conducted at local PFAS-impacted groundwater wellsite (Tempe, Arizona, USA). The well was momentarily taken off-line until an appropriate PFAS mitigation strategy could be developed. The existing 1000gpm wellhead pump was replaced before the PFAS mitigation (pilot-scale) study, by a 6gpm smaller sized pump (¾ HP, 3-inch diameter, 34-inch long multi-stage submersible pump -Grundfos; 5SEQ07-230-2). The reason for installing this smaller sized pump is twofold. It is to limit the total amount of water use, which was restricted by the City (i.e., not to exceed 500,000 gallons for the entire 5-6 months study) and also to minimize water wastage.

Once the smaller pump was installed at this PFAS contaminated wellsite, the pump's outlet (discharge side) was connected to a 1-inch diameter manifold. The manifold is installed with several components, including a check valve to prevent any backflow to the well, a pressure/flow control valve to adjust both the pressure and flowrate with two additional pressure gauges (installed before and after the control valve). A water-meter (totalizer) was also installed to this manifold to monitor the total amount of water (gallons) used throughout the study. The submersible pump was operated continuously, the feed pressure and flowrates (by adjusting the control valve) were monitored and adjusted as needed during the study. If the pump is stopped or bypassed, it was done momentarily (for a few minutes to an hour only). The bypass/stops were done to either change the cartridge filters (CF) or to collect the raw water samples for the bench-scale (RSSCT) study.

A 55-gallon HDPE drum covered with LDPE liners was used to collect and transport well-water to the laboratory for the bench-scale (RSSCT) studies. The well-water sample was used within the first two weeks of collection to minimize water quality degradation for the bench-scale RSSCT study. The raw water quality was routinely monitored during both the piloting (at least once a week) and the RSSCT study. Several handheld water quality probes were used at the field to measure pH, conductivity, and temperature during sample collection. During the changeout of CF, well water is usually diverted momentarily to a nearby dry well, located at the site.

Table 3.1 shows there is a slight variation in the water quality results between the historical water quality values and the samples collected during the PFAS mitigation (i.e., piloting) study, using the small pump. The water quality results, especially for the PFAS concentration, differ considerably from historical data. This difference in water quality means samples taken using the smaller pump represent shallower aquifer water and may not reflect the water quality for the entire production well. The entire production using the wellhead pump is a combination of blending waters from different zones of the entire aquifer. Primary water qualities of the raw water were: pH (n=71): 7.4 ± 0.2, turbidity (n=61): 0.12 ± 0.16, conductivity (n=71): 2028 ± 106 µS/cm, temperature (n=71) : 26.7 ± 2.4 °C, DOC (n=16): 1.2 ± 0.3 mg/L , all of which reflects low DOC water with high conductivity. The groundwater well, which serves as the feed water to this pilot-scale as well as the bench-scale studies, had varying influent PFAS concentration throughout the study. Table 3.2 shows the concentration of various PFAS compounds (or species) detected in the feed water (i.e., includes both pilot and RSSCT studies).

Table 3.1 Historical and pilot water quality summary for Tempe GW.

Water quality parameter	Historical data (1000gpm pump)	Pilot data (6gpm pump)
Arsenic, µg/L (n =9)	4.81	4.02
Calcium, mg/L (n =9)	93	117
Chloride, mg/L (n = 11)	346	401
Chromium, µg/L (n =9)	2.82	0.40
Conductivity, µmhos/cm at 25 °C (n = 71)	1829	2028
Total hardness (as $CaCO_3$), mg/L	386	475
Copper, µg/L (n =9)	1.43	13
Fluoride, mg/L	0.329	NA
Iron, mg/L (n =9)	0.02	0.002
Magnesium, mg/L (n =9)	37.4	44.82
Nitrate (as Nitrogen), mg/L (n =11)	4.33	3.68
pH, pH Units (n = 71)	7.03	7.40
Selenium, µg/L (n =9)	0.25	0.001
Silica, mg/L (n =9)	30	14
Sodium, mg/L (n =9)	231	226
Sulfate, mg/L (n =11)	114	103
Total Dissolved Solids, mg/L (n = 71)	1037	1115
Dissolved Organic Carbon, mg/L (n =16)	NA	1.2
Turbidity, NTU (n = 71)	0.918	0.12
Bromide (mg/L) (n = 11)	0.19	0.22
PFOS + PFOA (ng/L) (n =14)	57	21

Table 5.1 shows the physicochemical properties of the PFAS compounds listed in Table 3.2. Except for PFHxA, all the other PFAS compounds detected are under the UCMR 3 (Third Unregulated Contaminant Monitoring Rule) (U.S. EPA 2016). Even though the PFOS and PFOA are under the EPA health advisory limit of 70 ng/L for this well water, the PFOS and PFOA concentrations were approaching the EPA HAL. However, PFOA and PFOS values of this well water exceeded the limits set by many other States. For example, they are above the California notification limit of 6.5 ng/L for

PFOS and 5.1 ng/L for PFOA, respectively ("Perfluorooctanoic Acid (PFOA) and Perfluorooctanesulfonic Acid (PFOS)" 2020).

Furthermore, the PFOA value (Table 3.2) was above California's recently revised response level of 10 ng/L ("Response Levels Lowered for Water Systems Statewide as PFAS Investigation Continues" 2020). Also, the relative abundance of different PFAS compounds is of interest to this study. As PFAS contaminated groundwater may have a varying concentration of different PFAS species, it is important to evaluate the selective adsorption capacity of the adsorbent material (such as GACs and IX).

Table 3.2 PFAS compounds concentration in feed water samples (pilot and RSSCTs)

PFAS Compound	Pilot Average (n=14) (ng/L)	± SD	PFAS concentrations for each RSSCTs with Tempe GW (ng/L)				
			1&2	3&4	5, 6 & 9	7	8
PFBS(C4)	17.1	1.3	17.0	18.0	17.0	20.0	15.0
PFHxS(C6)	6.6	2.1	6.0	7.3	5.9	6.4	5.3
PFHpA(C7)	3.4	1.1	2.5	3.0	2.4	2.9	3.8
PFHxA(C6)	6.0	0.8	5.1	6.2	5.4	5.7	6.2
PFOA(C8)	11.1	4.8	7.2	9.0	8.0	9.3	19.0
PFOS(C8)	9.4	1.8	9.4	9.7	8.4	8.8	9.8
PFNA(C9)*	0.7	1.3	-	-	-	-	3.6
Total PFAS	54.2	7.7	47.2	53.2	47.1	53.1	62.7

* PFNA (n =2).
Notation: (N-ethyl perfluorooctanesulfonamidoacetic acid (NEtFOSAA), N-methyl perfluorooctanesulfonamidoacetic acid (NMeFOSAA), perfluorobutanoic acid (PFBS), perfluorodecanoic acid (PFDA), perfluorododecanoic acid (PFDoA), perfluoroheptanoic acid (PFHpA), perfluorohexanesulfonic acid (PFHxS), perfluorohexanoic acid (PFHxA), perfluorononanoic acid (PFNA), perfluorooctanesulfonic acid (PFOS), perfluorooctanoic acid (PFOA), Perfluorotetradecanoic acid (PFTA), Perfluorotridecanoic acid (PFTrDA), Perfluoroundecanoic acid (PFUnA)

3.2 Field Analyses

The field measurements included measuring basic water quality parameters at the field site such as pH, conductivity, and temperature (Hanna-99130), along with turbidity and iron measurements (Milwaukee Instruments). Field samples were collected twice per day for 3-times a week for the pilot-scale study. Some of the lab samples were collected 2-3 times a week, but others collected less frequently, once a week.

3.3 Laboratory Analyses

Influent and effluent samples of the pilot-scale and RSSCT studies were collected in 50-mL conical centrifuge sample tubes (except PFAS samples), filtered and stored at 4°C until analyzed. Samples were filtered using preashed (550°C) 0.7µm filter papers (Whatman glassfiber filters, GF/F).

Table 3.3 Water quality parameters and analysis.

WQ Parameter	Instrument/Method	Sample preparation/Measurement
Dissolved Organic Carbon	Shimadzu TOC-V$_{csh}$	Filtered samples in 23mL glass vials and acidified using HCl to pH 2-3.
UV$_{254}$ Absorbance	Hach DR 6000	Quartz cuvette of 1-cm path length was used as a sample cell, with Nanopure water as blank for each sample set.
Anions	Thermo Dionex ICS 5000 using EPA method 300.0	Filtered samples stored in 1.5mL IC vial.
Metals	Thermo Fisher X-Series 2	Filtered samples were stored in a 15mL centrifuge tubes and acidified using nitric acid to a final 2% acid by volume for preservation.
PFAS	EPA Method 537 by Eurofins Scientific	Influent and effluent of pilot and RSSCTs in 250mL HDPE bottles with 1.4 g tris hydrochloride and tris (hydroxymethyl) aminomethane as a preservative (15.5: 1 w/w).

Samples were analyzed for all major anions (IC), cations (ICP-MS), organics (DOC and UV_{254}), and also measured for 14 different types of PFAS analytes (using LC/MS/MS by a commercial lab). Table 3.3 shows the analysis details of the water quality parameters. Table 3.4 and Table 3.5 shows the average anions and metals measurement throughout this study for the feed water from the field (pilot-scale) study.

Table 3.4 Anions concentration of the pilot feed water (n=11).

Anions	Average (mg/L)	Standard Deviation (mg/L)
Nitrite*	0.7	0.8
Nitrate	16.3	28.9
Bromide	0.22	0.0
Chloride	400.8	11.8
Sulphate	102.6	1.6

*Nitrite (n=7)

Table 3.5 Metals concentration of the pilot feed water (n=9).

Metals	Average (µg/L)	Standard Deviation (µg/L)
Arsenic	4	0.45
Calcium	116,647	4,700
Magnesium	44,822	1,663
Sodium	226,444	8,330
Potassium	7,396	149
Aluminum	17	20
Chromium	0.40	0.11
Manganese	15	15
Copper	13	9
Iron	2	1
Zinc	54	26
Selenium	1	0.31
Silicon	14,286	269
Vanadium	7	1
Lithium	156	2
Nickel	2	0.16
Strontium	1,398	59

3.4 Adsorbent Description

Commercial adsorbent materials were used in the pilot-scale and the RSSCTs. The adsorbents and their designation with respective manufacturers are shown in Table 3.6. These designations will be used throughout this report. Adsorbents used in the pilot-scale columns were GAC1(Calgon) and GAC2(Norit), whose particle sizes varied from 1.68 mm to 0.42 mm (mesh number 12x40), whereas the IX(Purolite) resin varied from 0.75 mm to 0.60 mm. However, for the RSSCT columns, all these media were crushed to obtain smaller particle sizes varying from 0.105 mm to 0.088 mm (mesh number 140x170).

Table 3.6 Adsorbent description

Adsorbent	Manufacturer	Designation	Average Particle Size (mm)	
			Pilot	RSSCT
Filtrasorb 400	Calgon Carbon Corporation	GAC1	0.84	0.096
Norit GAC 400	Cabot Corporation	GAC2	0.84	0.096
PFA694E	Purolite	IX	0.67	0.096

3.5 Pilot/MobileNEWT Description

The pilot-scale (testbed) study was conducted at the MobileNEWT testbed (Figure 3.1). It is a dual-axial enclosed trailer (dimension: 14'Lx7'W) owned by Nanosystems Engineering Research Center (ERC) for Nanotechnology-Enabled Water Treatment (NEWT), located at ASU and could be hauled to any location. It is a testbed (i.e., mobile lab), insides fitted with several different types of water treatment modules, including several columns for loading any adsorbent materials of choice. The trailer can be hauled to the contaminated wellsite (groundwater) or to water treatment plants (WTPs) (surface water) in assessing the various type of conventional as well as novel/innovative water treatment technologies for any given pollutant types and in assessing their removal. Even

though the MobileNEWT has several different water treatment modules fitted inside, this study focused on columns loaded with adsorbent materials for PFAS removal. Columns were operated continuously throughout this study.

All three pilot columns (Figure 3.2) at the MobileNEWT were utilized during this PFAS mitigation (pilot-scale) study. Each column is 2-inches in diameter, and 26-inch in height, utilized to evaluate the effectiveness of commercially available two types of GAC materials and one ion-exchange (IX) media to adsorb PFAS from this groundwater. The raw water was continuously filtered through 5-um CF before it passed through all the columns. These columns were operated in a downflow-mode and were instrumented with several flowmeters as well as pressure gauges to monitor the flow rates and pressure drops across columns. The IX column was operated at a loading rate of 6.4 gpm/ft^2 under an EBCT of 1.3 minutes. The GAC columns were operated at a loading rate of 4.1 gpm/ft^2 with EBCT of 2.0 minutes for GAC1(Calgon) and EBCT of 1.9 minutes for GAC2(Norit). Sampling taps were used to collect effluent samples from various heights of the columns (i.e., influent, effluent, and mid-height of media). These columns were operated continuously for more than five (5) months to assess the long-term performance of PFAS removal by these two types of media (GAC and IX) in the field-setting.

Figure 3.1 Interiors of MobileNEWT

Figure 3.2 Pilot /MobileNEWT columns. Figure 4.5.2& 34:

3.6 Rapid Small-Scale Column Tests (RSSCTs) Setup and Design

The RSSCTs were conducted with Tempe GW to simulate the pilot columns and to closely match its performance in terms of operation and bed volumes (BVs) attained, in removing PFAS prior to the breakthrough. The hydraulic loading rate and empty bed contact time (EBCT) of the pilot columns were simulated at the RSSCT (for both IX resin and GAC beds) based on two different design criteria, CD and PD to simulate the pilot columns performance for both GAC1(Calgon) and GAC2(Norit) (0.84 mm particle diameter), as well as the IX resin (Purolite) (0.65 mm particle diameter). RSSCTs were designed using the scaling equations mentioned earlier. The RSSCT experimental matrix and design parameters are listed in Table 3.7 and Table 3.8

The RSSCT apparatus included 0.43 cm diameter low-density polyethylene tubing (as an adsorbent column), with polypropylene quick connectors and high-density polyethylene tubing, all these materials used are NSF approved for drinking water purposes. A piston pump (QG50, Fluid Metering Inc, Syosset, NY) was used to feed water to the RSSCT columns. Figure 3.3 represents the RSSCT setup.

Prior to the RSSCT study, all the adsorbents (i.e., GACs and IX) were wet crushed using a mortar and pestle and sieved to achieve the designed particle sizes. For IX, nitrile rubber gloves were packed with IX(Purolite) media before crushing. The reason for using the nitrile gloves was to localize the IX(Purolite) resin and increase the crushing throughput, as the resin beads were very slippery. Once crushed to targeted sizes, these adsorbents were washed and then wet packed into the RSSCT columns.

Table 3.7 Design parameters of RSSCTs mimicking pilot-scale columns.

Design Parameters	GAC 1			GAC 2			IX		
	Pilot-scale	RSSCT 1	RSSCT 2	Pilot-scale	RSSCT 3	RSSCT 4	Pilot-scale	RSSCT 5	RSSCT 6
Particle diameter (mm)	0.84	0.10	0.10	0.84	0.10	0.10	0.68	0.10	0.10
Column diameter (cm)	5.10	0.43	0.43	5.10	0.43	0.43	5.10	0.43	0.43
Column Length (cm)	33.40	1.60	5.43	30.90	1.65	5.02	32.84	1.60	4.30
EBCT (min)	2.00	0.03	0.23	1.85	0.02	0.21	1.26	0.03	0.18
Loading rate (m/h)	10.02	36.86	14.23	10.02	40.92	14.23	15.64	37.00	14.37
Re	6.90	2.90	1.10	6.90	3.20	1.10	8.60	2.90	1.10
Sc	893.70	893.70	893.70	893.70	893.70	893.70	893.70	893.70	893.70
Re x Sc	6154	2590	1000	6154	2875	1000	7719	2600	1010
Bed volume (mL)	674	0.24	0.80	631	0.24	0.74	674	0.23	0.63
flow rate (mL/min)	338.39	9.00	3.47	338.39	9.99	3.47	528.22	9.03	3.51
CD or PD	N/A	CD	PD	N/A	CD	PD	N/A	CD	PD

Table 3.8 Design parameters of RSSCTs mimicking full-scale columns.

Design Parameters	GAC 1		GAC 2		IX	
	Pilot-scale	RSSCT 7	Pilot-scale	RSSCT 8	Pilot-scale	RSSCT 9
Particle diameter (mm)	0.84	0.10	0.84	0.10	0.65	0.10
Column diameter (cm)	304.80	0.43	304.80	0.43	304.80	0.43
Column/Media Length (cm)	122.00	1.69	122.00	1.69	122.00	1.69
EBCT (min)	5.00	0.07	5.00	0.07	3.30	0.07
Loading rate (m/h)	14.67	14.23	14.67	14.23	24.44	14.04
Re	10.08	1.12	10.08	1.12	13.17	1.12
Sc	893.70	893.70	893.70	893.70	893.70	893.70
Re x Sc	9005	1000	9005	1000	11769	1000
Bed volume (mL)	8913637	0.23	8913637	0.23	9805001	0.25
flow rate (mL/min)	1782727	3.47	1782727	3.47	2971212	3.43
CD or PD	N/A	CD	N/A	CD	N/A	CD
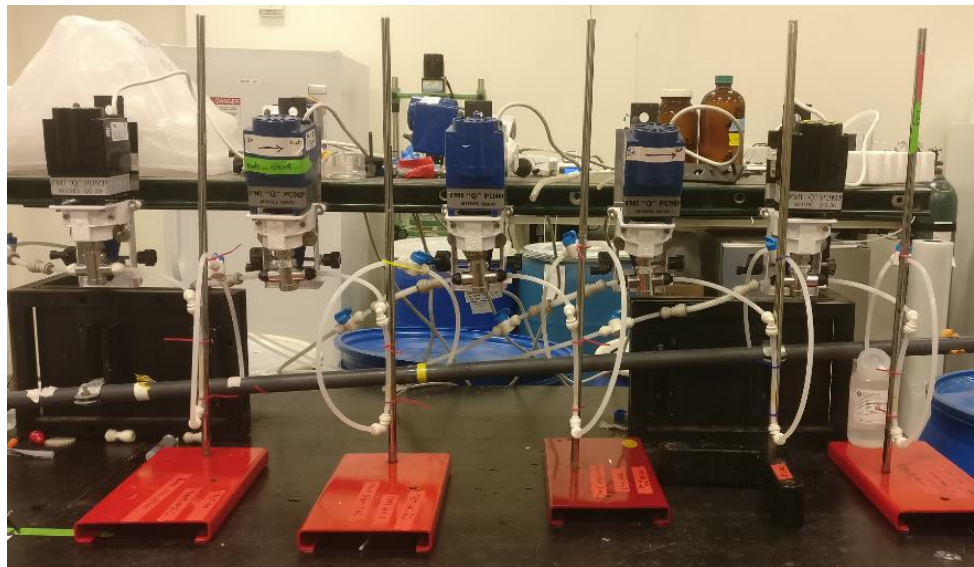
Figure 3.3 Representative RSSCT setup used in the study.

CHAPTER 4

RESULTS AND DISCUSSION FOR TEMPE GW

This chapter focuses on the PFAS breakthrough curves for the pilot columns, as well as the CD and PD based RSSCT columns. The main objectives here are to (1) Compare adsorbent capacity (i.e., the mass of PFAS/mass of media) of commercial granular activated carbons (GACs) and anion exchange resin (IX) material for PFAS removal at pilot-scale. (2) Determine if CD or the PD RSSCT columns breakthroughs match the breakthrough shape, concentrations, and adsorbent capacity of the pilot-scale columns.

Table 4.1 PFAS, DOC and UV$_{254}$ absorbance concentration of pilot and RSSCTs feed water.

Water Quality Parameter		Pilot			RSSCTs with Tempe GW				
		Average	Max	Min	1&2	3&4	5,6,9	7	8
PFAS for Tempe GW (ng/L) (n= 14)	PFBS (C4)	17.1	20	15	17	18	17	20	15
	PFHxS (C6)	6.6	12	2.9	6.0	7.3	5.9	6.4	5.3
	PFHpA (C7)	3.4	6.4	2.4	2.5	3.0	2.4	2.9	3.8
	PFHxA (C6)	6.0	7.5	5.1	5.1	6.2	5.4	5.7	6.2
	PFOA (C8)	11.1	24	7.2	7.2	9.0	8.0	9.3	19
	PFOS (C8)	9.4	14	6.4	9.4	9.7	8.4	8.8	9.8
	PFNA* (C9)	0.7	3.6	2.6	-	-	-	-	3.6
	Total PFAS	54.2	70.0	46.8	47.2	53.2	47.1	53.1	62.7
DOC (mg/L)		1.2	1.9	0.7	0.8	1.2	1.2	1.2	1.1
UV$_{254}$ (1/cm) (Abs)		0.012	0.021	0.004	0.009	0.009	0.010	0.010	0.013

* PFNA (n = 2)

4.1 PFAS Breakthrough in GAC and IX Using Pilot Columns

All three packed-bed pilot-scale columns (GAC1(Calgon), GAC 2(Norit), and IX (Purolite)) were operated continuously throughout the entire study. These columns were fed with well water over the entire 150 days (i.e., five months) of operation. The goal was to compare the adsorbent capacity of the sorbents (GACs and IX) in adsorbing PFAS. At the end of this study, a little over 100,00 gallons of well-water was used (which remains lower than the allocated amount, which also helped in minimizing the waste). The IX column was operated over 150,000 bed volumes (BVs), while the GAC columns were operated for nearly 100,000 BVs, as shown in Figure 4.1.
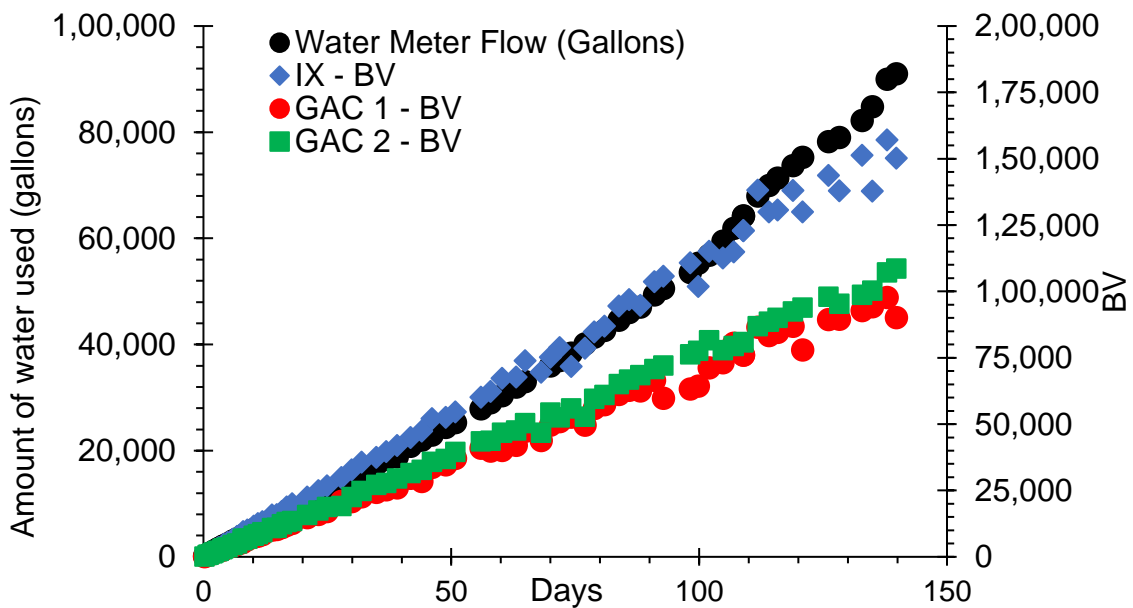
Figure 4.1 Water consumption and bed volumes processed for pilot columns.

Figure 4.1 also shows the total and individual water consumption of each column as a function of time. Table 4.1 shows the average (total) PFAS influent concentration during the field study. The average was about 54.2 ng/L, with maximum and minimum

70 ng/L and of 46.8 ng/L, respectively. Below the PFAS breakthrough for GACs and IX

for the pilot columns are further discussed and compared to each other.

4.1.1 PFAS Breakthrough in Pilot GAC Columns:

Columns at testbed were loaded with adsorbent media GAC1(Calgon) and

GAC2(Norit) for column 2 and column 3, respectively, while column 1 was loaded with

IX (Purolite) materials for the pilot-scale studies. Both GACs were bituminous type coal-

based carbon. Here the main objective of the study was to assess the difference between

these two GACs and to assess their ability to adsorb and remove PFAS from this

groundwater well at the pilot-scale. However, the comparison between these two

adsorbents will be discussed further and in more detail in the later part of this section. The

secondary objective of this pilot-scale study was to assess the effect of relative removal of

different PFAS compounds (or species) and their breakthrough patterns at the pilot

columns.

The groundwater is found to be of low DOC and with low specific ultraviolet

absorbance ($SUVA_{254}$) values (1.2 mg/L and 0.92 L mg-C^{-1} m^{-1} average, respectively).

Figure 4.2 shows the DOC and UV_{254}-absorbance breakthrough curves for the

GAC1(Calgon) and GAC 2(Norit), respectively. DOC and UV_{254}-absorbance show rapid

breakthrough for both the GACs (>80% breakthrough occurred within 25,000 BVs). This

early breakthrough suggests the presence of non-adsorbable DOM (dissolved organic

matter) fraction that is most likely not adsorbing to the carbons and not competing with

PFAS for adsorption sites.

Figure 4.3 shows the breakthrough curves of PFAS compounds as C/C$_0$ to BVs

(bed volumes) processed, where C$_0$ is the average influent concentration of respective

PFAS compound, as shown in Table 4.1 for both GAC1(Calgon) and GAC2(Norit), respectively. The normalized, non-dimensional dimensional numbers aid to directly compare different PFAS compounds (species) removal for any given sorbent type as well as to compare them against different sorbents type. The actual concentration breakthrough curves for the pilot-scale column for PFAS species removal by GACs and IX are shown in Figures 4.10-4.13.

Figure 4.3 shows for GACs, PFOS(C8) breakthroughs later in comparison to PFHxS(C6), and PFHxA(C6) for a similar number of BVs. The longer chain compounds (e.g., C8) are more hydrophobic than short-chain compounds (e.g., C6) (see Chapter 5). The long-chain compounds breakthrough slowly when compared to the shorter chain compounds, which are less hydrophobic and breakthrough faster despite varying influent concentration. Prior studies have also reported the same pattern on the chain length to media breakthrough (Park et al. 2020; Schaefer et al. 2019; Du et al. 2014; C. J. Liu, Werner, and Bellona 2019; McCleaf et al. 2017). Thus, the shorter chain compounds being less hydrophobic in nature and higher diffusivity (Park et al. 2020), have lesser interaction, thus are weakly adsorbed to GAC media as compared to longer chain compounds.

Similarly, Figure 4.3 shows the breakthrough in terms of functional groups; PFHxS (C6) is compared to PFHxA (C6), and PFOS(C8) is compared to PFOA(C8). It shows that compounds of the same carbon chain length, compounds with sulfonic acid functional group breakthrough later as compared to the carboxylic group, these trends are seen in other studies as well (Rodowa et al. 2020). The sulfonic group compounds breakthrough later due to additional per-fluorinated carbon in their hydrophobic tail, which increases the hydrophobicity of such compounds and results in greater adsorption to the GAC media.
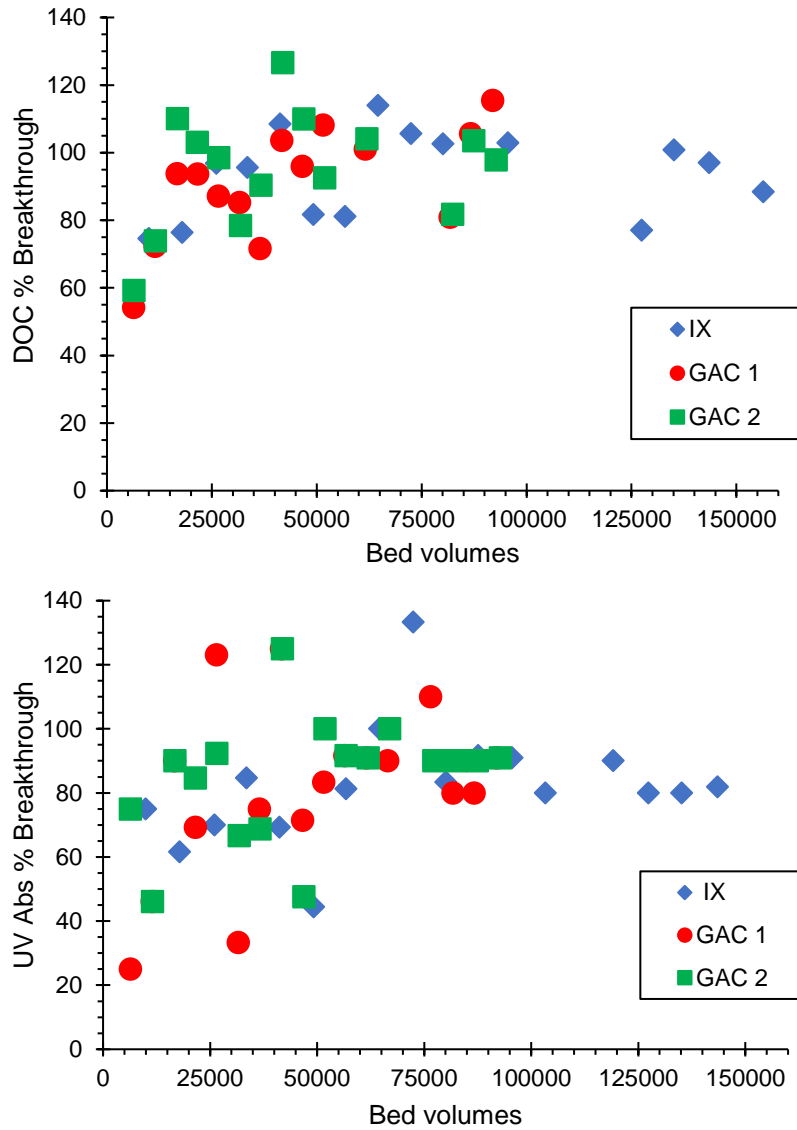
Figure 4.2 DOC (A) and UV_{254} Abs (B) fractional breakthrough curves for Tempe GW, pilot columns (GAC 1, GAC 2, and IX) as a function of BVs treated, with effluent normalized to influent values (DOC = 1.2mg/L and UV_{254}(Abs/cm) = 0.012).
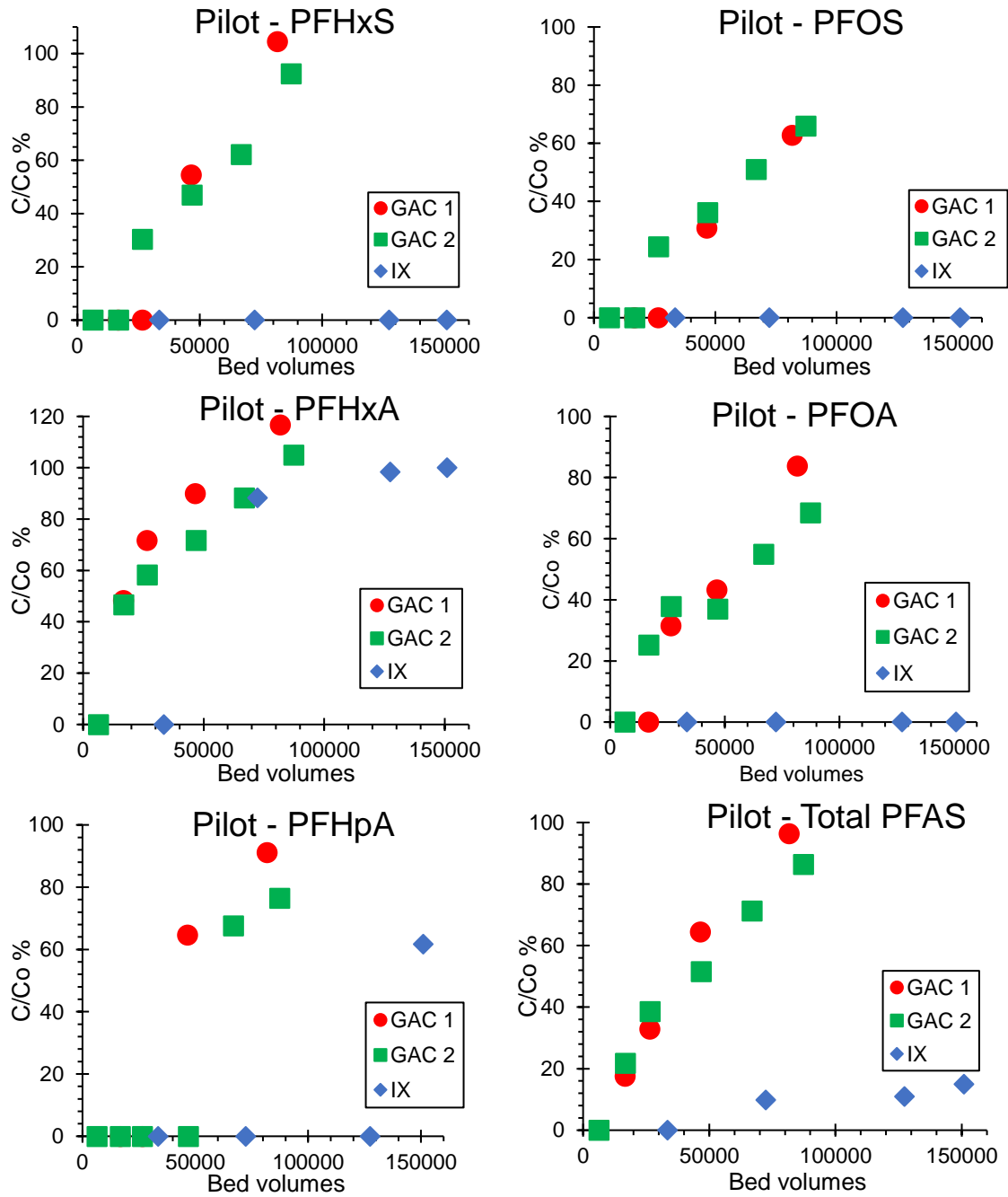
Figure 4.3 PFHxS (A), PFOS (B), PFHxA (C), PFOA(D), PFHpA (E) and Total PFAS (F) breakthrough curves for Tempe GW, pilot columns (GAC 1, GAC 2 and IX) as a function of BVs treated with effluent concentration (C) normalized to influent concentration (C_0) as shown in Table 4.1.

Thus, for GAC1(Calgon) and GAC2(Norit), the chain length and the functional group of PFAS compounds play an essential role in adsorption and overall breakthrough, even in dynamic influent water matrix at pilot-scale. The breakthrough generally happens in the order of increasing hydrophobicity, i.e., the longer chain being hydrophobic adsorbs more, resulting in slower breakthroughs (C4>C6>C8). Similarly, among functional groups, the sulfonic group PFAS compounds broke through slowly to the carboxylic groups for the same carbon chain length.

The breakthrough patterns, as mentioned earlier, were correlated with Log D and Log K_{ow} values at pH (pH 7.4) shown in Table 5.1. Log D and Log K_{ow} represents the hydrophobicity of the compounds. Figure 4.4 (A) shows the breakthrough curve of PFHxA, PFBS, PFOA, PFHxS, and PFOS for GACs at 46,000 BVs and Figure 4.4 (B) shows the breakthrough at 82,000 BVs and 87,000 BVs for the GAC1(Calgon) and GAC2(Norit) respectively. The general order of breakthrough, as seen in Figure 4.4 and at the majority of BVs for both the GACs were of the following order: PFHxA ≈ PFBS < PFOA ≈ PFHxS < PFOS except for PFHpA, which follows the increasing order of hydrophobicity, indicated by the increasing Log D values as shown in Table 5.1. Here PFHpA, although it was non-detect until 26,000 and 46,000 BVs for GAC1(Calgon) and GAC 2 (Norit), respectively, showed increased breakthrough at later BVs. This breakthrough behavior of PFHpA could be due to specific adsorption sites available for PFHpA combined with a low average influent concentration of PFHpA (3.4 ng/L), which is close to the analytical method's detection limit of 2 ng/L. A similar trend was seen in the PFHpA breakthrough in another study (C. J. Liu, Werner, and Bellona 2019).
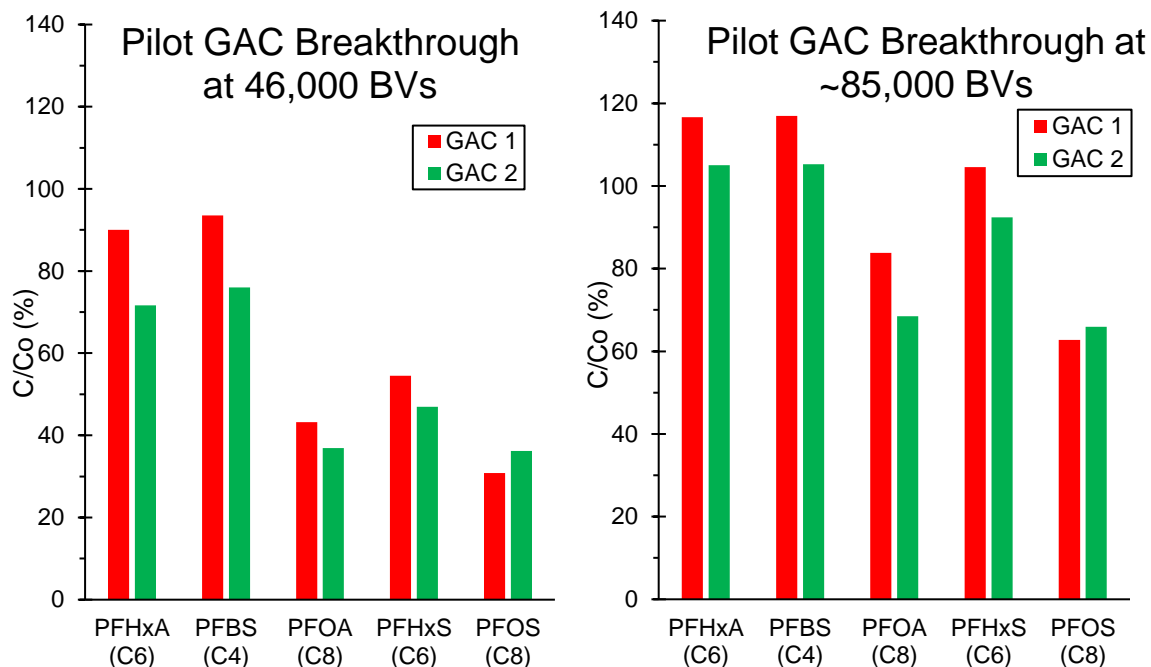
Figure 4.4 Breakthrough of PFHxA, PFBS, PFOA, PFHxS, and PFOS (A) at 46,000 bed volumes (B) 82,000 bed volumes for GAC 1 and 87,000 bed volumes for GAC 2.

  PFHxA and PFBS (Figure 4.3) completely broke through for both carbons (GAC1(Calgon), and GAC2(Norit)), and the effluent concentration was higher than 100%, this is due to chromatographic effect (Hand et al. 1997), which is typically due to desorption of already adsorbed PFBS. This occurs when the molecules are weakly adsorbed and are then replaced by more strongly adsorbed molecules; here, such compounds possibly could be PFHxS, PFOS, or adsorbable fraction of DOM. The above discussion suggests that the expected breakthrough order of PFAS compounds in pilot-scale GAC columns is dependent on the hydrophobicity of PFAS compounds and hence is their expected removal, despite varying influent PFAS concentration.

4.1.2 PFAS Breakthrough in Pilot IX Column

Column 1 of the pilot-scale was loaded with IX(Purolite) media, which is a special resin bead specifically made for PFAS removal. It is polystyrene crosslinked with divinylbenzene IX resin, with a "complex amino" functional group (not disclosed by manufacturer). The main objective was to evaluate the adsorption capacity of the PFAS selective IX resin. The IX resin column had a higher hydraulic loading rate and a shorter EBCT as compared to GAC columns (Columns 2 and 3). Thus, it was treated with a higher amount of water, as seen in Figure 4.1, even though all three columns were of similar height.

Figure 4.2 also shows the DOC and UV_{254}-absorbance breakthrough for the IX resin was rapid and was similar to the GAC columns. More than 80% of the breakthrough occurred within 25,000 BVs, and 30,000 BVs for DOC and UV_{254}, respectively. This early organic (DOC and UV_{254}) breakthrough suggests the presence of non-adsorbable DOM fraction that is most likely not adsorbed by the IX resin and does not compete with PFAS compounds for the adsorption sites. This early breakthrough suggests that IX, which is a PFAS selective resin, has higher selectivity towards PFAS compounds removal.

Figure 4.3 shows that among all the PFAS compounds detected in the influent water, only PFHxA broke through completely at ~125,000 BVs in IX columns, while PFHpA broke through 62% at ~150,000 BVs. PFHxA is the least hydrophobic among all the PFAS compounds detected. Additionally, PFHpA, even though it comes after PFBS according to the order of hydrophobicity (Log D), has an earlier breakthrough (62% at 150,000 BVs) compared to PFBS (no breakthrough). This early breakthrough of PFHpA

31

could be because the effluent concentration at 62% breakthrough was only 2.2 ng/L, which

is very close to the analytical detection limit of 2 ng/L.

Since IX(Purolite) is an anion exchange resin and can remove anions. Various water

quality parameters (such as nitrate, nitrite, bromide, chloride, and sulfate) were also

measured and analyzed for both influent and effluent samples to evaluate for any potential

competing ions. However, Figure 4.5 shows that almost all the anions measured broke

through almost instantaneously (>99% at ~2000 BVs), indicating this IX is highly selective

for PFAS removal. Additionally, nitrite and bromide seem to compete for the same

adsorption sites, as an increase in the effluent concentration of one is correlated with a

decrease in the other.
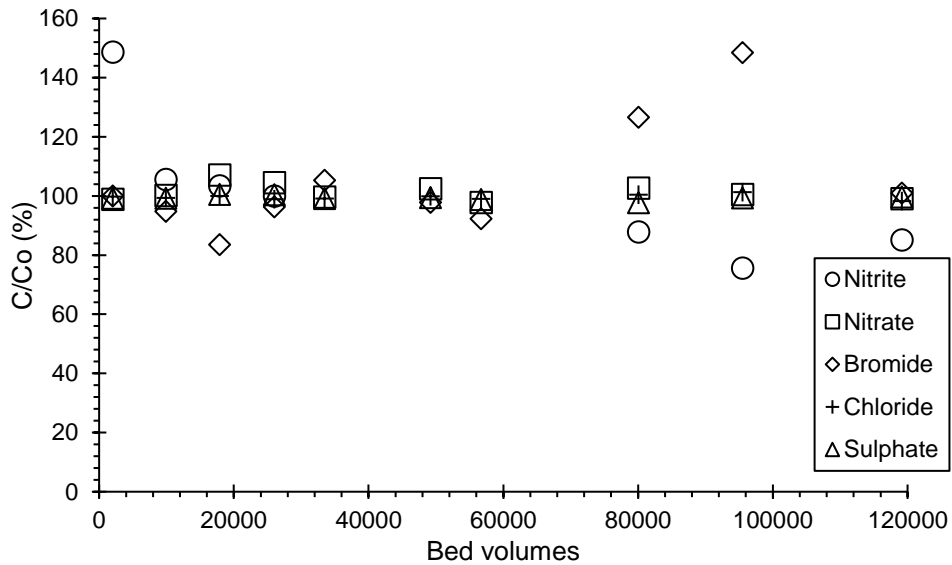
Figure 4.5 Bromide, Nitrate, Nitrite, Sulphate, and Chloride breakthrough curves for
Tempe GW, IX pilot column as a function of BVs treated with effluent concentration (C)
normalized to influent concentration (C_0) as shown in Table 4.1.

Unlike the GACs, the chain length or functional group dependence on PFAS

breakthrough could not be observed for IX at pilot columns with an EBCT of 1.3 minutes.

Most of the compounds did not break through even after 5-months of operation of 150,000

BVs of pilot-scale operation. However, multiple wells RSSCTs study (Chapter 5) and other studies (Schaefer et al. 2019) have shown similar results as GACs, i.e., longer carbon chain, and more hydrophobic compounds breakthroughs slower (or later) as compared to the shorter and less hydrophobic compounds. This breakthrough pattern indicates that, like GACs, hydrophobic interactions may be critical for IX resin too.

Thus, from the above results, it can be concluded that the IX resin used is highly effective in adsorbing most of the PFAS compounds in the testbed columns with primarily no breakthroughs. Only PFHxA and PFHpA are two compounds that broke through completely and partially, respectively; this is among varying influent PFAS concentrations and under variable water quality matrices.

4.1.3 Comparing Adsorption Capacity of Sorbents in Pilot-Scale

The adsorption capacity and performance of adsorbents in the pilot-scale testing are further compared. Table 4.2 shows the adsorbent capacity of GAC1(Calgon), GAC2(Norit), and IX(Purolite) at different BVs (bed volumes). These are compared for different PFAS compounds. The adsorption capacity of a sorbent is reported as the mass of contaminant (μg) adsorbed per unit mass (g) of the adsorbent.

Adsorption capacity (or the solid-phase loading) is calculated by integrating the area between the breakthrough curve and the influent concentration, normalized to the amount of adsorbent used. Adsorption capacity is mathematically calculated using Equation 6.

$$\text{Adsorbent capacity} \left(\frac{\mu g \text{PFAS}}{\text{g adsorbent}}\right) = \frac{\int_0^V (C - C_0)dV}{1000\, M} \tag{6}$$

where C and C_o are the effluent and influent PFAS concentration (ng PFAS/L) respectively; V is the volume of water processed through the bed (L), and M is the mass of adsorbent used (g), and 1000 is the conversion factor to have the units in (µg PFAS/ g adsorbent)

Figure 4.3 shows among GAC1(Calgon) and GAC2(Norit), the breakthrough curves were similar in shape for all the PFAS compounds, suggesting a similar mass transfer mechanisms (MTZ) and zone development in both GACs. However, Figure 4.3 and Table 4.2 suggests that the GAC2(Norit) performed slightly better than GAC1(Calgon), with a later breakthrough for most of the PFAS compounds and with a higher adsorption capacity for all PFAS compounds. At the end of testing, GAC2(Norit) had a higher total PFAS adsorption capacity of 5.31µg/g of adsorbent, which is 1.4 times that of GAC1(Calgon). Table 4.2 also shows that the adsorption capacities for lesser hydrophobic compounds like PFHxA, PFBS, and PFHpA were of much higher capacity at similar BVs (~42,000 and ~85,000) for GAC2(Norit) than GAC1(Calgon), respectively. In contrast, both the GACs were similar for more hydrophobic compounds like PFOS and PFOA.

The differences in GAC performance could be attributed to GAC characteristics. The GAC2(Norit) is slightly higher in surface area and with larger mesopore and micropore volume in comparison to GAC1(Calgon) (C. J. Liu, Werner, and Bellona 2019). Adsorbent's surface area and mesopores are important for the adsorption of more hydrophobic compounds. Moreover, the micropores are also important for less hydrophobic compounds (Park et al. 2020). Therefore, among the GACs, the GAC2(Norit) performed better than GAC1(Calgon), for any given number of BVs

Table 4.2 PFAS adsorption capacity of pilot columns (GAC 1, GAC 2, and IX).

Pilot Column	Bed Volumes Treated	Adsorption capacity (µg PFAS/ g media)						Total
		PFBS (C4)	PFHxS (C6)	PFHpA (C7)	PFHxA (C6)	PFOA (C8)	PFOS (C8)	
GAC 1	46528	0.75	0.51	0.25	0.23	0.78	0.76	3.28
GAC 2	46868	1.04	0.54	0.35	0.34	0.85	0.81	3.93
IX	33000	0.57	0.23	0.10	0.20	0.29	0.31	1.70
GAC 2	66904	1.15	0.67	0.45	0.40	1.11	1.05	4.83
IX	72000	1.24	0.50	0.21	0.33	0.62	0.67	3.57
GAC 1	81688	0.69	0.60	0.30	0.22	1.05	1.09	3.94
GAC 2	87349	1.15	0.74	0.49	0.40	1.30	1.22	5.31
IX	150900	2.59	1.05	0.41	0.37	1.29	1.39	7.10

Among the adsorbents tested at pilot columns, the IX resin outperformed the GACs, as shown in Figure 4.3, even after treating > 150,000 BVs, which is about 1.5 times higher than GACs. Only PFHxA and PFHpA broke through fully and partially, respectively; this is among all detected PFAS compounds. While the total PFAS almost reached a complete breakthrough >85% for both GAC1(Calgon) and GAC 2 (Norit). In comparison, the IX resin only reached ~15% of breakthrough, which means the IX resin has much larger adsorption capacity compared to the GAC materials.

However, Table 4.2 would show lesser adsorption capacity for IX compared to GACs at similar BVs (esp. between GAC 2 and IX at 67,000 and 72,000 BVs, respectively). This lower adsorption capacity is because IX, with a specific gravity of about 1.05, is twice as dense as GACs. For a given volume, IX would have twice the amount of mass as compared to GACs and thus lowers the adsorption capacity for similar BVs initially. Nevertheless, at the end of testing, the adsorption capacity of the IX pilot column for total PFAS at the end of the run was about 7.1µg/g of adsorbent, which is 1.3 times and 1.8 times greater than GAC1(Calgon) and GAC2(Norit), respectively. Since IX had only

<15% breakthrough, the complete breakthrough was not achieved, this later breakthrough for IX suggests that it would require much longer run time when all the compounds are ultimately adsorbed and saturated for a complete breakthrough to occur.

The larger adsorption capacity of the IX resin proves that this IX material is highly effective in removing PFAS from this groundwater well. However, PFAS selectivity at higher EBCTs needs to be further explored as our study was initially designed for shorter EBCT to expedite the breakthrough. Moreover, the capital cost, the media cost, and the replacement cost of IX systems are much higher than GACs. Thus, cost estimates on media based on pilot and RSSCT studies are necessary toward selecting appropriate media types based on performance and in designing a full-scale system.

Based on the pilot-scale study, it can be concluded that the hydrophobic interaction (i.e., PFAS to media) is most likely to be an important adsorption mechanism for the GACs. The breakthrough pattern was dictated by the carbon chain length as well as a functional group of PFAS compounds. Both the GACs (Calgon and Norit) were similar in performance with similar PFAS breakthrough curves, suggesting similar mass transfer mechanisms for both the GACs. However, when GACs are closely compared, the GAC2(Norit) with higher adsorption capacity tends to perform slightly better than GAC1(Calgon) in adsorbing PFAS compounds for a similar number of BVs processed. However, the IX resin has much larger adsorption capacity and outperformed the GACs in adsorbing and in removing PFAS from this dynamic groundwater well during the pilot-scale study.

4.2 PFAS Breakthrough in GAC and IX using CD-RSSCT

The RSSCTs based on CD design were performed to evaluate the following conditions. It was conducted, first to simulate pilot-scale columns PFAS breakthrough, and then also to study the effects of EBCT on PFAS removal.

The RSSCTs (RSSCT 1,3&5) simulating the pilot columns based on CD design were assessed for 100,000 BVs for two GACs, and 150,000 BVs for the IX. These RSSCTs simulating the pilot columns took about 2-3 days to complete. The time taken by RSSCTs is merely a fraction of the time taken for the pilot-scale study. Additionally, the RSSCTs (RSSCT 7,8&9) with a higher hydraulic loading rate (HLR) and longer EBCTs were also performed to evaluate the effects of EBCT on the breakthrough curves. Tables 3.7 and 3.8 show the design parameters of all these RSSCT runs.

4.2.1 PFAS Breakthrough in CD-RSSCTs Simulating Pilot Columns

The RSSCTs to simulate the pilot columns were performed in the same feed water (i.e., well water) as the pilot study under design parameters, as shown in Table 3.7. The RSSCT feed is of lower DOC and $SUVA_{254}$ values, 0.78 mg/L and 1.15 L mg-C^{-1} m^{-1} for the RSSCT 1, 1.21mg/L and 0.83 L mg-C^{-1} m^{-1} for RSSCT 2, and 0.92 mg/L and 0.98 L mg-C^{-1} m^{-1} for RSSCT 3, respectively. From Figure 4.6, it is evident that all the CD-RSSCTs results have a rapid breakthrough for both DOC and UV_{254}-absorbance (>70% within 20,000 BVs). As previously mentioned in the pilot columns section, these results suggest the presence of non-adsorbable DOM, which causes early breakthroughs. Additionally, an early breakthrough with the reduction of particle size in RSSCTs suggests, particle size did not have much effect on DOC adsorption kinetics and remains the same regardless of particle sizes.

37

Figure 4.7 shows the breakthrough of PFAS compounds for GAC RSSCTs (RSSCT 1 and RSSCT 2 for GAC1(Calgon) and GAC2(Norit) respectively) simulating the pilot columns, as a normalized value, C/C_0 to BVs, where C_0 is the average influent concentration, as shown in Table 4.1.
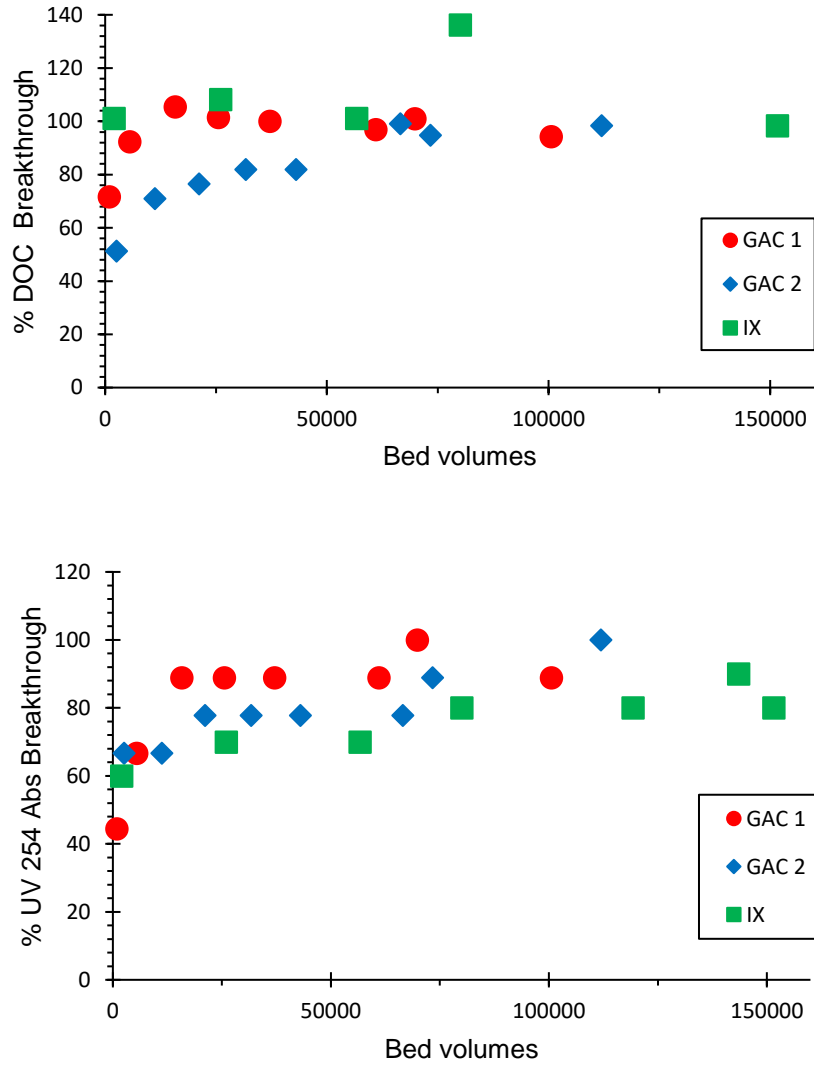
Figure 4.6 DOC (A) and UV_{254} absorbance (B) percentage breakthrough curves for Tempe GW, CD-RSSCTs (GAC 1, GAC 2, and IX). as a function of BVs treated with effluent normalized to influent values in Table 4.1.

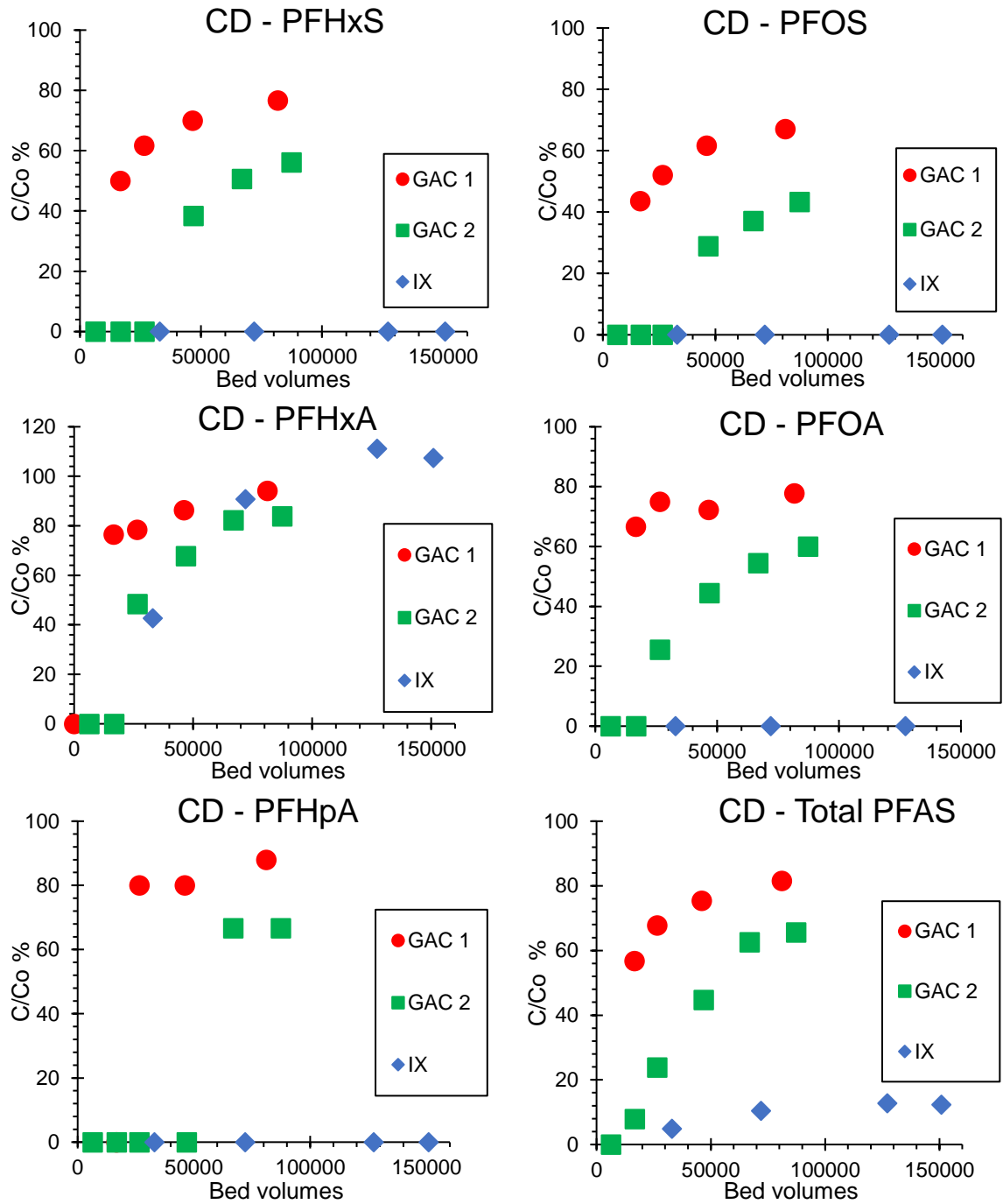**Figure 4.7** PFHxS(A), PFOS(B), PFHxA (C), PFOA(D), PFHpA(E) and Total PFAS (F) breakthrough curves for Tempe GW, CD - RSSCTs (GAC 1, GAC 2 and IX). as a function of bedvolumes treated with effluent concentration (C) normalized to influent concentration (C_0) in Table 4.1.

Figure 4.7 illustrates that CD-RSSCTs of GAC1(Calgon) and GAC2(Norit) have similar shapes of the breakthrough curves, and the breakthrough dependent on the chain length and its functional group. For example, PFOS (C8) broke through later compared to PFHxS(C6) and PFOA(C8). Similarly, PFOS (C8) broke through later compared to PFOA (C8), for a similar number of BVs. Therefore, the order of breakthrough according to chain length for a given functional group is C4>C6>C8, and for a given chain length, sulfonic group compounds breaking through later compared to a carboxylic group, were consistent in both CD-RSSCTs and pilot for GACs. Therefore, CD-RSSCTs was able to capture the breakthrough order successfully and possibly also the mass transfer zone (MTZ) similar to that of the pilot columns.

However, a closer look suggests the GAC2(Norit) seems to be more effective in adsorbing PFAS compared to GAC1(Calgon), as all the PFAS compounds breakthrough earlier for the latter. The difference seems to be significant for the more hydrophobic compounds such as PFOS and PFOA than the less hydrophobic compounds, such as PFHxA and PFHpA. The difference being less significant for less hydrophobic compounds could also be due to these compounds breaking through faster. Thus, the distinction between the two GACs is not very apparent. The early breakthrough of PFAS compounds for GAC1(Calgon) may also possibly be due to some operational issues related to the RSSCT 1 column operation, especially at the initial stages of operation, such as off-gassing of dissolved gas (if any) in the feed water. Therefore, it could be concluded that the CD-RSSCTs are effective in simulating the pilot columns and in capturing its breakthrough order and possibly capturing the mass transfer zone (MTZ) of the pilot columns.

However, the IX CD-RSSCT shows a complete breakthrough of PFHxA only, which is the least hydrophobic of all the PFAS compounds. There was also no PFHpA breakthrough as in the pilot columns, possibly due to its low concentration (2.4 ng/L) in the feed water as compared to pilot average feed concentration (3.4 ng/L), which is also close to the detection limit of the analytical method (2 ng/L). Nevertheless, these results suggest, the IX is the best performing adsorbent with a slower breakthrough, and the RSSCT column seems to reflect that for IX, even if it is only for the PFHxA compound.

Table 4.3 shows the adsorption capacity of CD-RSSCTs at different bed volumes. From comparing adsorption capacity for GACs at similar BVs (46,000 and ~85,000), as in pilot columns, GAC2(Norit) performs better than GAC1(Calgon). However, the total PFAS adsorption capacity for GAC 2 is 5.72 µg/g of adsorbent at the end of testing, which is 2.2 times GAC1. The larger difference between the two GACs as compared to pilot results could be due to the operational issue of RSSCT 1 mentioned earlier. Nevertheless, the results are consistent with the pilot-scale.

Table 4.3 PFAS adsorption capacity of CD-RSSCTs simulating pilot columns (GAC 1, GAC 2, and IX).

CD-RSSCTs simulating pilot	Bed Volumes Treated	Adsorption capacity (µg PFAS/ g media)						
		PFBS (C4)	PFHxS (C6)	PFHpA (C7)	PFHxA (C6)	PFOA (C8)	PFOS (C8)	Total
GAC 1	46528	0.63	0.27	0.13	0.16	0.27	0.48	1.93
GAC 2	46868	1.16	0.62	0.28	0.40	0.68	0.84	3.98
IX	33000	0.53	0.19	0.08	0.13	0.25	0.26	1.44
GAC 2	66904	1.40	0.78	0.36	0.46	0.86	1.10	4.95
IX	72000	1.24	0.50	0.21	0.33	0.62	0.67	3.57
GAC 1	81688	0.79	0.38	0.15	0.19	0.39	0.71	2.62
GAC 2	87349	1.56	0.92	0.40	0.50	1.02	1.33	5.72
IX	150900	2.44	0.85	0.34	0.19	1.15	1.21	6.18

Table 4.3 also shows that IX(Purolite) has lower adsorption capacity compared to GAC2(Norit) at similar BVs (67,000 and 72,000 for IX(Purolite) and GAC2(Norit) respectively), like the pilot-scale testing. However, IX CD-RSSCT, after 150,000 BVs and a simulated EBCT of 1.26 minutes, had about ~12% total PFAS breakthrough compared to >85% breakthrough for GAC RSSCTs after treating ~85,000 BVs with a simulated EBCT of 2 minutes. Thus, IX performed the best among the three media. RSSCTs adsorption capacity and order of performance among the sorbents were consistent with the pilot columns' results.

4.2.2 CD-RSSCTs to Study the Effect of EBCT on PFAS Breakthrough

The RSSCT columns were also run to simulate the full-scale columns under varying hydraulic loading rates (HLR) and EBCTs using the same feed water (groundwater well) as of the pilot-scale study; its design parameters are shown in Table 3.8.

The effect of EBCT and potential competition for the sorption sites for total PFAS breakthrough are evaluated for different sorbents (RSSCT 1 and RSSCT 7 for GAC1(Calgon)), (RSSCT 2 and RSSCT 8 for GAC2(Norit)), and (RSSCT 3 and RSSCT 9 for IX(Purolite)). Figure 4.8 compares the total PFAS breakthrough for different sorbents. Figure 4.8 shows the RSSCTs with longer EBCTs have lower or similar effluent concentrations as compared to the shorter EBCTs and also resulted in similar BVs. Suggesting that longer EBCTs have little or no effect of DOM preloading or other dissolved ions on adsorbent performance on PFAS removal. These results also suggest that the mass transfer zone (MTZ) is effectively captured even at short EBCT of 2 min for GAC1(Calgon) and GAC2(Norit), and 1.3 min for IX (Purolite), respectively.
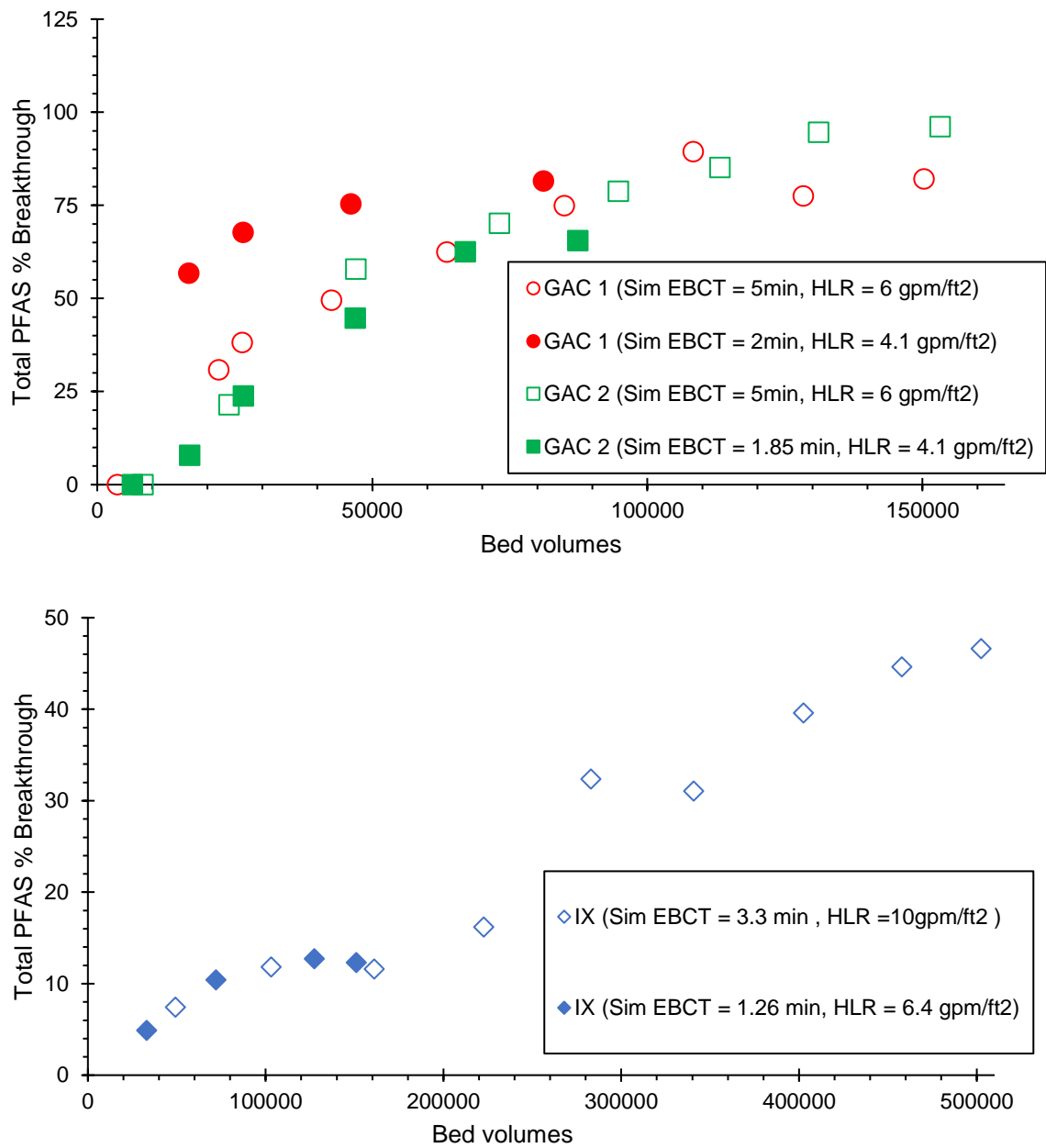
Figure 4.8 Total Fractional PFAS breakthrough curves for RSSCT 1,3,7&8 (A) and RSSCT 5&9 (B), where respective influent concentrations C_0 are as shown in Table 4.1.

4.3 PFAS Breakthrough of GAC and IX using PD-RSSCTs

The RSSCTs based on PD design was evaluated next. This was performed to simulate pilot columns PFAS breakthrough. The RSSCTs (RSSCT 2,4&6) simulating the pilot columns were performed for 100,000 BVs for both GACs and 150,000 bed volumes for the IX based on the PD design. These PD-RSSCTs took about 14-19 days to complete, even though it is much longer than the CD design, yet reasonable in terms of days required to complete a pilot-scale study. Table 3.7 shows the design parameters of all these RSSCTs runs.

Figure 4.9 shows the breakthrough of PFAS in GAC RSSCTs (RSSCT 2 and RSSCT 4 for GAC1(Calgon) and GAC2(Norit), respectively) simulating the pilot columns, as C/C_0 to BVs processed, where C_0 is the average influent concentration as shown in Table 4.1.

Figure 4.9 illustrates that GAC2(Norit) has the complete breakthrough of hydrophobic compounds, like PFHxA and PFBS, whereas the GAC1(Calgon) shows partial breakthrough of PFHxA (69%) and PFBS (59%), respectively at the end of runs. Moreover, the hydrophobic compounds like PFOS and PFHxS had no breakthrough in GAC 2 (Norit), whereas GAC1(Calgon) shows the breakthrough of the compounds (at the end of the RSSCT runs). The difference in breakthrough patterns among different PFAS compounds in PD-RSSCTs suggests that intraparticle diffusion may be more relevant for the longer/more hydrophobic compounds since the intraparticle diffusion is the rate-limiting step in the PD design. Moreover, the GACs' PD RSSCTs run was able to show (similarly to CD) the breakthrough is dependent on the chain length (C4>C6>C8) and functional group (sulfonic group breaking through later compared to the carboxylic group).

However, all the PFAS compounds breakthroughs were delayed in the PD design compared to the pilot columns or CD design, suggesting that PD design does not accurately reflect the pilot-columns and has much slower kinetics in comparison to the CD design.

The IX RSSCT PD-RSSCT had only one (i.e., PFHxA) PFAS compound among all compounds detected in the feed to breakthrough at the end of the column run. Thus, suggesting that IX is an effective adsorbent among three sorbents tested, to remove PFAS from the groundwater well.

Table 4.4 PFAS adsorption capacity of PD-RSSCTs simulating pilot columns (GAC 1, GAC 2, and IX).

PD-RSSCTs simulating pilot	Bed Volumes Treated	Adsorption capacity (µg PFAS/ g media)						
		PFBS (C4)	PFHxS (C6)	PFHpA (C7)	PFHxA (C6)	PFOA (C8)	PFOS (C8)	Total
GAC 1	46528	1.32	0.52	0.22	0.38	0.63	0.82	3.89
GAC 2	46868	1.39	0.69	0.29	0.52	0.86	0.92	4.67
IX	33000	0.53	0.19	0.08	0.13	0.25	0.26	1.44
GAC 2	66904	1.84	0.99	0.41	0.64	1.22	1.32	6.41
IX	72000	1.17	0.40	0.16	0.19	0.55	0.58	3.05
GAC 1	81688	1.93	0.84	0.38	0.52	0.99	1.35	6.02
GAC 2	87349	2.00	1.29	0.53	0.68	1.53	1.72	7.75
IX	150900	2.44	0.85	0.34	0.16	1.15	1.21	6.16

Table 4.4 shows the adsorption capacity of PD-RSSCTs at different BVs. GACs have much higher adsorption capacity for total PFAS compared to pilot (~1.5 times). Thus, showing that PD-RSSCTs overestimate the adsorption capacity. Additionally, since most of the compounds are yet to break through completely, the adsorption capacity would be much larger at the end of testing, leading to a greater discrepancy between pilot and PD-RSSCTs. On the other hand, IX PD-RSSCTs have similar adsorption capacity as CD-RSSCTs due to minimal breakthrough.
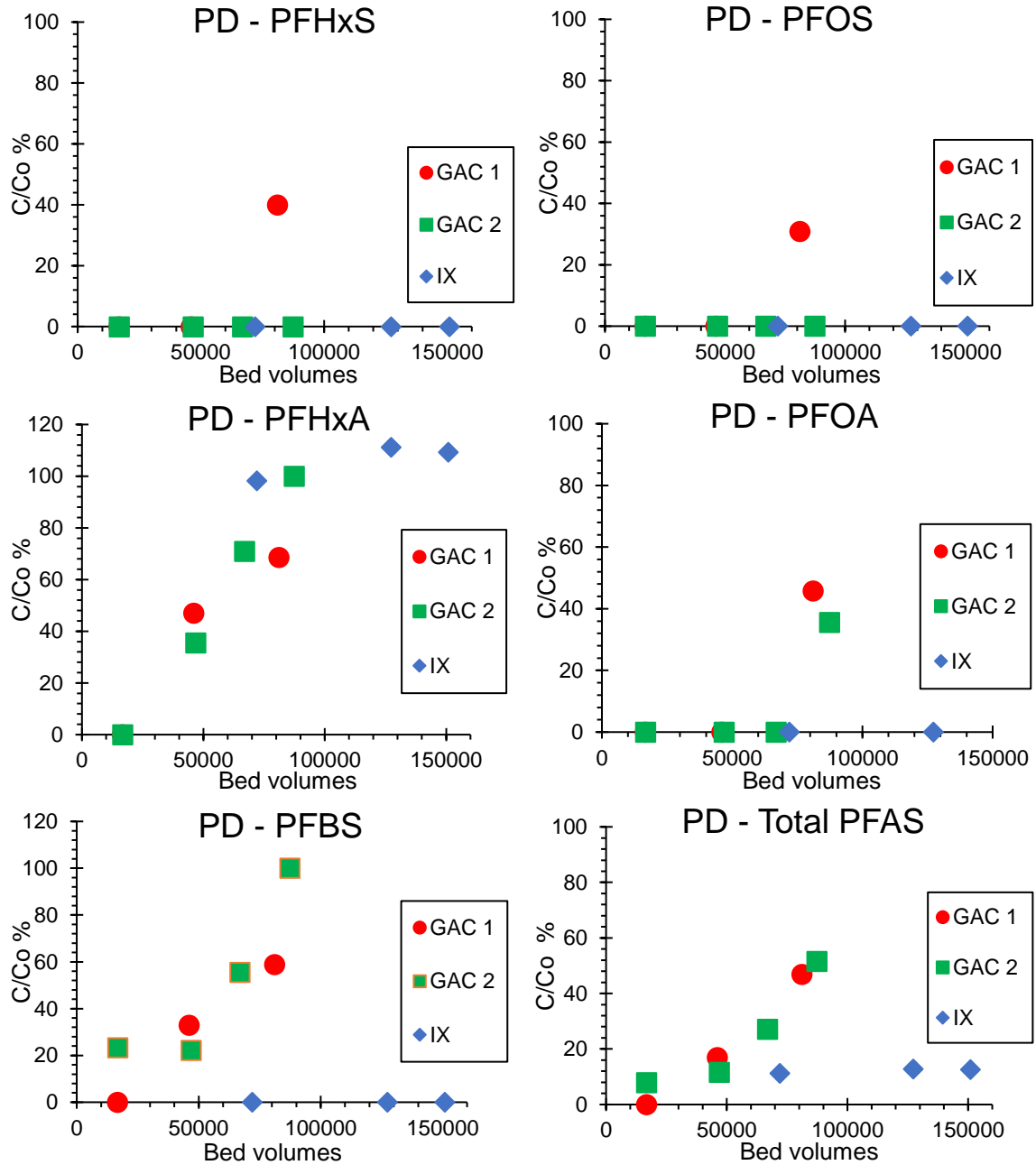
Figure 4.9 PFHxS(A), PFOS(B), PFHxA (C), PFOA(D), PFBS(E) and Total PFAS (F) breakthrough curves for Tempe GW, PD - RSSCTs (GAC 1, GAC 2 and IX). as a function of bed volumes treated with effluent concentration (C) normalized to influent concentration (C_0) as shown in Table 4.1.

4.4 Comparing RSSCT and Pilot Columns

The breakthrough curves from the field pilot testing were compared against the RSSCT results using both the CD and PD design based RSSCTs. The RSSCTs simulating the pilot columns were run with the same well water samples collected in 55-gallon drums from the field site. Therefore, to determine the best scaling design (CD or PD), RSSCTs were run to compare the PFAS breakthrough of the pilot columns in terms of effluent concentration (ng/L), normalized (C/C_o) concentration, and adsorption capacities basis. The section below discusses these findings.

4.4.1 Comparing Absolute PFAS Concentration Breakthrough Between RSSCTs And Pilot Columns

Figure 4.10 shows the total PFAS concentration breakthrough curves with BVs treated for both RSSCTs and pilot columns for GAC1(Calgon), GAC2(Norit), and IX(Purolite). Figure 4.1 shows that the CD-based RSSCT design matches the pilot-scale results closely than the PD design RSSCT for both GAC1(Calgon) and GAC2(Norit). These breakthrough curves (i.e., CD-RSSCT and pilot columns) have a similar shape. The slight difference between the pilot and CD-RSSCT (if any), could be attributed to the varying influent PFAS concentration for the pilot columns and other operational variations (e.g., stoppages due to change cartridge filters, off-gassing of dissolved gas) in the pilot and RSSCTs operations, etc. However, the similarities between the two GAC runs at the pilot to the CD based RSSCT results suggest a similar mass transfer zone (MTZ) adsorption between these two columns. Figure 4.10 suggests that CD-RSSCT to pilot columns agreement is slightly better for GAC2(Norit) than GAC1(Calgon), with visibly lesser

deviation. Whereas in general, the GAC1(Calgon) CD-RSSCT shows a slight overprediction of the breakthrough.

Figure 4.10 Total PFAS effluent concentration (C) for Tempe GW, pilot, and RSSCTs with CD and PD scaling relationship for GAC 1, GAC 2, and IX as a function of bed volumes.

Figure 4.11 PFBS(A), PFHpA (B), PFHxS (C), PFHxA (D), PFOS(E) and PFOA(F) effluent concentrations (C) for Tempe GW pilot and RSSCTs with CD and PD scaling relationship for GAC 1 as a function of BVs.

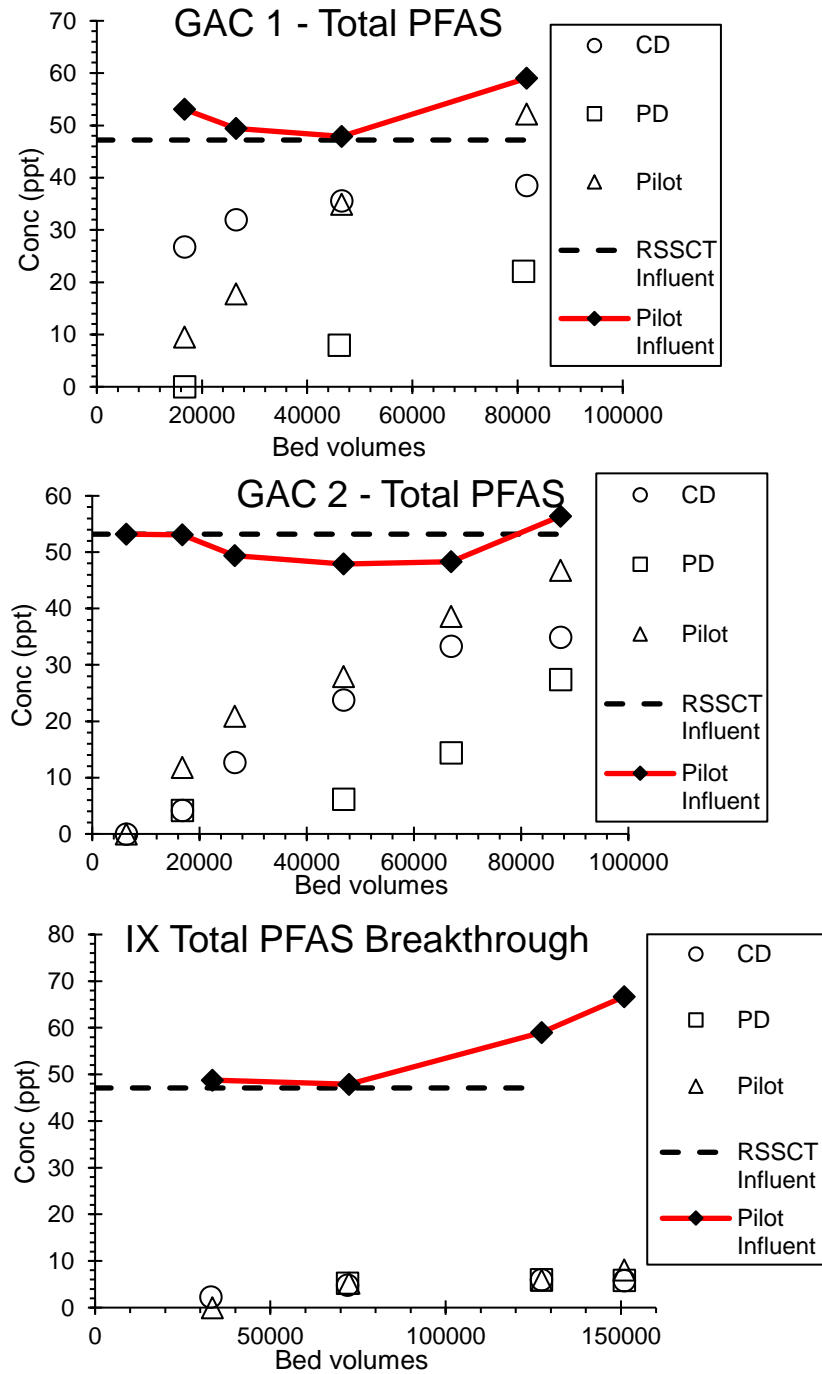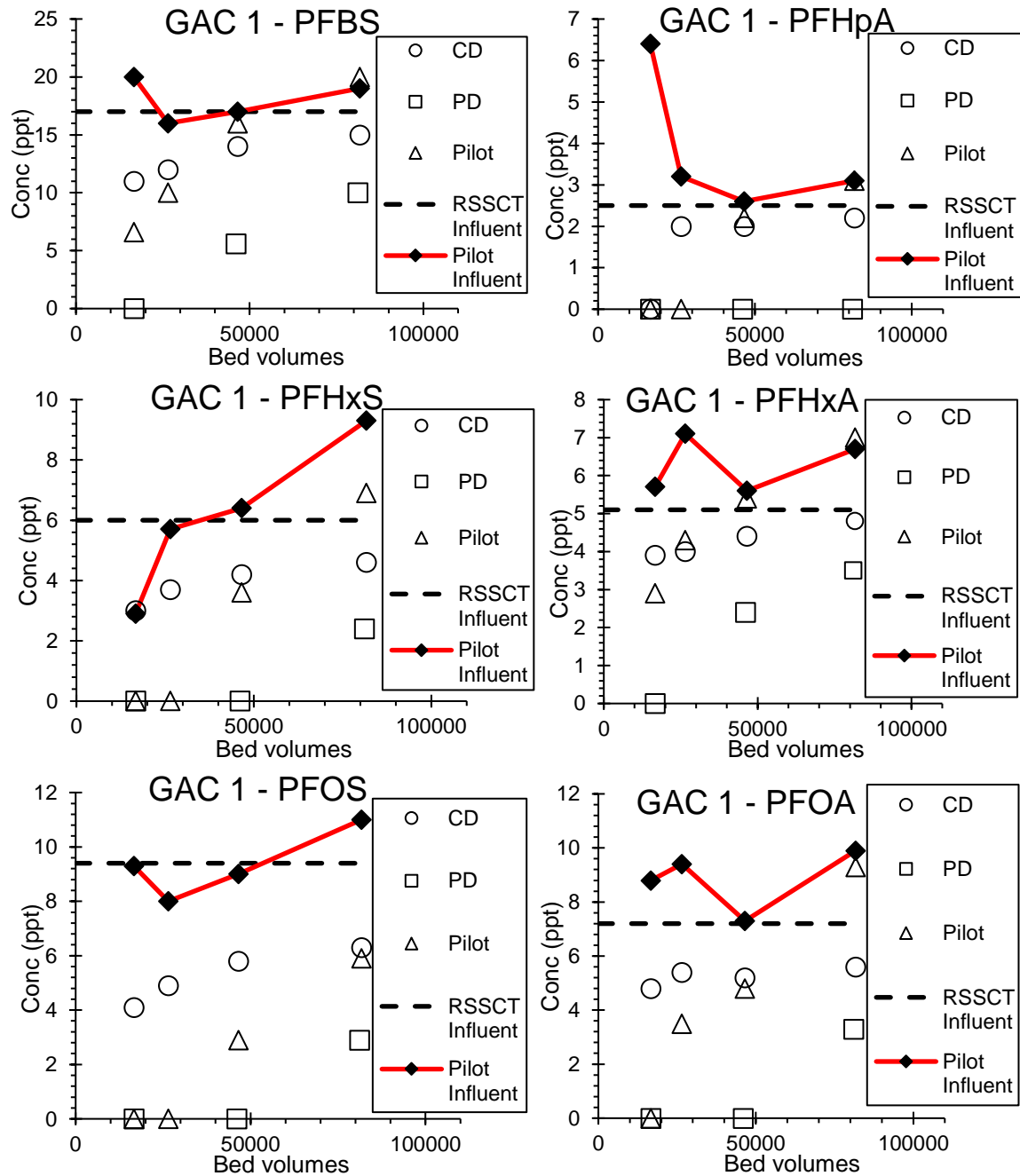**Figure 4.12** PFBS(A), PFHpA (B), PFHxS (C), PFHxA (D), PFOS(E) and PFOA(F) effluent concentrations (C) for Tempe GW pilot and RSSCTs with CD and PD scaling relationship for GAC 2 as a function of BVs.
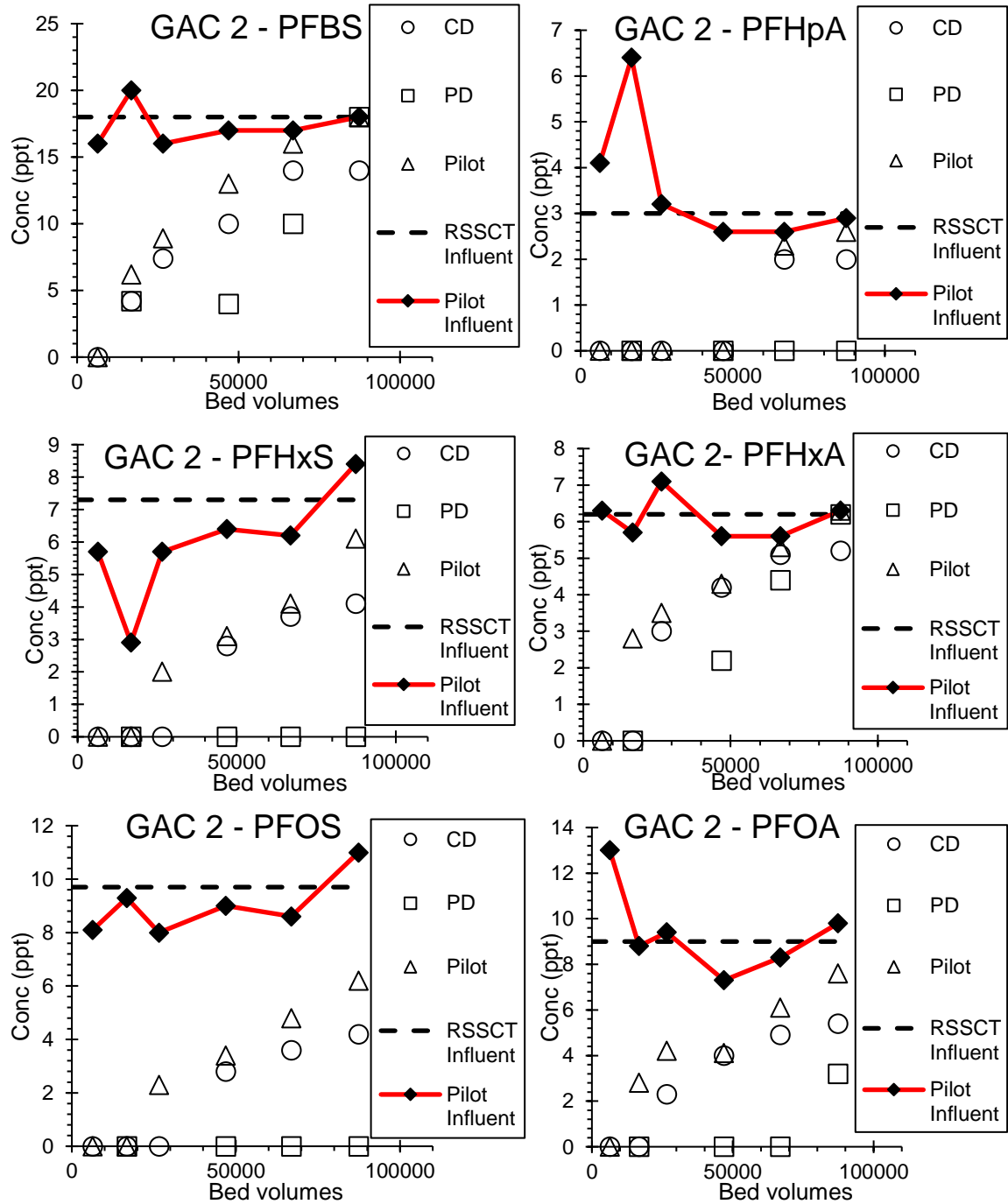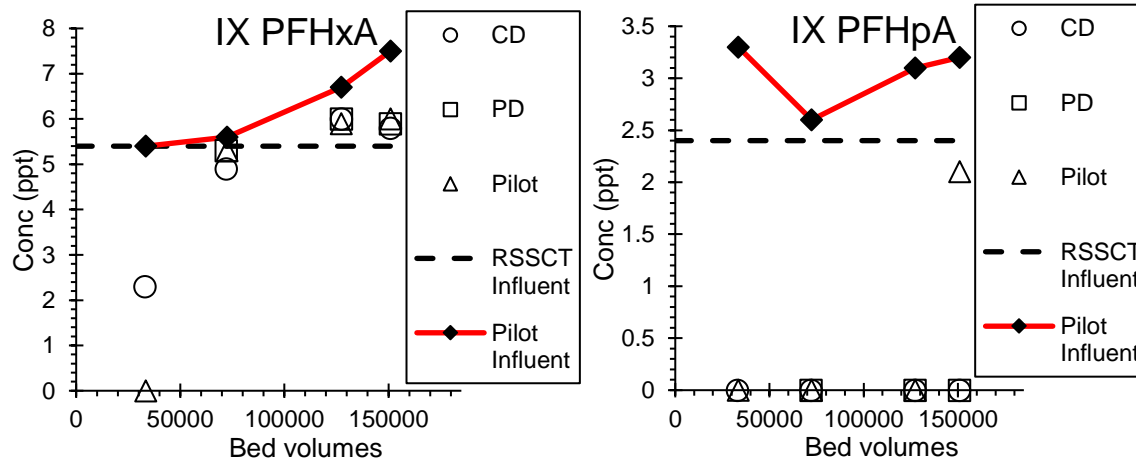
Figure 4.13 PFHxA(A) and PFHpA(F) effluent breakthrough concentrations(C) for Tempe GW pilot and RSSCTs with CD and PD scaling relationship for IX, as a function of BVs, treated.

Similarly, Figure 4.10 shows the IX results for the pilot columns against RSSCT based on CD, and PD design. All the columns (pilot, CD, and PD-RSSCT) show similar total PFAS (concentration) breakthrough, occurring at the same time for the entire run. Since the pilot, CD, and PD-RSSCTs, all show only minimal (<15%) breakthrough of PFAS compounds and makes it difficult to select the best RSSCT design (i.e., CD vs. PD) to simulate the pilot column for PFAS.

Figure 4.12 and 4.13 shows the breakthrough curves for individual PFAS compounds for GAC1(Calgon) and GAC2(Norit). In general, for all the compounds, it shows CD based RSSCT matches the pilot breakthrough more closely than PD. On the other hand, the PD based RSSCT design shows much slower or no breakthrough at all. The slight difference between CD-RSSCT to pilot columns could be due to varying influent (PFAS) concentration at the wellsite. Figure 4.11, 4.12, and 4.13, shows a gradual increase of PFAS compounds in the effluent at later stages of the pilot column runs. This rise in effluent concentrations could be due to an increase in influent (PFAS) concentration for both GAC1(Calgon) and GAC2(Norit) during later stages of testing.

51

Overall, CD based RSSCT matches the pilot breakthrough shape and concentrations of total PFAS and individual PFAS compounds more closely for GACs as compared to PD based RSSCT. Unlike pilot, the RSSCTs have stable, non- fluctuating feed water, which may not be the case for pilot or full-scale plants, where the water quality is dynamic (varies). Similarly, Figure 4.13 shows RSSCT based on CD and PD design for the IX resin matches the PFHxA breakthrough closely to the pilot columns. This is observed as all the three columns (CD, PD, and pilot), have a complete breakthrough (>100%) of this compound. However, the CD based RSSCT seems to conservatively predict the PFHxA breakthrough, as shown in Figure 4.13 where the CD breakthrough occurs before the pilot column. Moreover, the PFHpA breakthrough occurred only at the pilot columns. Therefore, it is difficult to assess the appropriate RSSCT fit for IX resins.

4.4.2 Comparing Fractional PFAS Concentration Breakthrough Between RSSCTs and Pilot Columns

Figure 4.14 shows the normalized (C/C_0) total PFAS breakthrough curves for the RSSCTs and the pilot columns for GAC1(Calgon), GAC2(Norit), and IX(Purolite). Since there is a difference in influent concentrations for pilot and RSSCT columns and a relative abundance of each PFAS compound, these normalized breakthrough curves provide a more explicit comparison between these two scales (i.e., RSSCT and pilot).

Figure 4.14 shows that for GACs, the CD based RSSCT design simulates the pilot column breakthrough better as compared to the PD based design, which is evident from the closeness of CD data to the pilot. Figure 4.14 also illustrates that the PD has the total PFAS breaking through much later in comparison to the CD and pilot-scale column results, for the GAC2(Norit). Similar conclusions could also be drawn for the GAC1(Calgon),

where the CD based design is slightly more conservative than the pilot-scale column results.

Figure 4.14 Total PFAS breakthrough curves for Tempe GW Pilot and RSSCTs with CD and PD scaling relationship for GAC 1, GAC 2, and IX as a function of BVs treated with effluent concentration (C) normalized to influent concentration (C_o) as shown in Table 4.1.

Figure 4.15 PFBS(A), PFHpA (B), PFHxS (C), PFHxA (D), PFOS(E) and PFOA(F) breakthrough curves for Tempe GW Pilot and RSSCTs with CD and PD scaling relationship for GAC 1 (Calgon F400) as a function of BVs treated with effluent concentration (C) normalized to influent concentration (C_o) as shown in Table 4.1.

Figure 4.16 PFBS(A), PFHpA (B), PFHxS (C), PFHxA (D), PFOS(E) and PFOA(F) breakthrough curves for Tempe GW pilot and RSSCTs with CD and PD scaling relationship for GAC 2 as a function of BVs treated with effluent concentration (C) normalized to influent concentration (C_o) as shown in Table 4.1.
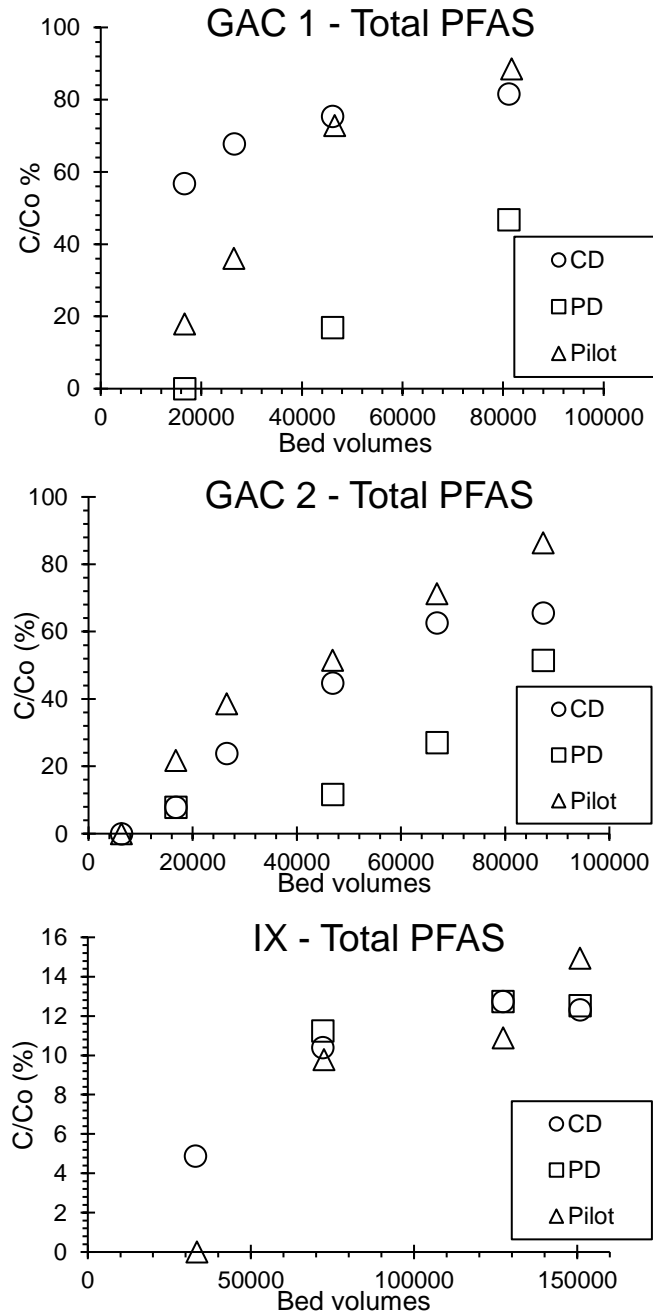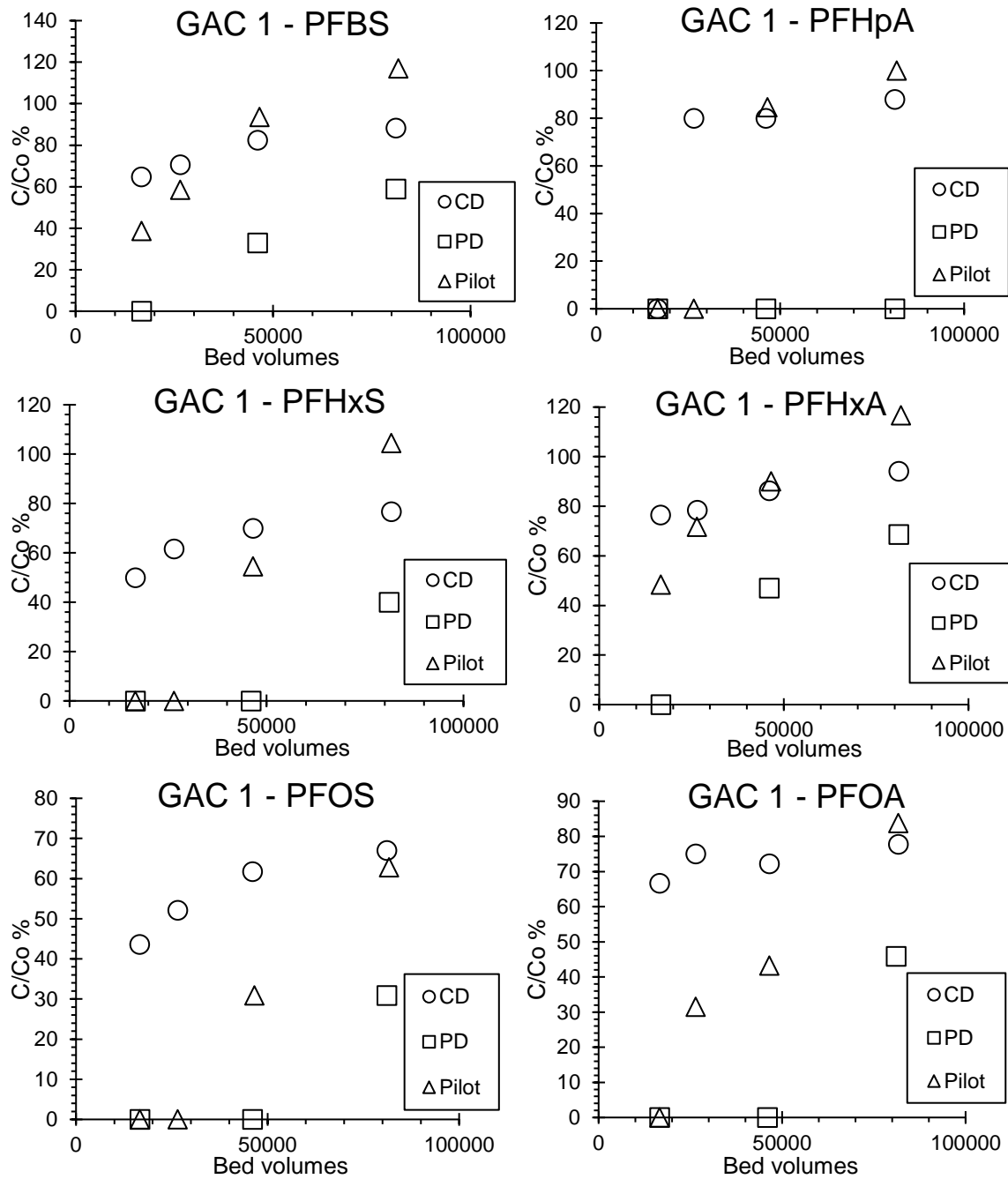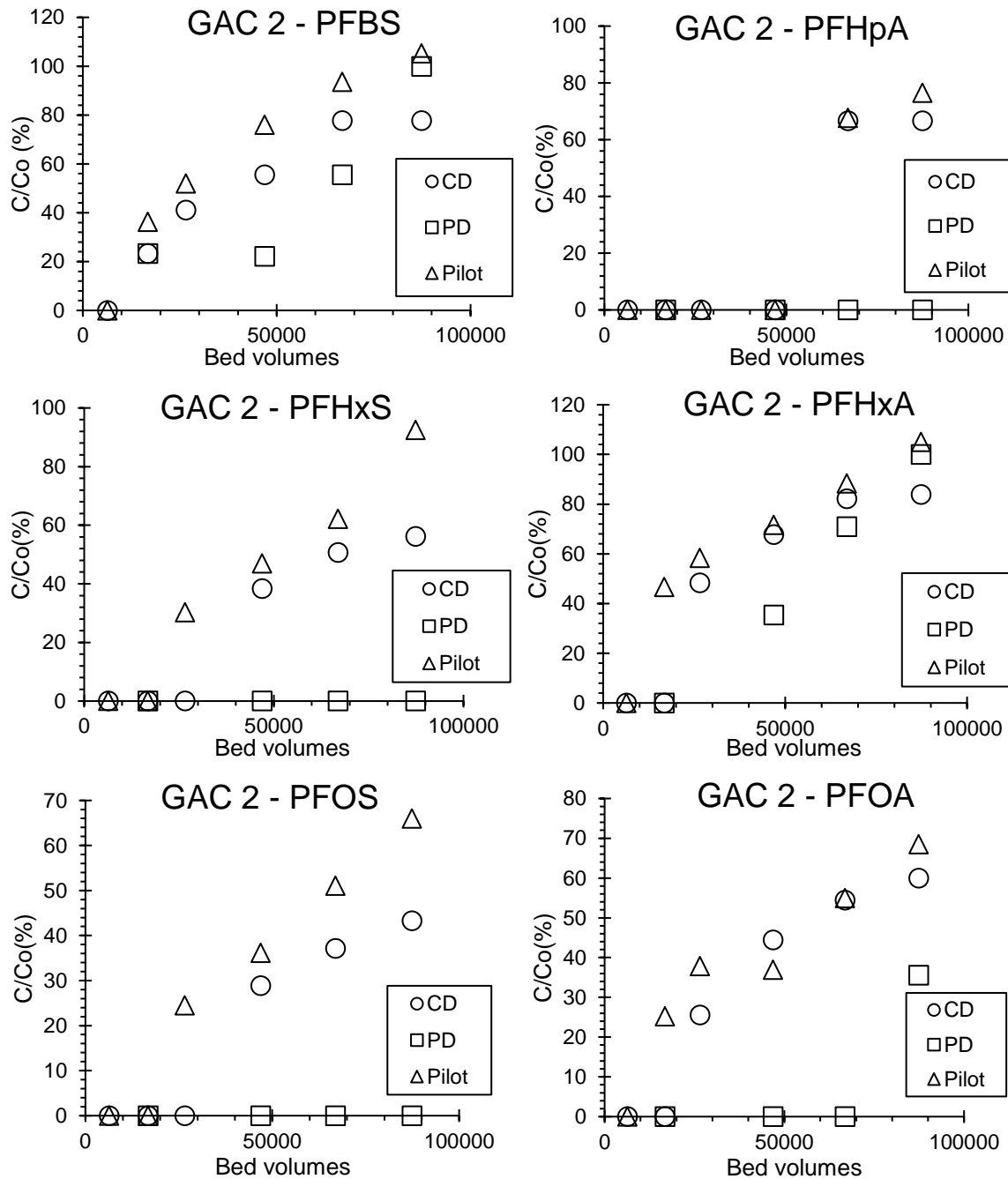
55
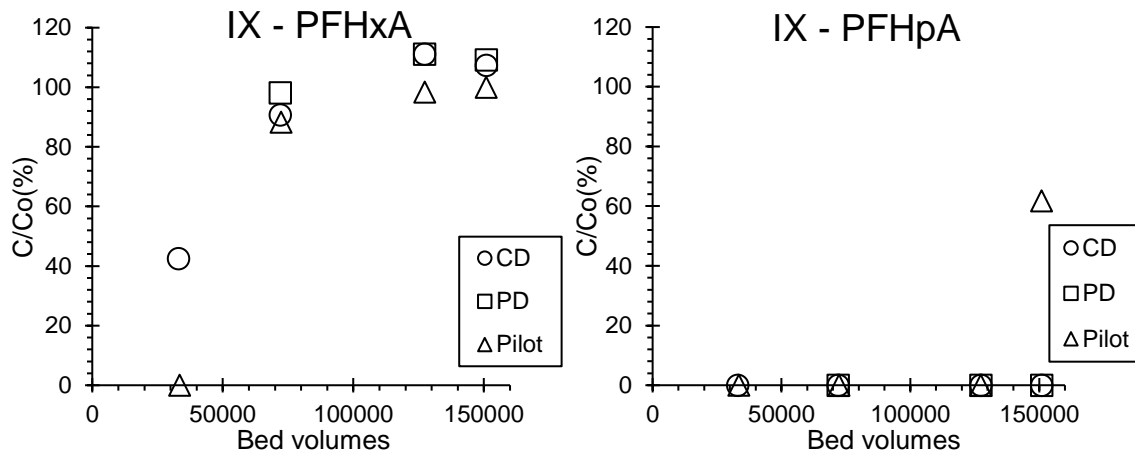
Figure 4.17 PFHxA(A) and PFHpA(B) breakthrough curves for Tempe GW pilot and RSSCTs with CD and PD scaling relationship for IX as a function of BVs treated with effluent concentration (C) normalized to influent concentration (C_o) as shown in Table 4.1.

Figure 4.15 and Figure 4.16 compares the CD and PD based RSSCT results to the pilot columns for all detected PFAS compounds for GACs. These results show that the short-chain PFBS breaks through almost completely (>85%) for all the three columns and within 100,000 BVs. On the other hand, the longer chain PFOS had only a 40% to 65% breakthrough based on both CD as well as the pilot at the end of the column runs.

Similar trends were observed for the PFHxA and PFOA breakthrough curves for both GAC2(Norit) and GAC1(Calgon). When PFOS and PFOA breakthrough curves are compared, the CD based RSSCT design results follow the similar breakthrough shape of the pilot-columns in general. However, the PD based design only shows breakthrough at the end of column testing at 82,000 BVs for GAC1(Calgon) and 87,000 BVs for GAC2(Norit), respectively. For GAC2 (Norit), the PD-RSSCT does not show any breakthrough for PFOS.

Therefore, the CD based design matches the pilot columns more closely across the different carbon chain lengths and functional groups than to the PD based methods for the GACs, which is visible from closer fitting of data points of CD-RSSCT to pilot.

Figure 4.17 shows the IX column results. It shows a complete breakthrough in PFHxA in all columns (pilot, CD, and PD-RSSCTs). This figure shows among all the PFAS compounds, only PFHxA and PFHpA broke through during this five-month-long pilot-scale study. Both RSSCTs based on CD and PD designs did not show breakthrough other than PFHxA. Due to the shorter duration (5 months) in column operation, especially for IX, a complete breakthrough could not be achieved. Thus, it is difficult to determine if the CD or the PD design would be appropriate for RSSCT to simulate the IX pilot column.

4.4.3 Comparing Adsorption Capacity of Adsorbents Between RSSCT and Pilot Columns

Figures 4.18-4.20 show different PFAS compounds adsorption capacity of GAC1(Calgon), GAC2(Norit), and IX(Purolite), RSSCT vs. pilot plotted at equal bed volumes, along with linear regression equation. The regression equation is of form $y = mx + c$. Therefore, for RSSCT to ideally fit the pilot results, slope (m) should be 1, and intercept (c) should be zero.

Figure 4.18 and 4.20 shows regression coefficients between pilot and CD-RSSCTs GACs at equal BVs for GAC1(Calgon), GAC2(Norit), and IX(Purolite). The adsorption capacity is calculated, as described in section 4.1.3. Figures 4.18-4.20 show, adsorbate loading (or capacity, i.e., the amount of adsorbate adsorbed per unit mass of adsorbent) between RSSCT (CD and PD) and pilot, and among the RSSCTs (CD vs. PD) for each adsorbent type (i.e., GACs and IX)

Figure 4.18 PFBS(A), PFHpA (B), PFHxS (C), PFHxA (D), PFOS(E) and PFOA(F), solid-phase loading (μg PFAS/g GAC) CD RSSCTs vs. pilot columns for GAC 1, GAC 2 and IX for Tempe GW at equal BVs.
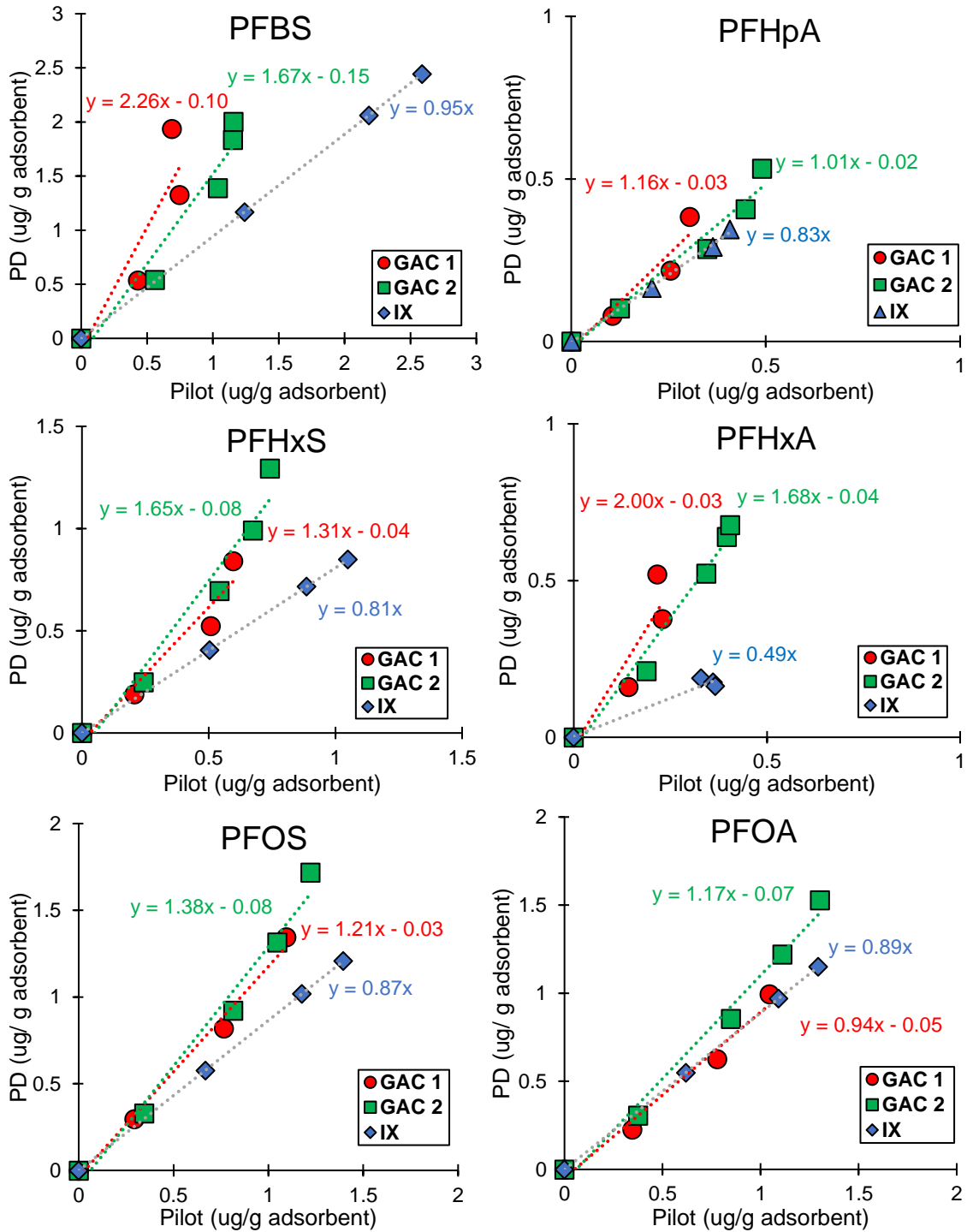
Figure 4.19 PFBS(A), PFHpA (B), PFHxS (C), PFHxA (D), PFOS(E) and PFOA(F), solid-phase loading (μg PFAS/g GAC) PD RSSCTs vs. pilot columns for GAC 1, GAC 2 and IX for Tempe GW at equal BVs.

Figure 4.20 Total PFAS solid-phase loading (μg PFAS/g GAC) comparison (A) CD vs. pilot (B) PD vs, pilot and (C) PD vs. CD columns, for GAC 1, GAC 2 and IX for Tempe GW at equal BVs.
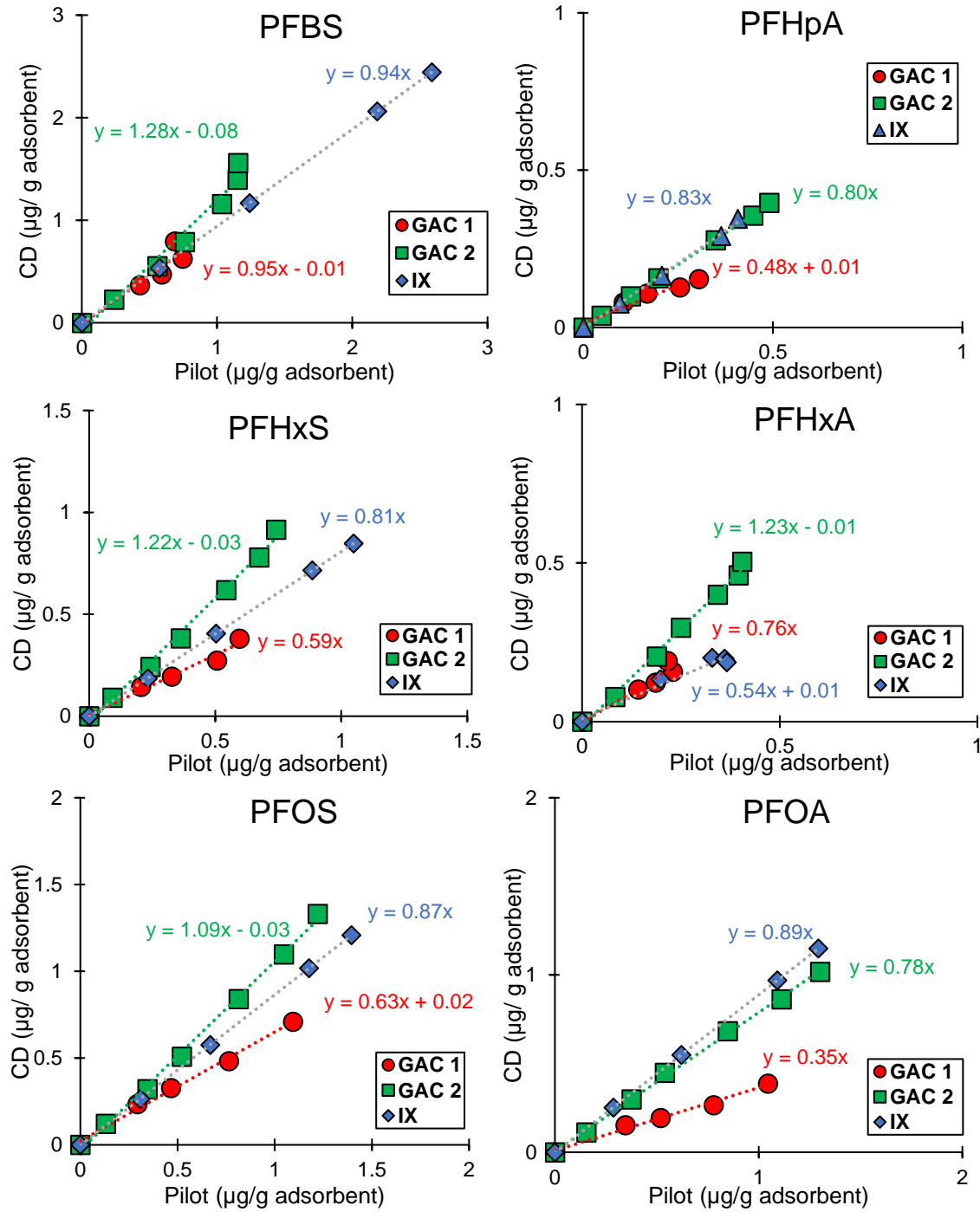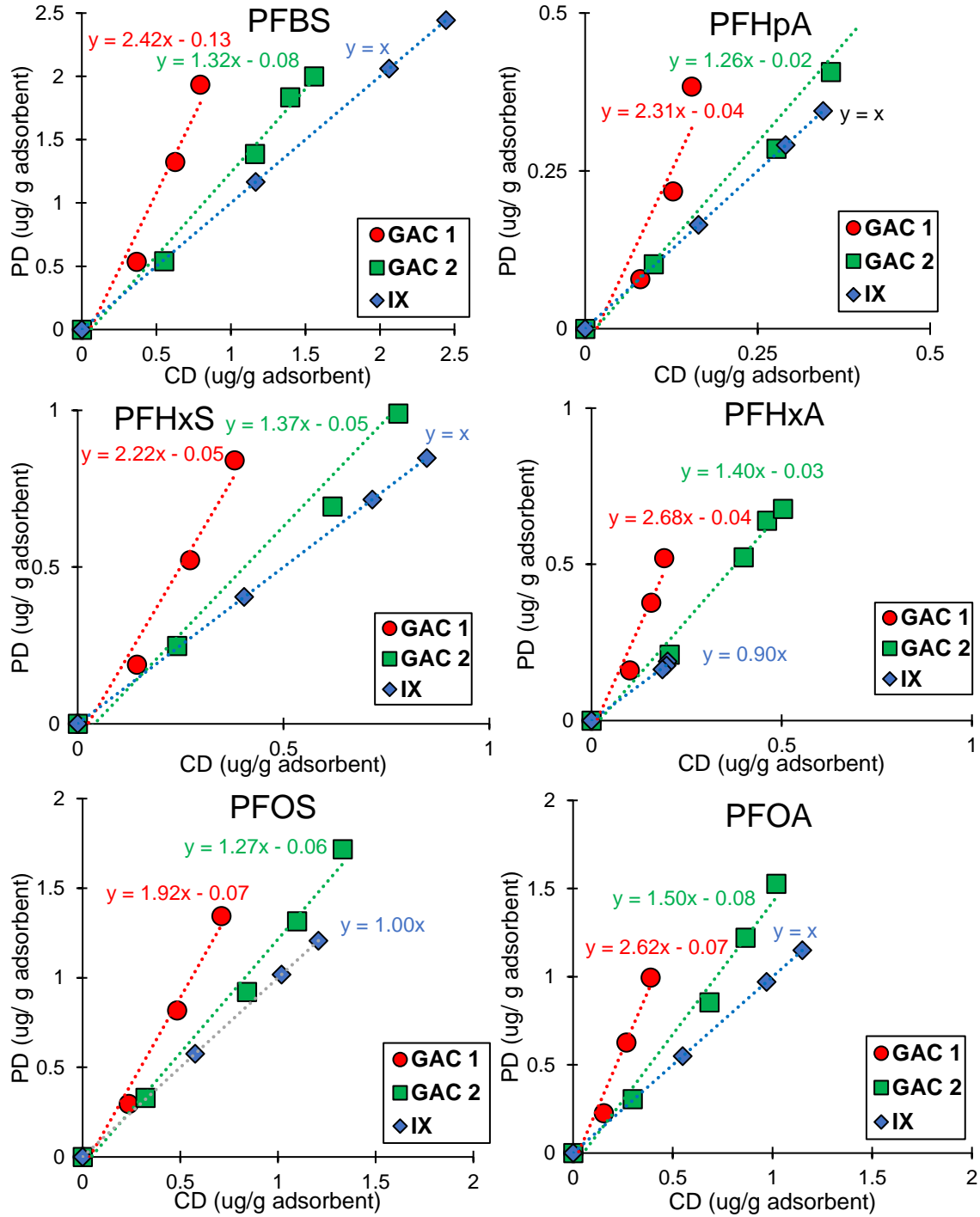
Figure 4.21 PFBS(A), PFHpA (B), PFHxS (C), PFHxA (D), PFOS(E) and PFOA(F), solid-phase loading (µg PFAS/g GAC) CD RSSCTs vs. pilot columns for GAC 1, GAC 2 and IX for Tempe GW at equal BVs.
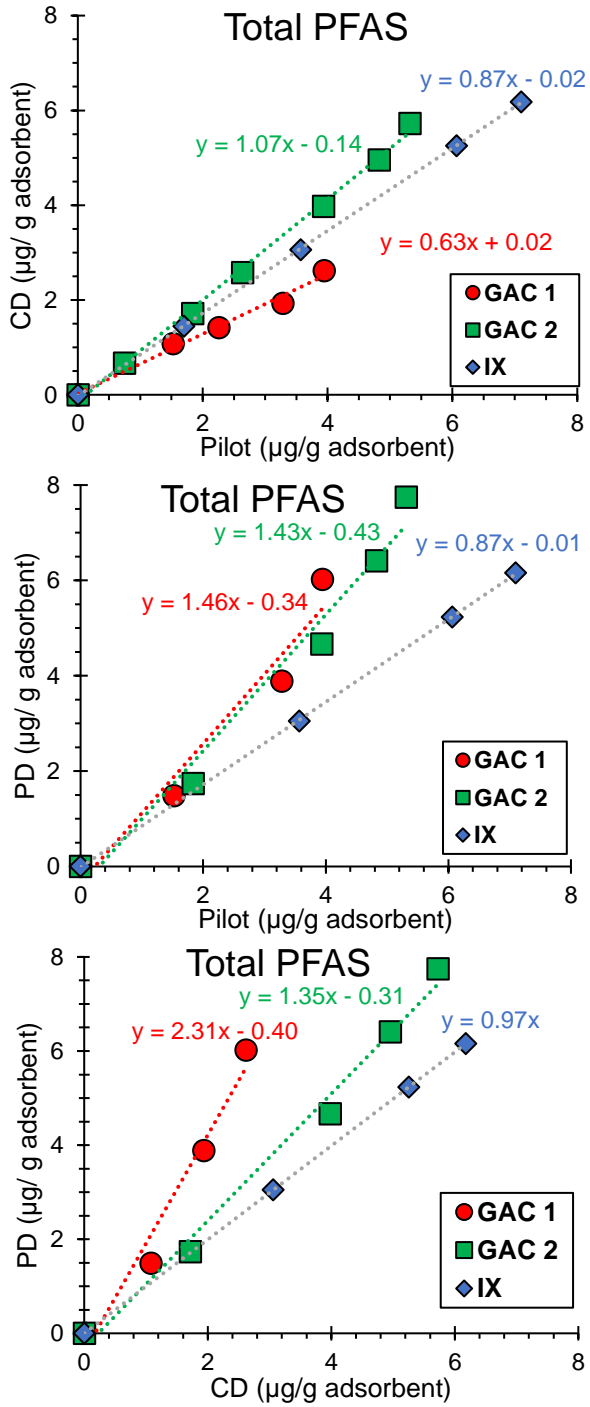
61

From Figure 4.18 and 4.20 for GACs adsorption capacity, the slope is generally less than 1 for GAC1 and close to 1 for GAC2, for all the PFAS compounds at equal BVs. On the other hand, from Figure 4.19, for pilot and PD-RSSCTs, the slope is greater than 1 for both the GACs. Since PD-RSSCTs are yet to achieve a complete breakthrough, the slope would increase at a complete breakthrough. Ideally, the slope would be 1 if RSSCTs perfectly simulate the pilot.

However, it is practically impossible for RSSCTs to perfectly simulate pilot due to the dynamic nature of water at the pilot-scale, where water quality varies with other operational challenges (pilot and RSSCTs). Therefore, from the point of design consideration, it is good to have the slope close to 1 or lesser than 1. Slope lesser than 1 is preferred because it would mean RSSCT is under predicting the adsorbent capacity, and thus full-scale systems designed based on this would be "conservative."

Furthermore, from Figure 4.21, the slope between PD and CD is always greater than 1 for all the PFAS compounds, emphasizing the overprediction of adsorbent capacity by PD as compared to CD. Therefore, the predicted sorbent replacement costs would be higher for systems designed based on CD-RSSCT as compared to PD-RSSCTs and would represent the higher side of the operational cost. However, from an engineering perspective, the system would be able to handle circumstances such as a momentary spike in influent PFAS concentrations (varying nature of the feed, in full-scale systems) in feed water without exceeding the treatment goals. For IX, all three slopes (*CD/Pilot, PD/Pilot, and CD/PD*) were nearly 1, which suggests similar adsorption capacity between all the three columns.

Therefore, it could be concluded from the above breakthrough and adsorbent capacity comparison results that, the CD based RSSCTs design seems to simulate the breakthrough shape and adsorption capacity of the pilot columns better for both GACs, for low organics (DOC < 1.5mg/L), PFAS impacted groundwater. Even though there are similarities in the IX pilot and RSSCT column in terms of performance, longer column run is necessary to determine the appropriate RSSCT method in simulating the pilot columns.

4.4.4 Statistical Comparison of Breakthrough Curves Between RSSCTs and Pilot Columns for GAC2(Norit)

Statistical tests were performed to compare breakthrough curves between pilot and RSSCTs (CD and PD), for GAC2(Norit). GAC2(Norit) was selected for comparison owing to the highest number of data points available to compare (CD(n=6), PD(n=4)) among all the media. Both Non-Parametric (Kulmugurov-Smirnov 2 Sample (K-S)) test and Parametric (Paired Student's- t-test) tests were performed to compare the adsorption capacity of both CD and PD to pilot for different PFAs compounds.

K-S is a nonparametric test (assumption of the normal distribution of the sample is not required). As shown in Figure 4.22, K-S 2 sample test compares the empirical cumulative distribution function of two sample groups and calculates the maximum difference between them. The K-S statistic is the maximum absolute difference in empirical CDF between the two sample groups. $D_{critical}$ value is calculated using Equation 7 (Young 1977). The significance level used in the K-S test is 0.05, i.e., 95% confidence level. If the K-S statistic calculated between the two data groups is higher than the $D_{critical}$ value, the data groups are statistically significant from each other. Therefore, the K-S statistic

between pilot and RSSCT (CD or PD) breakthrough data higher than $D_{critical}$ value would infer that they are statistically different.

$$D_{critical} = 1.368\sqrt{\frac{1}{a} + \frac{1}{b}} \tag{7}$$

where a and b are sample sizes of the two data groups being compared, respectively. Figure 4.23 shows the CD and PD RSSCT's $D_{critical}$ value for all the PFAS compounds along with respective $D_{critical}$ values. Figure 4.23 clearly shows that for all PFAS compounds, K-S statistic of both CD and PD are lesser than respective $D_{critical}$ values. Thus, both CD and PD breakthroughs are statistically similar to the pilot. Therefore, K-S two-sample test failed to distinguish between CD and PD.
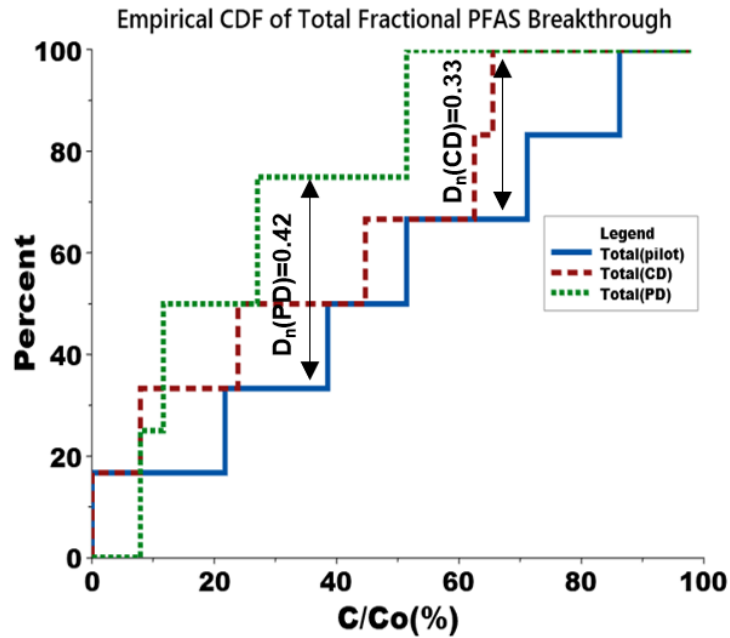
Figure 4.22 Empirical CDF plot of Total PFAS breakthrough curves of pilot, CD-RSSCT and PD-RSSCT for GAC2(Norit).
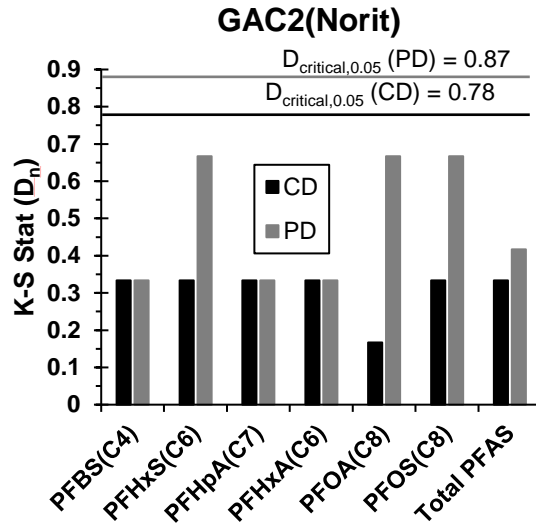
Figure 4.23 K-S Statistic value of CD and PD for all detected PFAS compounds in the feed with respective $D_{critical}$ values.

The student's *t*-test is a parametric test (assumes that data is normally distributed). To compare two breakthrough curves using Student *t*-test, fractional breakthrough data of pilot and RSSCT are treated as paired data. A paired sample *t*-test was conducted in Excel, with a confidence interval of 0.95. If the p-value calculated was greater than 0.05, then data groups compared were statistically similar.

Figure 4.24 shows the Student's t-test p-value of CD and PD with the pilot for all the PFAS compounds. Figure 4.24 illustrates that PD is statistically similar to the pilot for more compounds (PFBS, PFHxS, PFHpA, PFHxA, PFOS) than CD (PFHxS, PFHpA, PFHxA, and PFOA). Despite CD matching the breakthrough shape and visibly a better fit between CD and pilot breakthrough data, the t-test fails to distinguish between CD and PD. For instance, PD is tested statistically similar to the pilot for PFOS despite having no breakthrough in PD. Therefore, the student's t-test failed to distinguish between CD and PD as well.
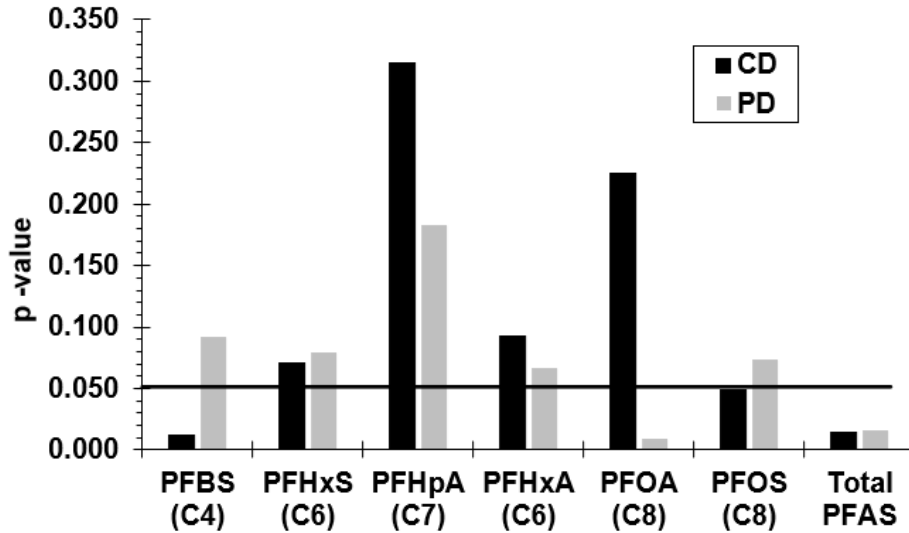
Figure 4.24 Student's *t*-test p-value of CD and PD for all detected PFAS compounds in the feed, the horizontal line represents p-value 0f 0.05.

Both K-S 2 sample test and Student's *t*-test failed to distinguish between the RSSCT models and the pilot most likely due to very few data points available for testing. Statistical tests show false-positive results for a small sample size (Forstmeier, Wagenmakers, and Parker 2017), which could have caused PD breakthroughs to be statistically similar to the pilot.

CHAPTER 5

AWWA PAPER: REMOVING PER- AND POLYFLUOROALKYL SUBSTANCES FROM GROUNDWATERS USING ACTIVATED CARBON AND ION EXCHANGE RESIN PACKED COLUMNS

[Text from: Chao Zeng, Ariel Atkinson, Naushita Sharma, Harsh Ashani, Annika Hjelmstad, **Krishishvar Venkatesh**, Paul Westerhoff. Removing per- and polyfluoroalkyl substances from groundwaters using activated carbon and ion exchange resin packed columns. *AWWA Water Science*, 2020, DOI: 10.1002/aws2.1172. I was involved in over 60% of the experiments in this published work (Zeng et al. 2020). The main objective of this Chapter is to document the trends in PFAS removal by GAC and IX based upon chain length and functional head-group moieties.

5.1 Abstract

Human exposure to per- and polyfluoroalkyl substances (PFAS) in drinking water is of growing concern due to increasing reports of occurrence and potential regulation. Adsorption of PFAS by granular activated carbon (GAC) or ion exchange (IX) resin is a suitable treatment technique. However, few studies compare PFAS removal in continuous flow GAC or IX adsorption systems using real drinking water sources. Herein, rapid small-scale column tests (RSSCTs) were used to investigate the effects of PFAS type and chain length on adsorption by GAC and IX resin for six groundwaters used as drinking water supplies. Seven PFAS substances with chain lengths of C4-C9 were detected in the groundwaters with the sum of their concentrations (ΣPFAS) ranging from 156 to 7044 ng/L. Adsorption capacities ($q_{\Sigma PFAS}$) were calculated to compare the removal capacity

among different sorbents. $q_{\Sigma PFAS}$ values ranged from 10.3 to 228 ng PFAS/mg sorbent after about 100,000 bed volumes treated. Coal-based GACs had higher adsorption capacity compared with coconut shell-based GAC, which was likely due to higher mesopore and macropore volumes. IX resins performed better than GAC in removing PFAS, but they were not effective in treating short-chain perfluorocarboxylic acids (PFCAs). Perfluorosulfonic acids (PFSAs) broke through later than PFCAs with the same chain length. Within PFSA or PFCA classes, shorter-chain PFAS species always broke through before longer-chain PFAS. Statistical analysis demonstrated that PFAS with higher hydrophobicity and molecular weight are more amenable to GAC adsorption. Empirical models were developed and predicted PFAS breakthrough. By quantifying PFAS selectivity and removal efficiency, this work provides benchmark data for commercially available treatment technologies and guidance towards specific PFAS classes where new treatment technologies may be most beneficial.

5.2 Introduction

Per- and polyfluoroalkyl substances (PFAS) are a group of man-made chemicals that have been used in industrial processes and consumer products, including surfactants, surface-protecting agents, and processing aids to produce polymers. They have been detected ubiquitously in the aquatic environment (Gawor et al. 2014; Rankin et al. 2016), biota, and humans (Ahrens and Bundschuh 2014; Vestergren and Cousins 2009). Human exposure to PFAS through consuming impacted drinking water is of growing adverse health concern (Emmett et al. 2006; Hurley et al. 2016). As such, many communities across the United States of America (USA) are, or will be, pursuing treatment techniques to remove PFAS from groundwaters serving as potable water supplies.

Perfluorooctanesulfonic acid (PFOS) and perfluorooctanoic acid (PFOA) are two dominant PFAS that occur in source waters. Their minimum reporting levels (MRLs) were 20 ng/L PFOA and 40 ng/L PFOS in USEPA's third Unregulated Contaminant Monitoring Rule (UCMR3) (USEPA 2017). There are hundreds of PFOA or PFOS alternatives, precursors, residuals, and transformation products (Wang et al. 2017). Due to recent regulations and restrictions on the use of long-chain PFAS (C8-C14), manufacturers shifted to short-chain alternatives (C4-C7) (Hu et al. 2016). Short-chain PFAS such as perfluorobutanoic acid (PFBS), perfluorohexanoic acid (PFHxA), perfluorohexanesulfonic acid (PFHxS), and perfluoropentanoic acid (PFPeA) have also been detected frequently in source waters (Appleman et al. 2014; Ateia et al. 2019; Hu et al. 2016; Oyetade et al. 2018). Appleman and coworkers (Appleman et al. 2014) investigated the occurrence of 23 PFAS in raw and treated waters from 20 utilities in the USA and found PFOS, PFHxA, and

PFHxS were the three most commonly occurring PFAS. Many other drinking waters related to PFAS occurrence studies are underway.

Adsorption using granular activated carbon (GAC) or ion exchange (IX) resin is emerging through research (Meng et al. 2014; Yang et al. 2018; Yu et al. 2009; Zhi and Liu 2015; 2016) and as commercially-available best available treatments for PFAS that many groundwater utilities are considering, or have recently installed. Carbon chain length and functional groups are important factors controlling PFAS adsorption; longer-chain PFAS are generally more amenable to GAC and IX resin adsorption than the shorter-chain PFAS, and perfluorosulfonic acid (PFSAs) normally have higher adsorption capacity and selectivity than perfluorinated carboxylic acids (PFCAs) (McCleaf et al. 2017; Rostvall et al. 2018; Xiao et al. 2017; Zaggia et al. 2016). Existing research focuses on treating PFOA and PFOS (Meng et al. 2014; Yang et al. 2018; Yu et al. 2009; Zhi and Liu 2016; 2015), often using model waters spiked with one or more PFAS compounds at equal concentrations, commonly at higher concentrations than detected in groundwaters used as drinking water supplies. Only a few comparative PFAS removal studies exist in continuous-flow adsorption systems in real groundwaters with ambient PFAS concentrations and ratios (Liu, Werner, and Bellona 2019; Patterson et al. 2019; Schaefer et al. 2019; Woodard, Berry, and Newman 2017; Xiao et al. 2017; Zaggia et al. 2016). This study aimed to quantify the ambient PFAS occurrence in six drinking water supplies and then determine the influence of type and chain length on PFAS removal using GAC and IX resin in continuous-flow packed beds. The groundwaters were drinking water supplies until PFAS were detected, when the wells were taken off-line until treatment could be installed. Rapid small scale column tests (RSSCTs) were performed, and the effects of

groundwater composition and ambient PFAS concentration/speciation was statistically correlated with adsorption capacity and PFAS breakthrough. By quantifying PFAS selectivity and removal efficiency, this work provides benchmark data for commercially-available treatment technologies and guidance towards specific classes of PFAS where new treatment technologies may be most beneficial.

5.3 Materials and Methods

5.3.1 Groundwater Sources

Water samples from six PFAS-impacted groundwaters (Arizona, USA) were collected in 2018-2019. The wells varied in capacity from 45 to >225 m^3/hr (198 to 991 gpm) and were previously used as drinking water supplies until PFAS was detected at which time they were taken off-line until treatment was installed. Wells were purged, and samples were collected in 55-gallon HDPE drums, transported to the laboratory, and used in experiments within 2 weeks. Water quality was monitored throughout the experiments and is summarized in Table S1.

5.3.2 Rapid Small Scale Column Test

RSSCTs are an approach using continuous-flow packed beds of adsorbent material that, through dimensionless analysis that considers both hydraulics and pollutant mass diffusion, can predict months to years of full-scale system performance. RSSCTs were operated for >25,000 to several hundred thousand bed volumes (BVs). Eighteen RSSCTs were conducted to simulate pilot columns. The loading rate was 15–24 m/h (6.0-10 gpm/ft^2), and empty bed contact time (*EBCT*) was 3.3 min for IX resin beds and 4.6 or 5.0 min for GAC beds. Constant diffusivity (CD) based scaling approach where liquid

diffusivity is assumed to be independent of particle radius. This approach is recommended for weakly polar, low molecular weight organics at trace concentrations when competition for sorption sites is limited (Crittenden et al. 1991; Cummings and Summers 1994). In addition, studies have demonstrated that a CD model is appropriate for PFAS in waters with low levels of organic carbon, such as the groundwaters used in this work (Schaefer et al. 2019). RSSCT details are presented in Tables S2 and S3. All the RSSCTs (except RSSCT-1) were operated in lead-lag configurations of two columns in series; this is a common system configuration for full-scale utilities that maximizes adsorption capacity prior to adsorbent change-out. Both lead- and lag-columns had the same BV, sorbent mass, and loading rate (i.e., $EBCT_{lead+lag} = 2 \times EBCT_{lead}$).

Commercial adsorbents were used in the RSSCTs: Filtrasorb 400 (Coal1) and Centaur 12×40 (Coal3) were purchased from Calgon Carbon Corporation; Norit GAC 400 (Coal2) and Hydrodarco 4000 (Coal4) were obtained from Cabot Corporation; AquaCarb 1230AWC (Coco1) and AquaCarb 1240CAT (Coco2) were from Evoqua Water Technologies; Purofine PFA694E IX resin (IX1) was from Purolite Corporation, and Dowex PSR-2 resin (IX2) was from Dow Chemical Company. Adsorbents were wet crushed using a mortar and pestle and sieved to achieve designed particle sizes. Then adsorbents were washed and wet packed into the columns. GAC properties (density, surface area, pore size distribution, elemental content, and surface charge) are provided in Tables S4-S7.

5.3.3 Analytical Methods

PFAS samples were collected in 250 mL HDPE bottles with 1.4 g tris hydrochloride and tris (hydroxymethyl) aminomethane as preservative (15.5: 1 w/w). The duration of sample collection was taken into consideration when calculating the BV for each sample. For example, for the column with a bed volume equals to 1 mL, the sampling process takes 250 BV. The value was calculated based on the mid-point between the start and the end BVs of sample collection. Samples were stored at 4 °C until analysis. 14 PFAS (list provided in *Supporting Information (Appendix A)*) were analyzed using EPA Method 537 by Eurofins Scientific at a (MDL) of 2.0 ng/L. For the samples with levels of PFAS compounds below MDL, their concentrations were considered as zero. Standard methods were employed to measure pH, conductivity, and dissolved organic carbon (DOC).
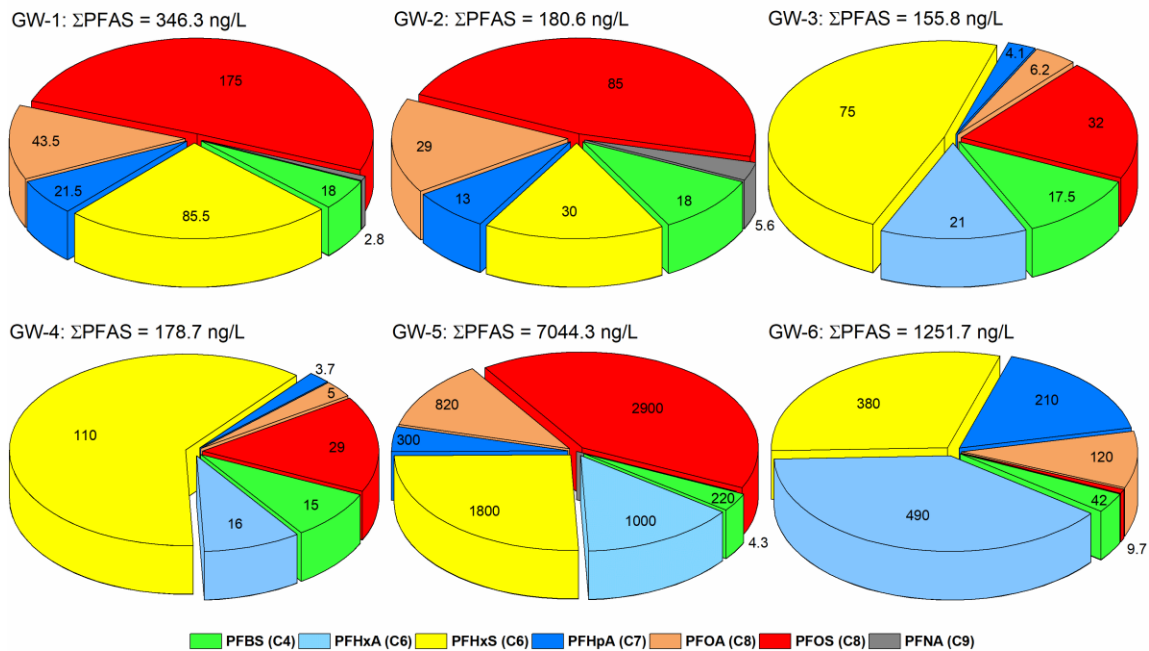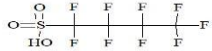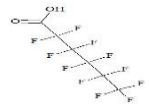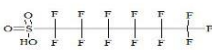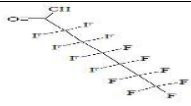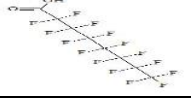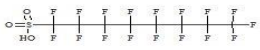
Figure 5.1 PFAS occurrence in the six groundwaters used in this study. The numbers in the pie charts show the concentrations of individual PFAS detected in the water

73

Table 5.1 Physicochemical properties of PFAS that vary substantially per species.

Chemical	Abbreviation	Formula	Chemical Structure	Molar mass	Log D[a] (pH=7.4)	Log Kow[b]
Perfluorobutanesulfonic acid	PFBS	$C_4HF_9O_3S$		300.01	0.25	1.82
Perfluorohexanoic acid	PFHxA	$C_6HF_{11}O_2$		314.05	0.18	3.48
Perfluorohexanesulfonic acid	PFHxS	$C_6HF_{13}O_3S$		400.11	1.65	3.16
Perfluoroheptanoic acid	PFHpA	$C_7HF_{13}O_2$		364.06	0.88	4.15
Perfluorooctanoic acid	PFOA	$C_8HF_{15}O_2$		414.07	1.58	4.81
Perfluorooctanesulfonic acid	PFOS	$C_8HF_{17}O_3S$		500.13	3.05	4.49
Perfluorononanoic acid	PFNA	$C_9HF_{17}O_2$		464.08	2.28	5.48

[a] ChemAxon [2014] MarvinSketch v 6.1.5.
[b] US EPA. [2019] Estimation Programs Interface Suite[TM] for Microsoft Windows, v 4.11. United States Environmental Protection Agency, Washington, DC, USA.

5.4 Results

5.4.1 PFAS Occurrence in Six Arizona Drinking Waters

Of the PFAS analyzed, seven that had with variable chain length (C#) and physico-chemical peroperties (Table 5.1) were detected in the groudwaters (Figure 5.1): PFBS (C4), PFHxA (C6), PFHxS (C6), perfluoroheptanoic acid (PFHpA) (C7), PFOA (C8), PFOS (C8), and perfluorononanoic acid (PFNA) (C9). The sum of concentrations for the seven detected PFAS (ΣPFAS) ranged from 156 to 7044 ng/L in the six drinking water supplies. Long-chain PFAS, including PFOS, were the predominant species in GW-1, GW-2, and GW-5, while higher concentrations of short-chain PFAS such as PFHxA and PFHxS were found in GW-3, GW-4, and GW-6. All seven PFAS were detected in GW-5; PFHxA was not detected in GW-1 and GW-2, and PFNA was below detection limit in GW-3, GW-4, and GW-6. The range in PFAS speciation and concentration, in conjunction with bulk water quality (DOC <1 mg/L, conductivity between 500 to 1000 µS/cm, and pH 7.5 to 8.5 (Table S1)), provide a range of real-world conditions typical for much of the southwestern USA.

5.4.2 RSSCT Breakthrough Curves For Combined PFAS Concentrations

Figure 5.2 compares ΣPFAS breakthrough in different groundwaters for two coal-based GACs. Typical S-shaped breakthrough curves were observed, with a lag period of BV treated with low or non-detectable PFAS concentrations before a gradual inrease in PFAS concentrations exiting the column (C) until plateauing near the influent PFAS concentration (C_0). This data implies the RSSCT captured the mass transfer zone within

the sorbent packed bed. Higher influent PFAS concentrations resulted in fewer BV treated prior to breakthrough. As shown in Figure 5.2, both GACs achieved effluent concentrations below the action limit of 70 ng/L (for PFOS+PFOA) after roughly 100,000 BVs for GW-1, GW-2, and GW-3. However, earlier breakthrough at only 40,000 BVs (to 70 ng/L level) occurred in GW-6. For reference, roughly 100,000 BV treated with a simulated EBCTs of ~5 minutes equates to one year of continous operation.
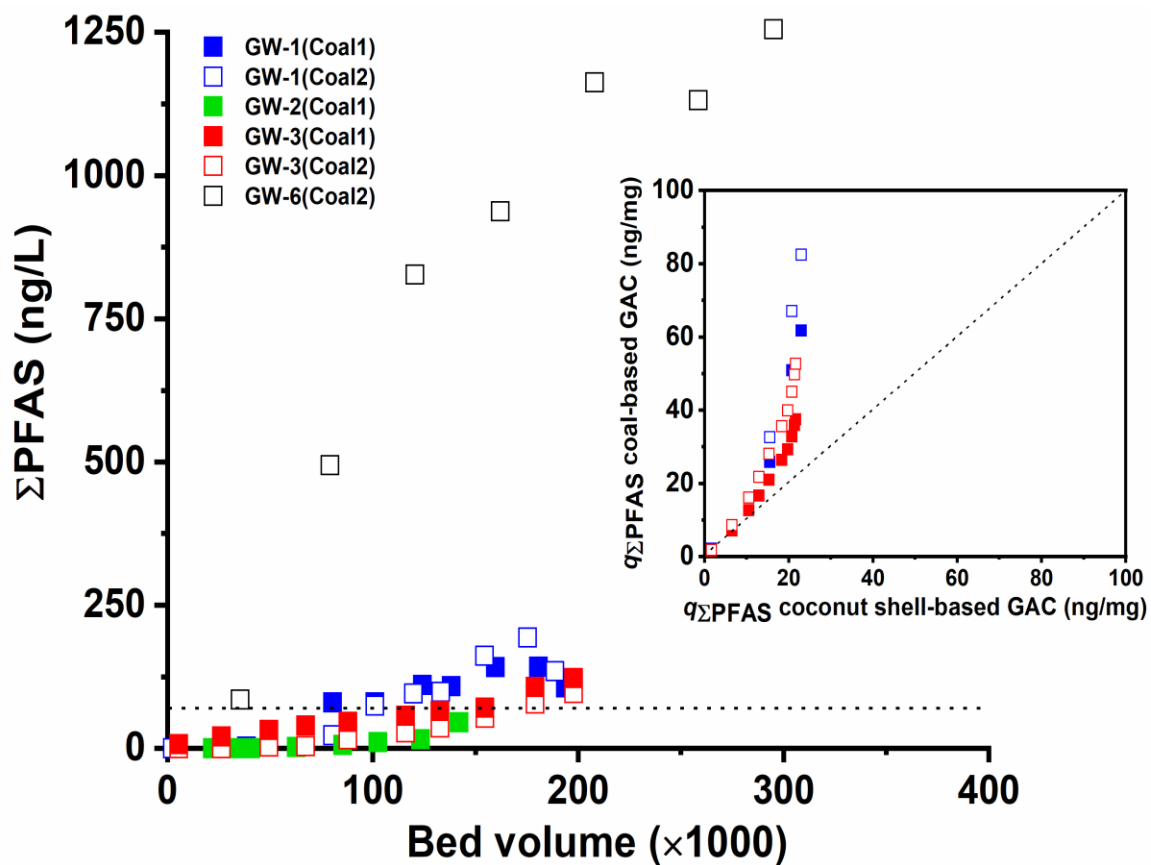
Figure 5.2 Breakthrough curve of ΣPFAS from Filtrasorb 400 (Coal1) and Norit 400 (Coal2) packed columns (Lead column) in treating GW-1 (C_0 = 346 ng/L), GW-2 (C_0 = 181 ng/L), GW-3 (C_0 = 156 ng/L), and GW-6 (C_0 = 1252 ng/L). The dotted line indicates 70 ng/L. Inset compares $q_{ΣPFAS}$ for coal- versus coconut shell-based GACs at 100,000 BV treated. AquaCarb 1230AWC (Coco1) was only used for GW-1; AquaCarb 1240CAT (Coco2) was only used for GW-3.
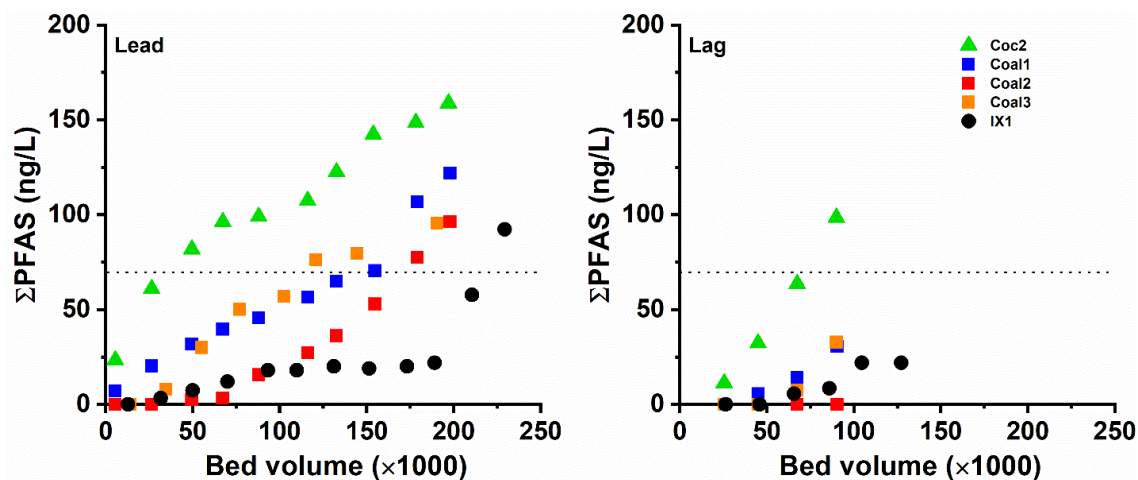
Figure 5.3 ΣPFAS breakthrough curves for RSSCT 7 to RSSCT 11 using GW-3. The dotted line indicates 70 ng/L.

Figure 5.3 shows the breakthrough curve for ΣPFAS in GW-3 with low PFAS concentration (ΣPFAS = 156 ng/L) and Figure 5.4 shows the breakthrough curve for ΣPFAS in GW-5 with high PFAS concentration (ΣPFAS = 7044 ng/L). All other breakthrough curves are provided in the Suppporting Information (Appendix A) (Figures S1-S4). Our results demonstrate that PFAS was adsorbed better by IX adsorbents than GAC, and coal-based GAC had higher adsorption capacity ($q_{ΣPFAS}$) compared with coconut shell-based GAC for the 6 groundwaters. $q_{ΣPFAS}$ was calculated using the integrated areas above the breakthrough curves and accounted for the volume of water treated and mass of adsorbent in the column. Calculated $q_{ΣPFAS}$ values (Table S2) ranged from 10.3 to 228 ng PFAS/mg sorbent after treating 100,000 BV. $q_{ΣPFAS}$ values were 3.6 times higher for Coal2 than Coco1 at 100,000 BV for GW-1 and 2.2 times higher for Coal2 than Coco2 at 200,000 BV for GW-3. As shown in Figure 5.2 (inset), $q_{ΣPFAS}$ were always higher for coal- than coconut shell-based GAC using all the data collected from GW-1 and GW-3.

IX resin columns treated more BVs before PFAS breakthrough than GAC columns treating the same groundwater. For example, 100% PFAS breakthrough from GW-6 was reached after about 500,000 BV in IX1, while breakthrough occurred at 200,000 and 300,000 BV for Coal4 and Coal2, respectively (Figure S4). However, due to their high density (~2x compared to GACs), the overall adsorption capacity ($q_{\Sigma PFAS}$) of IX resins is lower than coal-based GACs (Table S2).

The effect of potential competing adsorbates and EBCT on PFAS removal and capture of the mass transfer zone within the packed bed, was evaluated by comparing ΣPFAS breakthrough and the $q_{\Sigma PFAS}$ between *Lead* and *Lag* columns. As shown in Figure 5.3, 5.4 and Figures S1-S4, although PFAS are detected and eventually breakthrough in the *Lead* columns, the *Lag* columns generally have lower effluent PFAS concentrations for similar BVs treated. This indicates that longer EBCTs do not suffer from competing adsorbates (*e.g.*, ionic species, DOC), and the similar breakthrough curve shapes suggest shorter EBCTs (*i.e.,* ~ 2–5 minutes) capture the mass transfer zone. A lead-lag operational configuration allows near complete utilization of PFAS adsorption capacity. Table S8 shows that the ratios between the *Lead+Lag* to *Lead* column for $q_{\Sigma PFAS}$ were only slightly different from unity (1.07±0.12), implying that adsorption mechanisms are independent of EBCT. At full-scale, operating packed beds in lead-lag configurations allows complete media exhaustion in the lead column, while the lag column "polishes" PFAS compounds; operationally, the GAC in the lead column is replaced after exhaustion and then rotates to become the lag column, which maximizes sorbent adsorption capacity use while meeting low PFAS effluent concentrations.

78
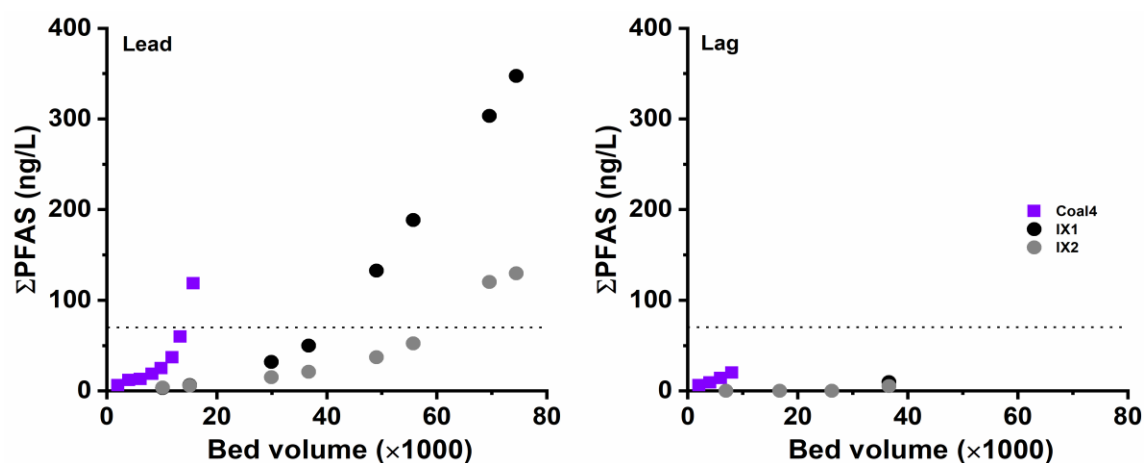
Figure 5.4 ΣPFAS breakthrough curves for RSSCT 13 to RSSCT 15 using GW-5. The dotted line indicates 70 ng/L.

5.4.3 Functional Groups and Chain Length Influence PFAS Removal Efficency

Figure 5.5 illustrates representative breakthrough curves for PFAS species in three groundwaters, normalized to the influent concentration of each species (C/C_0). PFSAs adsorb better (*i.e.*, break through later) than PFCAs with the same chain length (*e.g.,* PFOS and PFOA for C8 species). Within PFSA or PFCA classes, shorter-chain PFAS species break through before longer-chain PFAS. This breakthrough pattern is evident in all RSSCTs for GAC and IX resin (Figure S5–S22) (Figure S7–S24). When present, the PFAS species breakthrough order from least to best adsorbed was: PFHxA (C6), PFHpA (C7), PFOA (C8), and PFNA (C9) for PFCAs. For PFSA's, the order was PFBS (C4), PFHxS (C6), and PFOA (C8). When PFHxA (C6) existed in the groundwater (GW-3, 4, 5, and 6), it always broke through before any of the detected PFAS. While occurring in only GW-1 and GW-2 at low concentrations, PFNA (C9) breakthrough was only observed in the effluent of RSSCT-1 using coconut based GAC (*i.e.*, a poorly-performing GAC).

Additionally, as shown in Figure S22, IX resins were less effective in treating PFCAs than PFSAs, and all the PFCAs broke through earlier than PFSAs; the order was PFCAs (C6 > C7 > C8) before PFSAs (C4 > C6 > C8).
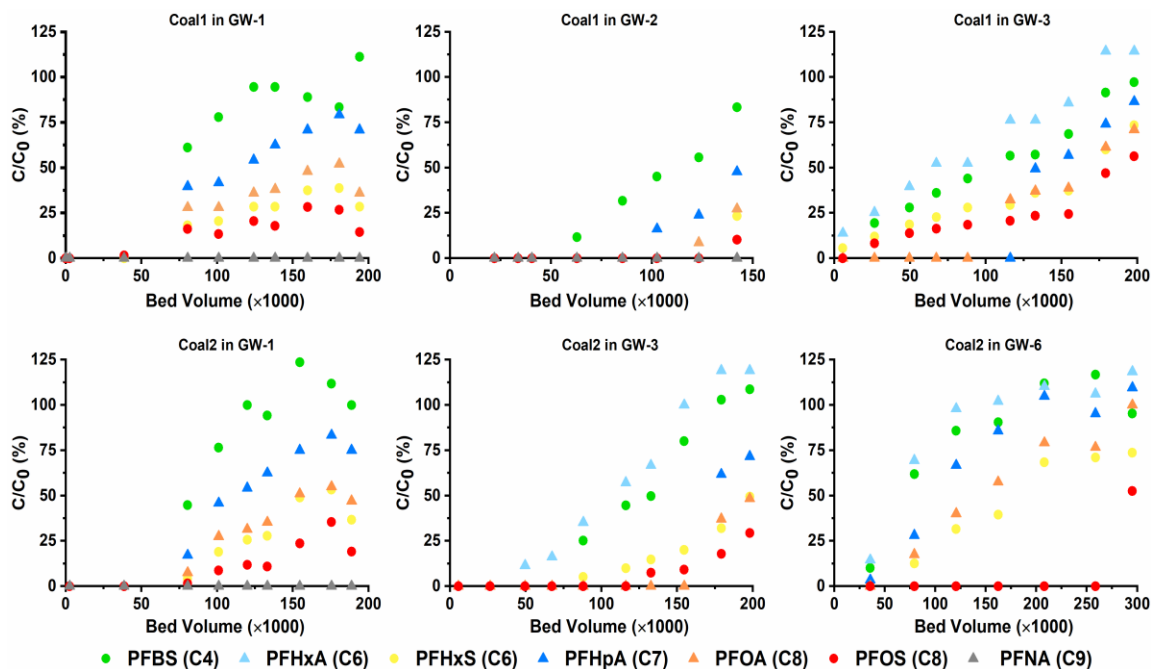
Figure 5.5 Representative RSSCT breakthrough curves in the Lead columns for three groundwaters and two carbon types (Coal1 and Coal2) as a function of BVs treated and PFAS effluent concentrations (C) normalized to PFAS influent concentration (C_0).

A statitical analysis was conducted to quantify the breakthrough behavior of different PFAS species (details provided in *Supporting Information (Appendix A)*). In 92% of PFCAs (n=144) and 84% of PFSAs (n=89) effluent samples, shorter-chain species broke through earlier than longer-chain species (Table S9). When comparing PFCAs with PFSAs of the same chain length, PFHxS broke through later than PFHxA (C6) in all samples (n=109), and PFOS adsorbed better than PFOA in 85% of the samples (n=80). Almost all outliers can be grouped into two catagories. First, because coconut-based GAC had low capacity for PFAS removal, breakthroughs of different PFAS were not distinguishable

from each other. Second, because the concentrations of PFHpA (4.1 ng/L) and PFOA (6.2 ng/L) in GW-3 were near the method detection limit (2 ng/L), rapid breakthrough of these compounds (from 0 to about 40–50% of C_0) was observed between ~100,000 and 200,000 BV (Figure 5.3).

Linear correlations performed between breakthrough trends (C/C_0 at all BV treated) with the physicochemical properties of PFAS (*i.e.,* molecular weight, *LogK$_{ow}$,* and *LogD*) yielded Pearson correlation coefficients (*R*) that are summarized in Table S10. PFAS with higher hydrophobicity and molecular weight were more amenable to GAC adsorption (statistically significant), especially for coal-based GAC (molecular weight: $R = 0.79$ to 0.96; *LogD*: R= 0.86 to 0.95). However, the *R* values were lower (not statisctially significant) for IX resins. This likely indicates differing PFAS adsorption mechanisms in IX resin and GAC, which are discussed below.

5.5 Discussion

The most general finding was that despite differing groundwater quality (e.g. pH, DOC, sulfate, and nitrate), similar trends in PFAS species breakthrough were observed across all the waters. Namely, higher PFAS in the influent led to higher $q_{\Sigma PFAS}$ and faster PFAS breakthrough, not all PFAS broke through at the same sorbent utilization rate (shorter-chain PFAS have lower $q_{\Sigma PFAS}$), and coal-based GAC had higher PFAS removal efficiency than coconut shell-based GAC in real groundwaters at ambient PFAS cocentrations. More detailed discussion is organized below around four themes.

5.5.1 Influence of Sorbent Materials

Coal-based GAC had higher PFAS removal efficiency than coconut shell-based GAC in real groundwaters at ambient PFAS cocentrations. However, coal-based GAC did have low affinity for the adsorption of short-chain PFCAs, and IX resin removed PFAS more effiently than GAC in all the groundwaters. GAC and IX resin performed very differently in the column tests, which can be explained by their different mechanisms for PFAS removal. Hydrophobic interaction is the main mechanism for PFAS adsorption onto GAC, while molecular size (versus pore size) and charge distribution on IX resins lead to electrostatic mechanisms which dominate for PFAS removal by IX resin. (Du et al. 2015).

The observation that coal-based GAC removes PFAS more efficiently than coconut shell-based GAC in real groundwaters at ambient PFAS concentrations is consistent with prior batch studies using synthetic water spiked with PFAS compounds at equal concentrations (1 µg/L–50 mg/L) (Appleman et al. 2013; Yu et al. 2009). As shown in Table S7, the values of point of zero charge range from 6.6 to 8.0 and coconut shell-based GACs are higher than coal-based GACs, which should result in more favorable electrostatic attraction of anionic PFAS. However, this did not lead to enhanced PFAS adsorption. In addition, Table S6 shows Coco1 and Coco2 also have lower polarity, which is expressed by combined nitrogen and oxygen contents because both nitrogen- and oxygen- containing surface functional groups can serve as hydrogen-bond donor or acceptor that facilitate water adsorption (Li et al. 2020). But more hydrophobic coconut shell-based GACs were not as effective as coal based GACs. Thus, GAC charge and hydrophobicity cannot explain the enhanced PFAS sorption by coal- compared against

coconut-shell based GAC. Instead, the higher removal efficiency from coal based GACs likely arises from the enhanced meso- and macro-porous structures. Porosity data from our study show the combined mesopore and macropore volume for GAC_{Coal2} is 2.2 times greater than GAC_{Coco2} (Table S5), while the larger portion of microporous structure of coconut shell-based GAC may be unaccessible for PFAS (*e.g.,* PFOA and PFOS).

5.5.2 Influence of Groundwater Composition

This study was not designed to systematically investigate competitive sorption effects from nitrate, sulfate or other anions on PFAS removal by IX resins or GAC. However, some insights can be gained from the influent groundwater quality (Table S1). For the 3 groundwaters where IX was investigated, IX resins exhibited the higher $q_{\Sigma PFAS}$ than GAC. These waters had comparable nitrate levels (1-2 mg NO_3-N/L) and 2 groundwaters (GW-3, GW-4) both had about twice the level of chloride and sulfate than GW-6. Despite this limited variability in anionic composition, the $q_{\Sigma PFAS}$ was lower in the groundwaters with elevated sulfate and chloride. For all six groundwaters, a Pearson Correlation analysis showed no significant dependence between DOC and $q_{\Sigma PFAS}$. The lack of a dependence was most likely due to the narrow range of DOC levels that exist in Arizona groundwaters (e.g., 0.2-0.9 mgDOC/L). Adsorption of short-chain PFAS by GAC or IX resin may be more affected by DOC level in the water and pore blockage by hydrophobic molecules or even other competing ions (McCleaf et al. 2017). However, while from a mechanistic viewpoint it is clearly established in literature that large differences in anion and/or DOC concentrations influence PFAS adsorption, the

operational significance of these water quality parameters were limited within the groundwaters and study areas considered herein.

5.5.3 Impact of PFAS chain length on adsorption

Long-chain PFAS compounds (*e.g.,* PFOA and PFOS) are preferentially removed over short-chain PFAS species when normalized to species influent concentrations. This trend occurred in all six waters, despite the groundwaters containing different PFAS species mixtures and initial concentrations. This selective adsorption of PFAS originates from differences in physicochemical properties beween longer-chain and shorter-chain species (as well as PFCAs and PFSAs) (Appleman et al. 2014, Du et al. 2014, Zhang et al. 2016). For example, PFAS with longer C-F chains generally have higher hydrophobicity (indicated in Table 5.1 by *LogKow* and pH corrected *LogD*). Similarly, compared against PFCAs of similar chain lengths, the additional flurinated carbon (CF_2) on the molecules tail for PFSAs makes PFSAs more hydrophobic than PFCAs. Higher hydrophobicity favors attachment of longer-chain PFAS onto the sorbent surfaces.

Additionally, longer chain-PFAS such as PFOS with strong hydrophobic interactions can lead to the formation of molecular aggregates or micelles on adsorption sites, although this is less likely to happen for comparatively hydrophilic PFBA and PFBS (Zaggia et al. 2016).

5.5.4 Benefits and Limitations of RSSCT Scaling Models

RSSCTs are valuable tools to examine relative pollutant removals for different adsorbents and water qualities. Limited research is currently available comparing adsorption capacity or breakthrough curves for CD- or PD-RSSCTs against pilot- or full-scale data (Schaefer et al. 2019). One challenge for PFAS is the long number of bed volumes, and associated run time (likely years) to detectable breakthrough in many full-scale systems. Such studies are currently ongoing in our laboratory. We have seen that CD-RSSCTs have earlier breakthrough than PD-RSSCTs, and thus considering results from CD-RSSCTs to design full-scale systems would be "conservative". That is to say, the sorbent replacement costs would be higher for CD- compared with PD-RSSCTs, and thus potentially represent an upper bound in potential sorbent costs. A limitation of any RSSCT is that they operate for a "grab" water sample, whereas full-scale systems often see variable water quality over seasons or years, as groundwater quality can be influenced by localized pumping patterns or recharge events.

5.5.5 Benefits and Limitations of Empirical Models

Complying with health advisory and pending regulatory limits depends on mass concentrations rather than fractional removal. Even though some PFAS are not mechanistically as well removed as other PFAS, the ability of a packed bed to meet mass based PFAS regulation limits will depend on fractional removal and initial PFAS concentration. To this end, we developed two empirical regression models to predict the breakthrough of PFAS and combined PFOA and PFOS mass concentrations for the

drinking waters in the study. Central tendency models have been used by the USEPA to predict and develop drinking water regulations related to disinfection by-products (Amy et al. 1998, Obolensky and Singer 2008) and controlling DOC, which is a key DBP precursor (Black, Harrington, and Singer 1996; Edwards 1997). A similar central-tendency power function was used in the multiple regression model. *Supporting Information (Appendix A)* provides modeling details and outcomes of additional central-tendency modeling with individual PFAS species. Using $\alpha = 0.05$ resulted in only a few terms being statistically significant (sorbent type, BV treated, DOC, and PFHxS, PFHxA, and PFHpA); the other terms were not statistically significant for our database, and thus they do not emerge as parameters in the final stepwise regression equation. The log regression model (Equation S1) (n=126, $p < 0.001$, S = 0.60, $R^2 = 87.64\%$, $R^2_{adj} = 86.3\%$) was transformed into the following power function model:

$$[\Sigma PFAS] = e^{-18.00x_1 - 18.61x_2 - 18.58x_3 - 18.57x_4 - 15.71x_5 - 16.97x_6 - 19.56x_7 - 20.38x_8} \cdot BV^{1.2284} \cdot$$

$$[PFHxS]^{1.069} \cdot [PFHxA]^{-0.492} \cdot [PFHpA]^{0.999}[DOC]^{-2.01} \tag{8}$$

where $\Sigma PFAS$ is concentration of all the PFAS detected in the effluent; x_1, x_2, x_3, x_4, x_5, x_6, x_7, and x_8 represent sorbents Coal1, Coal2, Coal3, Coal4, Coco1, Coco2, IX1, and IX2, respectively ($x = 1$, if use the sorbent; $x = 0$, if not); and *[PFHxS]*, *[PFHxA]*, and *[PFHpA]* are the concentrations of those PFAS species in the groundwaters. The regression coefficients in the two models indicate the affinity of different sorbents on PFAS adsorption: IX resins > coal-based GACs > coconut shell-based GACs. Figure 5.6A plots all 126 data points as observed versus predicted (Equation 8) for ΣPFAS, which yields a

near 1:1 regression through the data of $\Sigma PFAS_{Predicted} = 0.99 \times \Sigma PFAS_{Observed} - 5.54$ ($R^2 =$ 0.92). For one water, Figure 5.6B shows the ΣPFAS breakthrough as a function of BVs treated was predicted using Equation 8 and compared against observed breakthrough data.
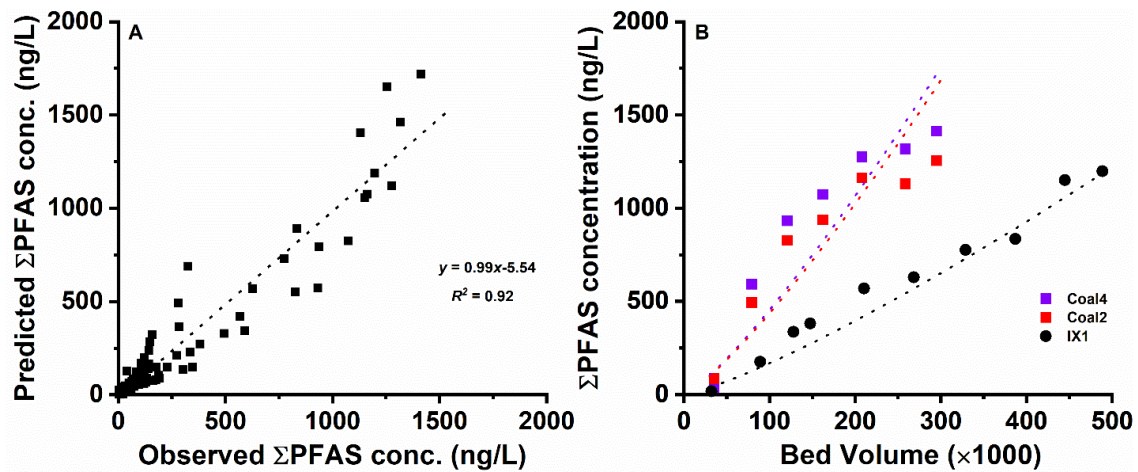
Figure 5.6 (A) Comparison between observed ΣPFAS concentrations and predicted ΣPFAS concentrations using all the data acquired from Lead columns in the RSSCTs. **(B)** Breakthrough of ΣPFAS from Lead columns using GW-6 (ΣPFAS = 1252 ng/L): solid symbols represent observed data, while dotted lines are the predicted breakthrough curves (right panel)

The model differentiates well between GAC and IX performance. However, the predicted shape of the GAC breakthrough curve does not necessarily match the observed s-shaped breakthrough curve. This limitation originates from the type of data we use in the model (i.e., fractional breakthrough as number of bed volumes treated from our entire dataset). This is very different than models which parameterize logistic-shaped models for each breakthrough curve, and then relate those parameters to different RSSCT or pilot runs (Black, Harrington, and Singer 1996). However, overall the model predicts well the number of BVs when influent and effluent GAC column ΣPFAS concentrations are equal and achieve fits that are typical of central-tendency models. A value of the central tendency

87

models is that they show which parameters were most influential on PFAS removal under the conditions tested. In our case that was type of adsorbent, number of bed volumes treated, concentrations of dominant PFAS species, and to a limited extent the DOC concentration in the water, while other water quality or performance data emerged as not statically relevant as independent parameters to predict PFAS breakthrough. We believe this type of model is helpful for the "case study" and could be mimicked in other regions where groundwater quality may be different.

5.6 Conclusions

Our results provide "benchmark" performance assessments of commercially available adsorption technologies for PFAS removal. As numerous funding agencies, companies, and research groups are seeking innovative PFAS treatment technologies (including but not limited to sorbents), this work provides adsorption capacity metrics and expected operational run time that can be used in future techno-economic analyses. Specifically, this work highlights the less efficient sorption of shorter-chain species by commercial sorbents, which should encourage research on technologies targeting their removal.

5.7 Acknowledgements

from University of Massachusetts Lowell kindly helped by measuring the point of zero charge for the GACs used in this study. Laurel Passantino provided technical editing of the manuscript.

CHAPTER 6

SUMMARY AND CONCLUSIONS

A pilot-scale study was conducted at a local groundwater PFAS contaminated wellsite to evaluate PFAS removal by commercial GACs and IX resins. The bench-scale method to simulate the pilot columns included the RSSCT under CD and PD based design. CD vs. PD designs were evaluated to validate their accuracy in simulating the pilot column breakthrough, in terms of breakthrough curve shape, breakthrough concentration prediction, and also in terms of adsorbent capacity. Additionally, RSSCTs based on CD design on multiple GWs were performed to document the trend of PFAS removal by GAC and IX.

The objective 1 of this thesis was to compare the adsorbent capacity of commercial granular activated carbon (GAC) vs. anion exchange resin (IX) materials to adsorb PFAS from groundwater, in a field pilot-scale study. Key observations answering objective 1 are as follows.

- The IX resin was highly effective in adsorbing PFAS from the groundwater wells at the pilot column. Only ~15% breakthrough of total PFAS at 150,000 BVs was observed. In contrast, the GACs had >85% breakthrough at 82,000 BVs and 87,000 BVs for both GAC1(Calgon) and GAC 2 (Norit), respectively.

- The adsorption capacity of the IX pilot column for total PFAS at the end of the run was about 7.1μg/g of adsorbent, which is 1.3 times and 1.8 times greater than GAC 1(Calgon) and GAC 2 (Norit), respectively. Since IX had only <15% breakthrough,

the complete breakthrough was not achieved; IX would have a much higher adsorption capacity if all the compounds breakthrough.

- Overall, the adsorption capacity at the end of testing followed the order: IX > GAC2(Norit) > GAC1(Calgon).

Objective 2 of this thesis was to compare CD vs. PD-RSSCTs breakthrough curves with GAC and IX to each other and against pilot-scale performance. Key observations answering objective 2 are as follows.

- The CD based RSSCT breakthrough curves show similar shape as the GAC in pilot-scale columns for various PFAS compounds. Therefore, in CD vs. PD, the CD is significantly better. Similar shapes suggest similar mass transfer zone (MTZ) development between pilot and CD-RSSCTs.

- The slope of adsorption capacity *CD vs. Pilot* was close to 1 for most PFAS compounds for GAC2(Norit) and slightly above 1 for GAC1(Calgon). Thus, CD-RSSCTs for GAC either closely predict or under predicts the adsorbent capacity of pilot columns.

- The slope of adsorption capacity for PD *vs. Pilot and PD vs. CD* was greater than 1, for most PFAS compounds for GACs. Therefore, PD overpredicts the adsorption capacity in comparison.

- The CD-RSSCT simulates the PFAS breakthrough and adsorbent capacity of GACs more closely for this low DOC groundwater as compared to PD-RSSCT.

- For the IX, overall breakthrough achieved is <15% in pilot columns, thus difficult to select if the CD or PD based RSSCTs is better to simulate the pilot columns.

91

- The effect of EBCTs for the CD based RSSCT results shows that mass transfer zone (MTZ) could be effectively captured even with a much shorter EBCT of 2 minutes for both the GACs and 1.3 minutes for the IX (Purolite). Similar breakthrough curves for varying EBCTs show that the longer EBCTs were not affected by DOM or dissolved ions in PFAS removal.

Objective 3 of this thesis was to document the trends in PFAS removal by GAC and IX based upon chain length and functional head-group moieties. Key observations answering objective 3 are as follows.

- The PFAS breakthrough in GACs columns was dictated mainly by PFAS carbon chain length and by its functional group, even with varying influent PFAS concentrations in groundwater well.
- The PFAS compounds of the same carbon chain length with sulfonic acid functional groups broke through later as compared to the carboxylic functional groups.
- For PFAS compounds of the same functional group, the shorter carbon chain PFAS compounds broke through much faster than, the longer chain PFAS compounds. The order of breakthrough was C4 > C6 > C8.
- In general, the breakthrough of PFAS compounds is based on the hydrophobicity of the compounds. More hydrophobic compounds breakthrough slower (more adsorption) compared to less hydrophobic compounds, which can be seen with inverse proportionality between the breakthrough order of the compound and its Log D value.

- The same trend of chain length (C4 > C6 > C8) and functional group (PFCAs > PFSAs) dependent breakthrough was observed in PFAS breakthrough in GACs for both pilot and RSSCT (CD and PD) columns.

- The pilot IX column had no breakthrough for most of the PFAS compounds. Therefore, a complete breakthrough pattern could not be assessed. However, the RSSCT results from other well sites (Chapter 5), shows the IX resin from longer-term testing shows similar results on chain length and functional group dependence on the breakthrough.

Future work:

CD and PD RSSCTs simulating MobileNEWT columns, using different particle diameter sizes (0.09 mm and 0.16mm), were performed on Tempe GW with spiked PFAS concentration (3000 ng/L Total PFAS), results are awaited. For GAC2(Norit), PFAS breakthrough curves for both the particle sizes are expected to coincide, which indicates that intraparticle diffusion is independent of particle size. This result is expected because CD is the valid model based on pilot and RSSCT results discussed in this study. The goal of performing different particle size RSSCTs is to extend the body of evidence and conclusively verify the validity of the CD model for GACs. IX RSSCTs were run up to 300,000 BVs and are expected to achieve a significant breakthrough for all PFAS compounds and to determine appropriate the appropriate RSSCT model.

Even though IX outperformed GACs in the experiments, consultants and design engineers should perform techno-economic analysis for scale up decisions which would include capital expenditure, media cost, operation, and management cost. They would help

in selecting cost-effective sorbent. The pilot-scale columns, especially for the IX, should be extended for much longer BVs to achieve a complete breakthrough curve. Thus, the RSSCT designs (PD versus CD) could be evaluated more effectively. The PFAS contaminated well/surface water with higher DOC concentration should also be tested under the pilot-scale operation and test the validity of RSSCTs in more extensive ranges of water quality. Furthermore, other novel and innovative technologies in PFAS removal or PFAS transformation to neutral compounds, rather than just separation, could also be investigated at both pilot and bench-scale levels.

REFERENCES

ADEQ. 2019. "Arizona's Public Water System Screening for Perfluorooctanoic Acid (PFOA) and Perfluorooctane Sulfonate (PFOS) Final Report." 2019. http://azdeq.gov/PFOA/PFOS.

Ahrens, Lutz. 2011. "Polyfluoroalkyl Compounds in the Aquatic Environment: A Review of Their Occurrence and Fate." Journal of Environmental Monitoring. https://doi.org/10.1039/c0em00373e.

Ahrens, Lutz, and Mirco Bundschuh. 2014. "Fate and Effects of Poly- and Perfluoroalkyl Substances in the Aquatic Environment: A Review." Environmental Toxicology and Chemistry. https://doi.org/10.1002/etc.2663.

Amy, Gary, Mohamed Siddiqui, Kenan Ozekin, Hai W. Zhu, and Charlene Wang. 1998. "Empirically Based Models for Predicting Chlorination and Ozonation By-Products: Trihalomethanes, Haloacetic Acids, Chloral Hydrate and Bromate." https://nepis.epa.gov/Exe/ZyPDF.cgi/200021CF.PDF?Dockey=200021CF.PDF.

Appleman, Timothy D., Eric R.V. Dickenson, Christopher Bellona, and Christopher P. Higgins. 2013. "Nanofiltration and Granular Activated Carbon Treatment of Perfluoroalkyl Acids." *Journal of Hazardous Materials*. https://doi.org/10.1016/j.jhazmat.2013.06.033.

Appleman, Timothy D., Christopher P. Higgins, Oscar Quiñones, Brett J. Vanderford, Chad Kolstad, Janie C. Zeigler-Holady, and Eric R.V. Dickenson. 2014. "Treatment of Poly- and Perfluoroalkyl Substances in U.S. Full-Scale Water Treatment Systems." *Water Research*. https://doi.org/10.1016/j.watres.2013.10.067.

Arvaniti, Olga S., and Athanasios S. Stasinakis. 2015. "Review on the Occurrence, Fate and Removal of Perfluorinated Compounds during Wastewater Treatment." Science of the Total Environment. https://doi.org/10.1016/j.scitotenv.2015.04.023.

Ateia, Mohamed, Amith Maroli, Nishanth Tharayil, and Tanju Karanfil. 2019. "The Overlooked Short- and Ultrashort-Chain Poly- and Perfluorinated Substances: A Review." Chemosphere. https://doi.org/10.1016/j.chemosphere.2018.12.186.

Black, Bryan D., Gregory W. Harrington, and Philip C. Singer. 1996. "Reducing Cancer Risks by Improving Organic Carbon Removal." *Journal / American Water Works Association*. https://doi.org/10.1002/j.1551-8833.1996.tb06570.x.

Butt, Craig M., Derek C.G. Muir, and Scott A. Mabury. 2014. "Biotransformation Pathways of Fluorotelomer-Based Polyfluoroalkyl Substances: A Review." Environmental Toxicology and Chemistry. https://doi.org/10.1002/etc.2407.

Chaplin, Brian P. 2014. "Critical Review of Electrochemical Advanced Oxidation Processes for Water Treatment Applications." Environmental Sciences: Processes and Impacts. Royal Society of Chemistry. https://doi.org/10.1039/c3em00679d.

Crittenden, John C., John K. Berrigan, and David W. Hand. 1986. "DESIGN OF RAPID SMALL-SCALE ADSORPTION TESTS FOR A CONSTANT DIFFUSIVITY." Journal of the Water Pollution Control Federation 58 (4): 312–19.

Crittenden, John C., Parimi Sanjay Reddy, Harish Arora, John Trynoski, David W. Hand, David L. Perram, and R. Scott Summers. 1991. "Predicting GAC Performance With Rapid Small-Scale Column Tests." Journal - American Water Works Association. https://doi.org/10.1002/j.1551-8833.1991.tb07088.x.

Crittenden, John, R. Rhodes Trussell, David W. Hand, Kerry J. Howe, and George Tchobanoglous. 2014. MWH Water Treatment Principles and Design. GPSA 12 Ed 2004 - FPS. https://doi.org/10.1016/B978-0-12-382092-1.00019-1.

Cummings, Laura, and R. Scott Summers. 1994. "Using RSSCTs to Predict Field-Scale GAC Control of DBP Formation." Journal / American Water Works Association. https://doi.org/10.1002/j.1551-8833.1994.tb06212.x.

Du, Ziwen, Shubo Deng, Yue Bei, Qian Huang, Bin Wang, Jun Huang, and Gang Yu. 2014. "Adsorption Behavior and Mechanism of Perfluorinated Compounds on Various Adsorbents-A Review." Journal of Hazardous Materials. https://doi.org/10.1016/j.jhazmat.2014.04.038.

Du, Ziwen, Shubo Deng, Youguang Chen, Bin Wang, Jun Huang, Yujue Wang, and Gang Yu. 2015. "Removal of Perfluorinated Carboxylates from Washing Wastewater of Perfluorooctanesulfonyl Fluoride Using Activated Carbons and Resins." *Journal of Hazardous Materials*. https://doi.org/10.1016/j.jhazmat.2014.12.037.

Edwards, Marc. 1997. "Predicting DOC Removal during Enhanced Coagulation." *Journal / American Water Works Association*. https://doi.org/10.1002/j.1551-8833.1997.tb08229.x.

Emmett, Edward Anthony, Frances Susan Shofer, Hong Zhang, David Freeman, Chintan Desai, and Leslie Michael Shaw. 2006. "Community Exposure to Perfluorooctanoate: Relationships between Serum Concentrations and Exposure Sources." *Journal of Occupational and Environmental Medicine*. https://doi.org/10.1097/01.jom.0000232486.07658.74.

Fernandez, Nerea Abad, Lucia Rodriguez-Freire, Manish Keswani, and Reyes Sierra-Alvarez. 2016. "Effect of Chemical Structure on the Sonochemical Degradation of

Perfluoroalkyl and Polyfluoroalkyl Substances (PFASs)." Environmental Science: Water Research and Technology. https://doi.org/10.1039/c6ew00150e.

Forstmeier, Wolfgang, Eric Jan Wagenmakers, and Timothy H. Parker. 2017. "Detecting and Avoiding Likely False-Positive Findings – a Practical Guide." Biological Reviews. https://doi.org/10.1111/brv.12315.

Gagliano, Erica, Massimiliano Sgroi, Pietro P. Falciglia, Federico G.A. Vagliasindi, and Paolo Roccaro. 2020. "Removal of Poly- and Perfluoroalkyl Substances (PFAS) from Water by Adsorption: Role of PFAS Chain Length, Effect of Organic Matter and Challenges in Adsorbent Regeneration." Water Research. https://doi.org/10.1016/j.watres.2019.115381.

Gawor, A., C. Shunthirasingham, S. J. Hayward, Y. D. Lei, T. Gouin, B. T. Mmereki, W. Masamba, et al. 2014. "Neutral Polyfluoroalkyl Substances in the Global Atmosphere." Environmental Sciences: Processes and Impacts. https://doi.org/10.1039/c3em00499f.

Gole, Vitthal L., Asher Fishgold, Reyes Sierra-Alvarez, Pierre Deymier, and Manish Keswani. 2018. "Treatment of Perfluorooctane Sulfonic Acid (PFOS) Using a Large-Scale Sonochemical Reactor." Separation and Purification Technology. https://doi.org/10.1016/j.seppur.2017.11.009.

Granum, Berit, Line S. Haug, Ellen Namork, Solvor B. Stølevik, Cathrine Thomsen, Ingeborg S. Aaberge, Henk Van Loveren, Martinus Løvik, and Unni C. Nygaard. 2013. "Pre-Natal Exposure to Perfluoroalkyl Substances May Be Associated with Altered Vaccine Antibody Levels and Immune-Related Health Outcomes in Early Childhood." Journal of Immunotoxicology 10 (4): 373–79. https://doi.org/10.3109/1547691X.2012.755580.

Hand, D. W., J. C. Crittenden, D. R. Hokanson, and J. L. Bulloch. 1997. "Predicting the Performance of Fixed-Bed Granular Activated Carbon Adsorbers." Water Science and Technology. https://doi.org/10.1016/S0273-1223(97)00136-4.

Hölzer, Jürgen, Thomas Göen, Knut Rauchfuss, Martin Kraft, Jürgen Angerer, Peter Kleeschulte, and Michael Wilhelm. 2009. "One-Year Follow-up of Perfluorinated Compounds in Plasma of German Residents from Arnsberg Formerly Exposed to PFOA-Contaminated Drinking Water." International Journal of Hygiene and Environmental Health. https://doi.org/10.1016/j.ijheh.2009.04.003.

Hu, Xindi C., David Q. Andrews, Andrew B. Lindstrom, Thomas A. Bruton, Laurel A. Schaider, Philippe Grandjean, Rainer Lohmann, et al. 2016. "Detection of Poly- and Perfluoroalkyl Substances (PFASs) in U.S. Drinking Water Linked to Industrial Sites, Military Fire Training Areas, and Wastewater Treatment Plants." *Environmental Science and Technology Letters*. https://doi.org/10.1021/acs.estlett.6b00260.

Hurley, Susan, Erika Houtz, Debbie Goldberg, Miaomiao Wang, June Soo Park, David O. Nelson, Peggy Reynolds, et al. 2016. "Preliminary Associations between the Detection of Perfluoroalkyl Acids (PFAAs) in Drinking Water and Serum Concentrations in a Sample of California Women." *Environmental Science and Technology Letters*. https://doi.org/10.1021/acs.estlett.6b00154.

Lapworth, D. J., N. Baran, M. E. Stuart, and R. S. Ward. 2012. "Emerging Organic Contaminants in Groundwater: A Review of Sources, Fate and Occurrence." Environmental Pollution. https://doi.org/10.1016/j.envpol.2011.12.034.

Li, Fan, Jun Duan, Shuting Tian, Haodong Ji, Yangmo Zhu, Zongsu Wei, and Dongye Zhao. 2020. "Short-Chain per- and Polyfluoroalkyl Substances in Aquatic Systems: Occurrence, Impacts and Treatment." Chemical Engineering Journal. https://doi.org/10.1016/j.cej.2019.122506.

Li, Lei, Patricia A. Quinlivan, and Detlef R.U. Knappe. 2002. "Effects of Activated Carbon Surface Chemistry and Pore Structure on the Adsorption of Organic Contaminants from Aqueous Solution." *Carbon*. https://doi.org/10.1016/S0008-6223(02)00069-6.

Liu, Charlie J., David Werner, and Christopher Bellona. 2019. "Removal of Per- And Polyfluoroalkyl Substances (PFASs) from Contaminated Groundwater Using Granular Activated Carbon: A Pilot-Scale Study with Breakthrough Modeling." Environmental Science: Water Research and Technology. https://doi.org/10.1039/c9ew00349e.

Liu, Jiaoqin, Ruijuan Qu, Zunyao Wang, Itza Mendoza-Sanchez, and Virender K. Sharma. 2017. "Thermal- and Photo-Induced Degradation of Perfluorinated Carboxylic Acids: Kinetics and Mechanism." Water Research. https://doi.org/10.1016/j.watres.2017.09.003.

McCleaf, Philip, Sophie Englund, Anna Östlund, Klara Lindegren, Karin Wiberg, and Lutz Ahrens. 2017. "Removal Efficiency of Multiple Poly- and Perfluoroalkyl Substances (PFASs) in Drinking Water Using Granular Activated Carbon (GAC) and Anion Exchange (AE) Column Tests." Water Research. https://doi.org/10.1016/j.watres.2017.04.057.

Meng, Pingping, Shubo Deng, Xinyu Lu, Ziwen Du, Bin Wang, Jun Huang, Yujue Wang, Gang Yu, and Baoshan Xing. 2014. "Role of Air Bubbles Overlooked in the Adsorption of Perfluorooctanesulfonate on Hydrophobic Carbonaceous Adsorbents." *Environmental Science and Technology*. https://doi.org/10.1021/es504108u.

Obolensky, Alexa, and Philip C. Singer. 2008. "Development and Interpretation of Disinfection Byproduct Formation Models Using the Information Collection Rule Database." *Environmental Science and Technology*. https://doi.org/10.1021/es702974f.

Oyetade, Oluwaseun A., G. Bishwa Bidita Varadwaj, Vincent O. Nyamori, Sreekantha B. Jonnalagadda, and Bice S. Martincigh. 2018. "A Critical Review of the Occurrence of Perfluoroalkyl Acids in Aqueous Environments and Their Removal by Adsorption onto Carbon Nanotubes." *Reviews in Environmental Science and Biotechnology*. https://doi.org/10.1007/s11157-018-9479-9.

Patterson, Craig, Jonathan Burkhardt, Donald Schupp, E. Radha Krishnan, Stephen Dyment, Steven Merritt, Lawrence Zintek, and Danielle Kleinmaier. 2019. "Effectiveness of Point-of-use/Point-of-entry Systems to Remove Per- and Polyfluoroalkyl Substances from Drinking Water." *AWWA Water Science*. https://doi.org/10.1002/aws2.1131.

Park, Minkyu, Shimin Wu, Israel J. Lopez, Joseph Y. Chang, Tanju Karanfil, and Shane A. Snyder. 2020. "Adsorption of Perfluoroalkyl Substances (PFAS) in Groundwater by Granular Activated Carbons: Roles of Hydrophobicity of PFAS and Carbon Characteristics." Water Research. https://doi.org/10.1016/j.watres.2019.115364.

"Perfluorooctanoic Acid (PFOA) and Perfluorooctanesulfonic Acid (PFOS)." 2020. https://www.waterboards.ca.gov/drinking_water/certlic/drinkingwater/PFOA_PFOS.html .

Rahman, Mohammad Feisal, Sigrid Peldszus, and William B. Anderson. 2014. "Behaviour and Fate of Perfluoroalkyl and Polyfluoroalkyl Substances (PFASs) in Drinking Water Treatment: A Review." Water Research. https://doi.org/10.1016/j.watres.2013.10.045.4

Rankin, Keegan, Scott A. Mabury, Thomas M. Jenkins, and John W. Washington. 2016. "A North American and Global Survey of Perfluoroalkyl Substances in Surface Soils: Distribution Patterns and Mode of Occurrence." Chemosphere. https://doi.org/10.1016/j.chemosphere.2016.06.109.

Rappazzo, Kristen M., Evan Coffman, and Erin P. Hines. 2017. "Exposure to Perfluorinated Alkyl Substances and Health Outcomes in Children: A Systematic Review of the Epidemiologic Literature." International Journal of Environmental Research and Public Health. https://doi.org/10.3390/ijerph14070691.

"Response Levels Lowered for Water Systems Statewide as PFAS Investigation Continues." 2020. 2020. https://www.waterboards.ca.gov/press_room/press_releases/2020/pr02062020_pfoa_pfos_response_levels.pdf.

Rodowa, Alix E., Detlef R. U. Knappe, Sheau-Yun Dora Chiang, Dirk Pohlmann, Catharine Varley, Adria Bodour, and Jennifer A. Field. 2020. "Pilot Scale Removal of Per- and Polyfluoroalkyl Substances and Precursors from AFFF-Impacted Groundwater by Granular Activated Carbon." Environmental Science: Water Research & Technology. https://doi.org/10.1039/c9ew00936a.

Rostvall, Ande, Wen Zhang, Wiebke Dürig, Gunno Renman, Karin Wiberg, Lutz Ahrens, and Pablo Gago-Ferrero. 2018. "Removal of Pharmaceuticals, Perfluoroalkyl Substances and Other Micropollutants from Wastewater Using Lignite, Xylit, Sand, Granular Activated Carbon (GAC) and GAC+Polonite® in Column Tests – Role of Physicochemical Properties." *Water Research*. https://doi.org/10.1016/j.watres.2018.03.008.

Schaefer, Charles E., Dung Nguyen, Paul Ho, Jihyon Im, and Alan Leblanc. 2019. "Assessing Rapid Small-Scale Column Tests for Treatment of Perfluoroalkyl Acids by Anion Exchange Resin." Industrial and Engineering Chemistry Research. https://doi.org/10.1021/acs.iecr.9b00858.

Sunderland, Elsie M., Xindi C. Hu, Clifton Dassuncao, Andrea K. Tokranov, Charlotte C. Wagner, and Joseph G. Allen. 2019. "A Review of the Pathways of Human Exposure to Poly- and Perfluoroalkyl Substances (PFASs) and Present Understanding of Health Effects." Journal of Exposure Science and Environmental Epidemiology. Nature Publishing Group. https://doi.org/10.1038/s41370-018-0094-1.

U.S. EPA. 2016. "The Third Unregulated Contaminant Monitoring Rule (UCMR 3): Data Summary." Office of Water, EPA 815-S-16–0. https://doi.org/http://water.epa.gov/lawsregs/rulesregs/sdwa/ucmr/ucmr3/upload/UCMR3_FactSheet_List1.pdf.

USEPA (2017) "The Third Unregulated Contaminant Monitoring Rule (UCMR 3) ." Washington, DC.

Vecitis, Chad D., Hyunwoong Park, Jie Cheng, Brian T. Mader, and Michael R. Hoffmann. 2009. "Treatment Technologies for Aqueous Perfluorooctanesulfonate (PFOS) and Perfluorooctanoate (PFOA)." Frontiers of Environmental Science and Engineering in China. https://doi.org/10.1007/s11783-009-0022-7.

Vestergren, Robin, and Ian T. Cousins. 2009. "Tracking the Pathways of Human Exposure to Perfluorocarboxylates." *Environmental Science and Technology*. https://doi.org/10.1021/es900228k.

Wang, Zhanyun, Jamie C. Dewitt, Christopher P. Higgins, and Ian T. Cousins. 2017. "A Never-Ending Story of Per- and Polyfluoroalkyl Substances (PFASs)?" *Environmental Science and Technology*. https://doi.org/10.1021/acs.est.6b04806.

Westerhoff, Paul, David Highfield, Mohammad Badruzzaman, and Yeomin Yoon. 2005. "Rapid Small-Scale Column Tests for Arsenate Removal in Iron Oxide Packed Bed Columns." Journal of Environmental Engineering. https://doi.org/10.1061/(ASCE)0733-9372(2005)131:2(262).

Woodard, Steve, John Berry, and Brandon Newman. 2017. "Ion Exchange Resin for PFAS Removal and Pilot Test Comparison to GAC." Remediation. https://doi.org/10.1002/rem.21515.

Xiao, Xin, Bridget A. Ulrich, Baoliang Chen, and Christopher P. Higgins. 2017. "Sorption of Poly- and Perfluoroalkyl Substances (PFASs) Relevant to Aqueous Film-Forming Foam (AFFF)-Impacted Groundwater by Biochars and Activated Carbon." Environmental Science and Technology. https://doi.org/10.1021/acs.est.7b00970.

Yang, Yiqiong, Qiao Ding, Minhui Yang, Yin Wang, Ning Liu, and Xiaodong Zhang. 2018. "Magnetic Ion Exchange Resin for Effective Removal of Perfluorooctanoate from Water: Study of a Response Surface Methodology and Adsorption Performances." *Environmental Science and Pollution Research*. https://doi.org/10.1007/s11356-018-2797-1.

Yu, Qiang, Ruiqi Zhang, Shubo Deng, Jun Huang, and Gang Yu. 2009. "Sorption of Perfluorooctane Sulfonate and Perfluorooctanoate on Activated Carbons and Resin: Kinetic and Isotherm Study." *Water Research*. https://doi.org/10.1016/j.watres.2008.12.001.

Young, I. T. 1977. "Proof without Prejudice: Use of the Kolmogorov Smirnov Test for the Analysis of Histograms from Flow Systems and Other Sources." Journal of Histochemistry and Cytochemistry. https://doi.org/10.1177/25.7.894009.

Zaggia, Alessandro, Lino Conte, Luigi Falletti, Massimo Fant, and Andrea Chiorboli. 2016. "Use of Strong Anion Exchange Resins for the Removal of Perfluoroalkylated Substances from Contaminated Drinking Water in Batch and Continuous Pilot Plants." *Water Research*. https://doi.org/10.1016/j.watres.2015.12.039.

Zeng, Chao, Ariel Atkinson, Naushita Sharma, Harsh Ashani, Annika Hjelmstad, Krishishvar Venkatesh, and Paul Westerhoff. 2020. "Removing Per- and Polyfluoroalkyl Substances from Groundwaters Using Activated Carbon and Ion Exchange Resin Packed Columns." AWWA Water Science. https://doi.org/10.1002/aws2.1172.

Zhang, Di, Qi Luo, Bin Gao, Sheau Yun Dora Chiang, David Woodward, and Qingguo Huang. 2016. "Sorption of Perfluorooctanoic Acid, Perfluorooctane Sulfonate and Perfluoroheptanoic Acid on Granular Activated Carbon." *Chemosphere*. https://doi.org/10.1016/j.chemosphere.2015.10.124.

Zhang, Xianming, Rainer Lohmann, Clifton Dassuncao, Xindi C. Hu, Andrea K. Weber, Chad D. Vecitis, and Elsie M. Sunderland. 2016. "Source Attribution of Poly- and Perfluoroalkyl Substances (PFASs) in Surface Waters from Rhode Island and the New York Metropolitan Area." *Environmental Science and Technology Letters*. https://doi.org/10.1021/acs.estlett.6b00255.

 Zhi, Yue, and Jinxia Liu. 2016. "Surface Modification of Activated Carbon for Enhanced Adsorption of Perfluoroalkyl Acids from Aqueous Solutions." *Chemosphere*. https://doi.org/10.1016/j.chemosphere.2015.09.097.

Zhi, Yue, and Jinxia Liu. 2015. "Adsorption of Perfluoroalkyl Acids by Carbonaceous Adsorbents: Effect of Carbon Surface Chemistry." *Environmental Pollution*. https://doi.org/10.1016/j.envpol.2015.03.019.

APPENDIX A

SUPPORTING INFORMATION

1. Materials and Methods

Groundwater

All the water samples were natural groundwaters directly taken from different well sites. The only exception was GW-4, which was a PFAS-impacted groundwater taken after being treated by UV peroxide advanced oxidation to remove 1,4–dioxane and TCE. The groundwaters were stored in 55-gallon HDPE barrels. Before use, all the water samples were passed through a polypropylene cartridge filter (filter grade = 1 µm). pH, conductivity, turbidity, DOC, and UV254 were measured. Table S1 summarizes water quality information. The peroxide concentration in GW-4 was measured by a Hach hydrogen peroxide test kit. Peroxide residual was below the detection limit (0.2 mg/L). Feed water samples were taken before and after column tests for PFAS analysis.

Table S1. Water quality of groundwaters used in column experiments.

	GW-1	GW-2	GW-3	GW-4	GW-5	GW-6
pH	7.5	7.6	8.5	8.1	7.9	8.1
Conductivity (µs/cm)	884	964	682	691	496	525
Alkalinity (mg/L as $CaCO_3$)	130	136	200	178	153	133
Turbidity (NTU)	0.26	0.40	0.1	0.07	1.21	0.28
DOC (mg/L)	0.88	0.95	0.21	0.30	0.80	0.40
UV254	0.008	0.01	0.003	0.002	0.010	0.006
Chloride (mg/L)	150	163	40	40	9.3	15.8
Sulfate (mg/L as SO_4)	76	75	183	180	68.3	97.4
Nitrate (mg/L as N)	5.7	4.7	2.0	2.0	1.0	1.2

Rapid small scale column tests (RSSCTs)

RSSCTs were designed to simulate pilot columns (120 cm length by 305 cm diameter) packed with GAC (12×40 mesh, geometric mean diameter of 0.84 mm) or IX resin (diameter of 0.65 mm). The RSSCT experimental matrix is in Table S2, and design parameters are in Table S3. The empty bed contact time (EBCT) of small-column is determined from the following equation:

$$\frac{EBCT_{SC}}{EBCT_{LC}} = \left[\frac{d_{p,SC}}{d_{p,LC}}\right]^{2-X} = \frac{t_{SC}}{t_{LC}} \qquad \text{(Eq. S1)}$$

where SC=small column (*i.e.*, RSSCT column); LC=large column (*i.e.*, pilot column); d_p is the diameter of sorbent packed in the column; t represents the test duration; X defines the dependence of intraparticle diffusivity on particle size: $X=0$ when diffusivity is constant (CD); $X=1$ when diffusivity is linearly proportional to sorbent particle size (PD). Only two RSSCTs (RSSCT-4 and RSSCT-6 with IX resin) were designed based on proportional diffusivity (PD) assumption, and the rest used the CD assumption. The number of BV treated equals the volume passed through the column at any given time divided by EBCT×flow rate.

We confirmed through control studies that there was no leaching of PFAS from any RSSCT apparatus components. The RSSCT apparatus included polyethylene columns (0.43 cm diameter) with polypropylene connecters, polyethylene tubing, and piston pumps (QG50, Fluid Metering Inc, Syosset, NY). Columns were packed under wet conditions with glass wool supporting the base sieved media. Columns were backwashed prior to experiments to remove fines.

Table S2. Summary of 18 rapid small scale column tests (RSSCTs) conducted in this study. 16 RSSCTs were designed using CD scaling assumptions, and 2 were designed (*) using PD assumptions.

RSSCT	Groundwater	Sorbent[a]	at ~100,000 BV[b]		at ~200,000 BV[b]	
			$q_{\Sigma PFAS}$ (ng/mg)	$\Sigma PFAS$ (C/C$_0$, %)	$q_{\Sigma PFAS}$ (ng/mg)	$\Sigma PFAS$ (C/C$_0$, %)
1		Coco1 (140×170)	22.9	94	N/A	N/A
2	GW-1	Coal1 (140×170)	61.7	22	103.8	29
3		Coal2 (140×170)	82.4	18	132.6	33
4		IX1 (140×170)*	15.2	0	67.8	0
5	GW-2	Coal1 (100×140)	33.7	6	N/A	N/A
6		IX1 (140×170)*	10.3	0	20.7	0
7		Coal1 (140×170)	29.7	36	37.5	78
8		Coal2 (140×170)	34.9	18	52.6	62
9	GW-3	Coco2 (140×170)	16.1	69	21.7	102
10		Coal3 (140×170)	32.4	28	54.6	58
11		IX1 (140×170)	19.7	9	36.4	28
12	GW-4	IX1 (140×170)	18.3	7	32.8	13
13		Coal4 (60×70)	250.5[c]	1.7	N/A	N/A
14	GW-5	IX1 (140×170)	486.9[d]	5	N/A	N/A
15		IX2 (140×170)	515.4[d]	1.8	N/A	N/A
16		Coal4 (140×170)	219.5	75	260.7	102
17	GW-6	Coal2 (140×170)	228.1	66	282.4	100
18		IX1 (140×170)	145.6	27	212.0	45

[a] The numbers show in the brackets indicate the standard sieve used to prepare the sorbents.

[b] Only lead column results are reported.

[c] q is reported at ~15,000 BV.

[d] q is reported at ~75,000 BV

Table S3. Summary of RSSCT design parameters.

Design Parameters	Pilot Scale	RSSCT 1, 2, and 3
Particle diameter (mm)	0.84	0.096
Column diameter (cm)	365.76	0.43
Column diameter (ft)	12	0.014
EBCT (min)	4.60	0.06
Loading rate (m/h)	23.8	79.7
Loading rate (gpm/ft^2)	9.74	32.60
Re	6.0	2.4
Sc	1581	1581
Re $\times$ Sc	9860	3779
Bed volume (mL)	17052334	1.17
Flow rate (mL/min)	4163953	19.5
Flow rate (gpm)	1100	0.005
CD or PD	N/A	CD
Column configuration	N/A	Lead + Lag

Design Parameters	Pilot Scale	RSSCT 5
Particle diameter (mm)	0.84	0.105
Column diameter (cm)	365.76	0.43
Column diameter (ft)	12	0.014
EBCT (min)	4.60	0.07
Loading rate (m/h)	23.8	83.5
Loading rate (gpm/ft^2)	9.74	34.16
Re	6.0	2.7
Sc	1581	1580.8
Re $\times$ Sc	9860	4324.5
Bed volume (mL)	17052334	1.46
Flow rate (mL/min)	4163953	20.4
Flow rate (gpm)	1100	0.005
CD or PD	N/A	CD
Column configuration	N/A	Lead + Lag

Design Parameters	Pilot Scale	RSSCT 4 and 6
Particle diameter (mm)	0.65	0.096
Column diameter (cm)	381	0.43
Column diameter (ft)	12.5	0.014
EBCT (min)	3.30	0.51
Loading rate (m/h)	22.0	6.8
Loading rate (gpm/ft^2)	9.0	2.8
Re	11.9	0.8
Sc	893.7	893.7
Re × Sc	10592.6	750.0
Bed volume (mL)	5638248	1.12
Flow rate (mL/min)	1708560	2.21
Flow rate (gpm)	451	0.0006
CD or PD	N/A	PD
Column configuration	N/A	Lead + Lag

Design Parameters	Pilot Scale	RSSCT 7-10, 16, and 17
Particle diameter (mm)	0.84	0.096
Column diameter (cm)	304.8	0.43
Column diameter (ft)	10	0.014
EBCT (min)	5.00	0.07
Loading rate (m/h)	14.7	14.2
Loading rate (gpm/ft^2)	6.0	5.82
Re	10.1	1.1
Sc	893.7	893.7
Re × Sc	9006	1000
Bed volume (mL)	8913637	0.23
Flow rate (mL/min)	1782727	3.47
Flow rate (gpm)	471	0.0009
CD or PD	N/A	CD
Column configuration	N/A	Lead + Lag

Design Parameters	Pilot Scale	RSSCT 11, 12, 14, 15, and 18
Particle diameter (mm)	0.65	0.096
Column diameter (cm)	304.8	0.43
Column diameter (ft)	10	0.014
EBCT (min)	3.30	0.07
Loading rate (m/h)	24.4	14.0
Loading rate (gpm/ft^2)	10	5.73
Re	13.2	1.1
Sc	893.7	893.7
Re $\times$ Sc	11769.7	1000.0
Bed volume (mL)	9805001	0.25
Flow rate (mL/min)	2971212	3.43
Flow rate (gpm)	785	0.0009
CD or PD	N/A	CD
Column configuration	N/A	Lead + Lag

Design Parameters	Pilot Scale	RSSCT 13[a]
Particle diameter (mm)	0.84	0.23
Column diameter (cm)	304.8	1.1
Column diameter (ft)	10	0.036
EBCT (min)	5.00	0.37
Loading rate (m/h)	14.7	6.0
Loading rate (gpm/ft^2)	6.0	2.38
Re	10.1	1.1
Sc	893.7	893.7
Re $\times$ Sc	9006	1000
Bed volume (mL)	8913637	3.5
Flow rate (mL/min)	1782727	9.45
Flow rate (gpm)	471	0.0009
CD or PD	N/A	CD
Column configuration	N/A	Lead + Lag

[a] 1.1 cm (ID) glass column was used in this experiment to avoid wall effect.

Sorbents

Table S4. Sorbent data for column experiments.

Identifier Name	Brand Name	Description	Apparent Density (g/mL)
Coal1	Filtrasorb 400	bituminous coal, reagglomerated	0.54
Coal2	Norit GAC 400	bituminous coal, reagglomerated	0.45-0.51
Coal3	CENTAUR 12×40	bituminous coal, reagglomerated	0.56
Coal4	HYDRODARCO 4000	Lignite coal based	0.34-0.54
Coco1	AquaCarb 1230AWC	catalytic coconut shell-based	0.45-0.52
Coco2	AquaCarb 1240CAT	catalytic coconut shell-based	0.49
IX1[a]	Purofine PFA694E	Polystyrenic gel	1.04-1.12
IX2[b]	Dowex PSR-2	Polystyrenic gel	1.1

[a] Functional group: complex amino; total exchange capacity > 0.65 eq/L.
[b] Functional group: quaternary amine; total exchange capacity > 0.65 eq/L.

Surface area and pore size distribution

The specific surface area and porosity of GAC were determined by nitrogen adsorption at 77.35 K using a Trisatr II 3020 instrument (Micromeritics Instrument Corp., Norcross, GA, USA). Pore width ranged from 1.7 nm to 300 nm.

Table S5. Surface area and pore distribution of GACs used in this study.

Adsorbent	Surface area[a] (m^2/g)	Pore Volume (cm^3/g)	Mesopore[b] (cm^3/g)	Macropore[c] (cm^3/g)	Mesopore+Macropore (cm^3/g)
Coal1	824	0.200	0.148	0.011	0.159
Coal2	770	0.196	0.153	0.012	0.165
Coal3	755	0.107	0.076	0.007	0.084
Coal4	573	0.458	0.367	0.075	0.442
Coco1	1011	0.101	0.061	0.002	0.063
Coco2	852	0.088	0.072	0.001	0.074

[a] BET surface area; [b] 2-50 nm; [c] > 50 nm.

Elemental content

Carbon (C), hydrogen (H), nitrogen (N), and oxygen (O) content were measured by Huffman Hazen Laboratories. C and H were determined on a Thermo Flash EA 1112 Series elemental analyzer. The technique is the classical Dumas method with thermal conductivity detection. The method is described in ASTM D5373 (coal) and ASTM D5291 (petroleum products). Weighed samples were combusted in oxygen at 1000 °C. The combustion products were swept with a helium carrier gas through catalysts, scrubbers, and reduced copper. C and H were then separated on a chromatography column and measured by thermal conductivity detection. N was measured on a different Flash EA 1112 Series elemental analyzer using the same technique and method as C and H. O was determined on a LECO CHNS-932 with VTF-900 Oxygen Analyzer. This method is described in

ASTM D5622. A sample was pyrolyzed at 1300 °C in a carbon pyrolysis tube to convert oxygen in the sample to CO_2 which is then measured by non-dispersive infrared detection.

Table S6. Elemental content of GACs used in this study.

Adsorbent	C (wt. %)	H (wt. %)	N (wt. %)	O (wt. %)	N + O (wt. %)
Coal1	82.05	0.53	0.38	8.36	8.74
Coal2	77.57	0.72	0.35	12.64	12.99
Coal3	78.15	0.58	0.60	12.69	13.29
Coal4	64.68	1.69	0.36	20.12	20.48
Coco1	90.48	0.40	0.16	6.12	6.28
Coco2	84.58	0.32	0.22	8.34	8.56

Surface charge

The pH of point of zero charge (PZC) was determined by the pH drift method. Briefly, six 0.01M NaCl solutions with different pH values (2–12) were prepared using distilled and deionized water that was purged with nitrogen to remove dissolved CO_2. The pH was adjusted by adding 0.5M HCl or NaOH and measured using a VWR SB80PC (VWR International, West Chester, PA) conductivity/pH meter. Then, 10 mg of each activated carbon were added to 10 mL of 0.1 M NaCl solutions with different initial pH values in 15 mL vials. Sealed vials were shaken at room temperature (25 ± 1 °C) on an orbit shaker at 150 rpm for 24h. Blanks with no activated carbon were also run with the samples. All samples were run in duplicate.

Table S7. PZC of the GACs used in this study.

Adsorbent	PZC
Coal1	7.1
Coal2	7.4
Coal3	7.2
Coal4	6.6
Coco1	8.0
Coco2	7.6

PFAS analytical method

14 compounds are included in EPA Method 537: N-ethyl perfluorooctanesulfonamidoacetic acid (NEtFOSAA), N-methyl perfluorooctanesulfonamidoacetic acid (NMeFOSAA), perfluorobutanoic acid (PFBS), Perfluorodecanoic acid (PFDA), perfluorododecanoic acid (PFDoA), perfluoroheptanoic acid (PFHpA), perfluorohexanesulfonic acid (PFHxS), perfluorohexanoic acid (PFHxA), perfluorononanoic acid (PFNA), perfluorooctanesulfonic acid (PFOS), perfluorooctanoic acid (PFOA), Perfluorotetradecanoic acid (PFTA), Perfluorotridecanoic acid (PFTrDA), Perfluoroundecanoic acid (PFUnA).

2. Results and Discussion

Breakthrough curves for combined PFAS
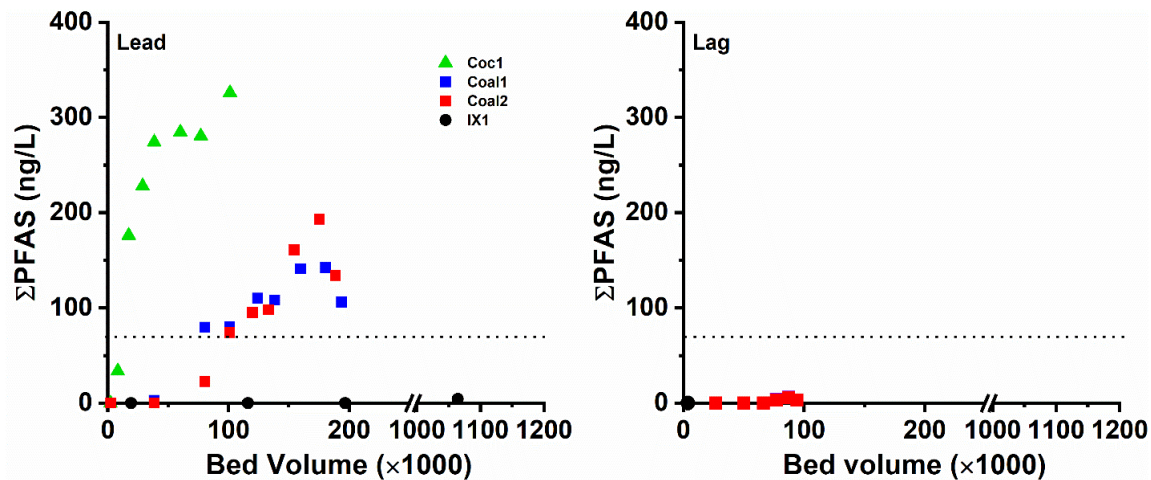
Figure S1. ΣPFAS breakthrough curves for RSSCT 1 to RSSCT 4 using GW-1. The dotted line indicates 70 ng/L.
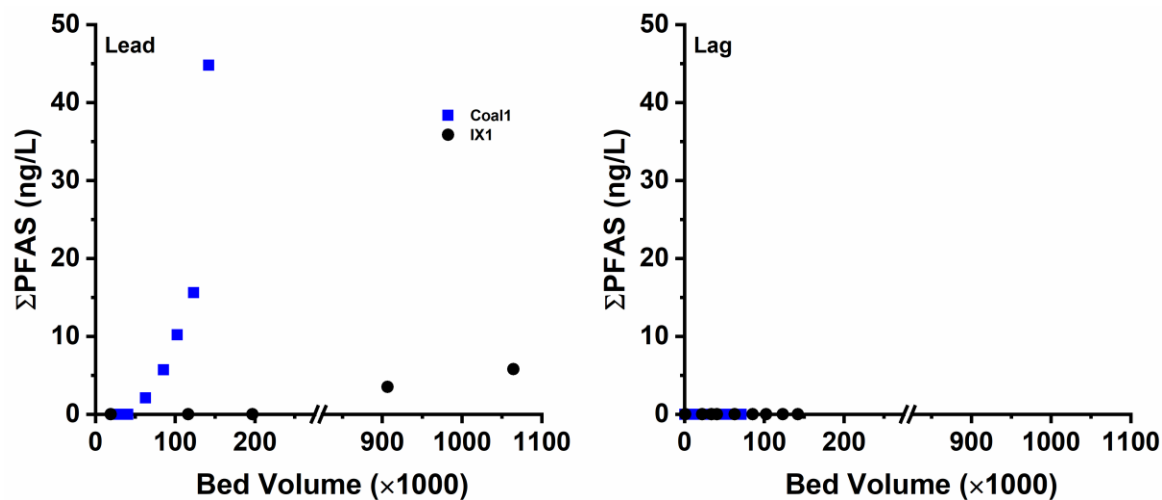
Figure S2. ΣPFAS breakthrough curves for RSSCT 5 and RSSCT 6 using GW-2. The dotted line indicates 70 ng/L.
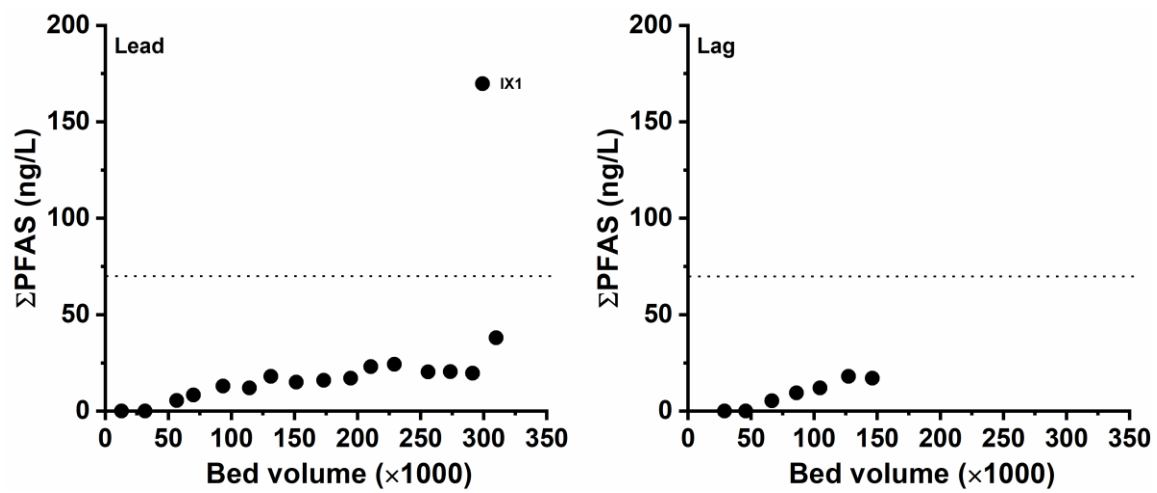
Figure S3. ΣPFAS breakthrough curves for RSSCT 12 using GW-4. The dotted line indicates 70 ng/L.
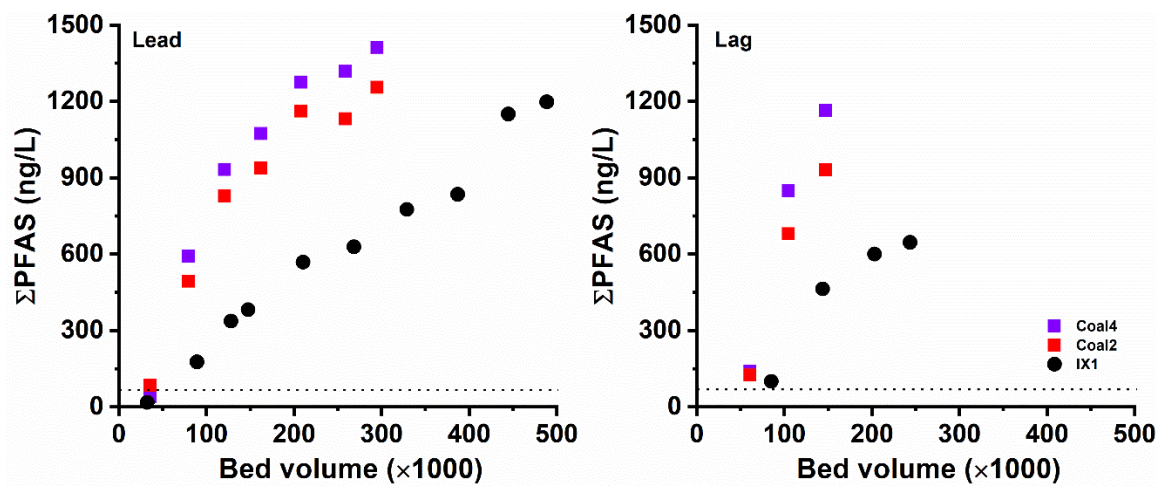
Figure S4. ΣPFAS breakthrough curves for RSSCT 16 to RSSCT 18 using GW-6. The dotted line indicates 70 ng/L.

PFAS adsorption capacity

Table S8. ΣPFAS breakthrough and PFAS adsorption capacity ($q_{\Sigma PFAS}$) for Lead and Lead+Lag columns.

RSSCT[a]	Bed Volume	Lead		Lead+Lag		$q_{Lead+Lag}$ / q_{lead} (%)
		ΣPFAS (C/C$_0$, %)	$q_{\Sigma PFAS}$ (ng/mg)	ΣPFAS (C/C$_0$, %)	$q_{\Sigma PFAS}$ (ng/mg)	
GW-1 (ΣPFAS=346.3 ng/L)						
2-Coal1	~100,000	22	61.7	3.2	63.3	103
3-Coal2	~100,000	18	82.4	0.7	79.5	97
GW-2 (ΣPFAS=180.6 ng/L)						
5-Coal1	~60,000	2	20.9	0.0	20.6	99
GW-3 (ΣPFAS=155.8 ng/L)						
7-Coal1	~90,000	29	20.9	19.5	24.7	118
8-Coal2	~90,000	10	28.0	0.0	29.4	105
9-Coco2	~90,000	64	15.4	63	21.5	140
10-Coal3	~90,000	27	29.0	21	31.6	109
11-IX1	~100,000	9	19.7	11	19.0	96
GW-4 (ΣPFAS=178.7 ng/L)						
12-IX1	~150,000	8	23.9	10	23.2	97
GW-6 (ΣPFAS=1251.7 ng/L)						
16-Coal4	~150,000	80	234.8	93	260.2	111
17-Coal2	~150,000	71	245.3	74	276.1	113
18-IX1	~240,000	48	232.5	52	234.8	102

[a]All the RSSCTs (except RSSCT 1) were operated in lead-lag configurations of two columns in series at same EBCT. Essentially, Lead+Lag system can be treated as one column with 2 times of the EBCT compared to the Lead column alone. In addition, by using this setup the total bed volume treated from Lead+Lag column was half of that in Lead column. To evaluate the effect of EBCT on PFAS removal, the results acquired at (or near) the end of the experiments were used. Results from RSSCT 4, RSSCT 6, and RSSCTs 13–15 were not included as less than 2% of ΣPFAS breakthrough was observed at the end of the experiment. PFAS adsorption capacity ($q_{\Sigma PFAS}$) was acquired by calculating the area above the breakthrough curve.

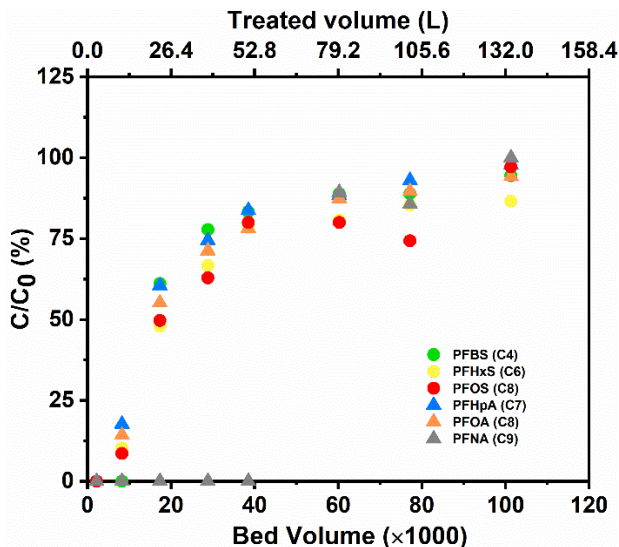Breakthrough curves for PFAS species (C/C$_0$) for each RSSCT

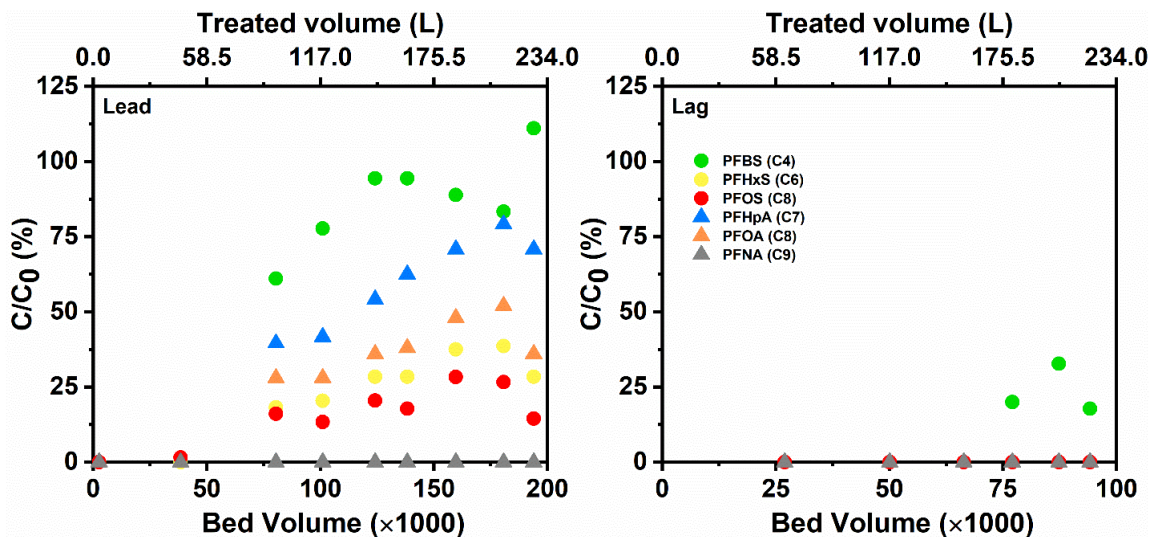Figure S5. PFAS breakthrough curve for RSSCT-1 (feed water: GW-1; packing material: Coco1).

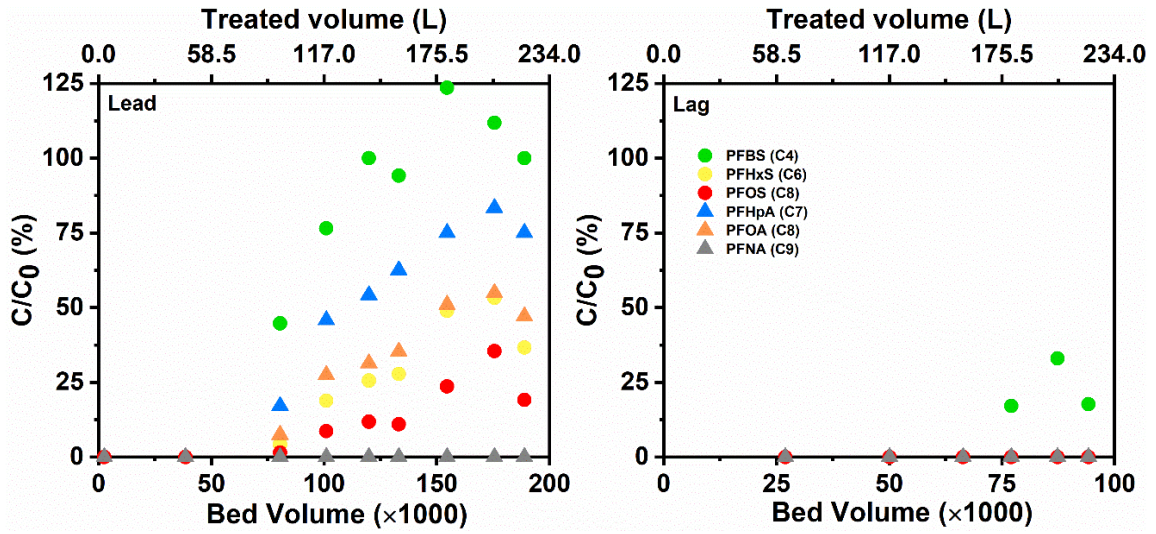Figure S6. PFAS breakthrough curve for RSSCT-2 (feed water: GW-1; packing material: Coal1).

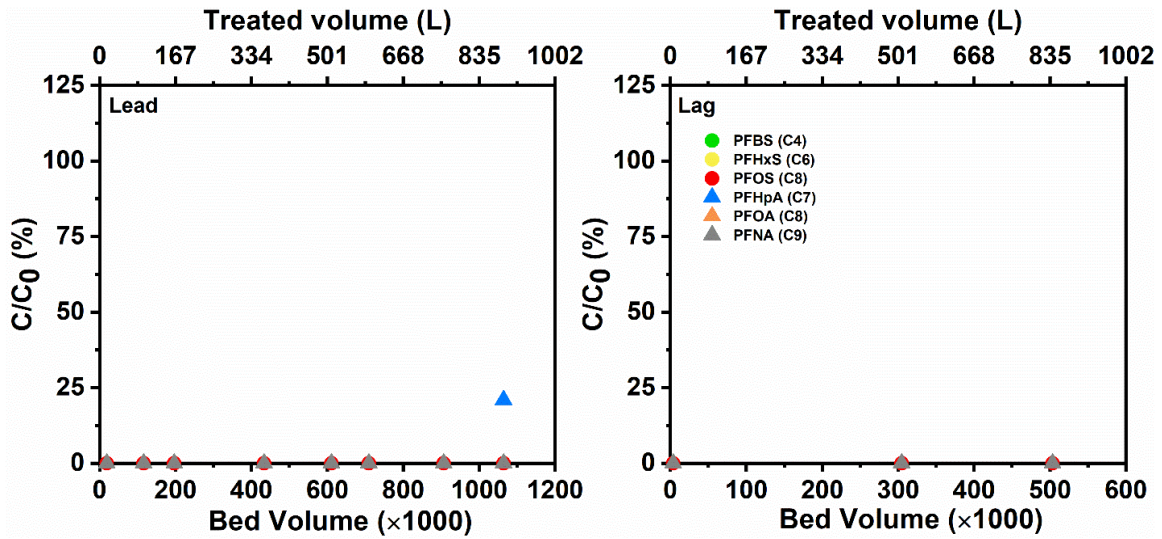Figure S7. PFAS breakthrough curve for RSSCT-3 (feed water: GW-1; packing material: Coal2).

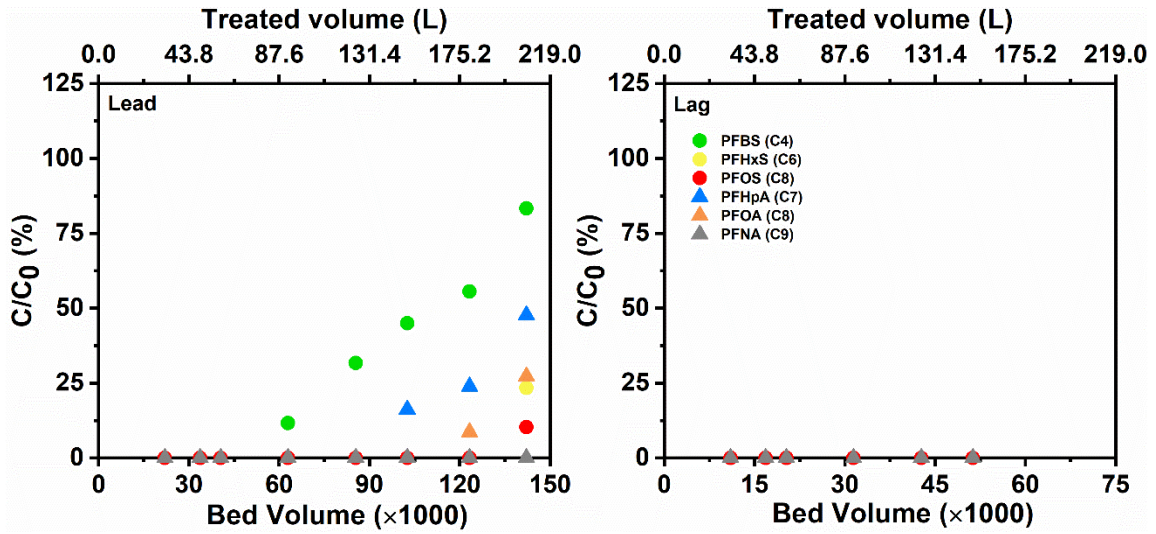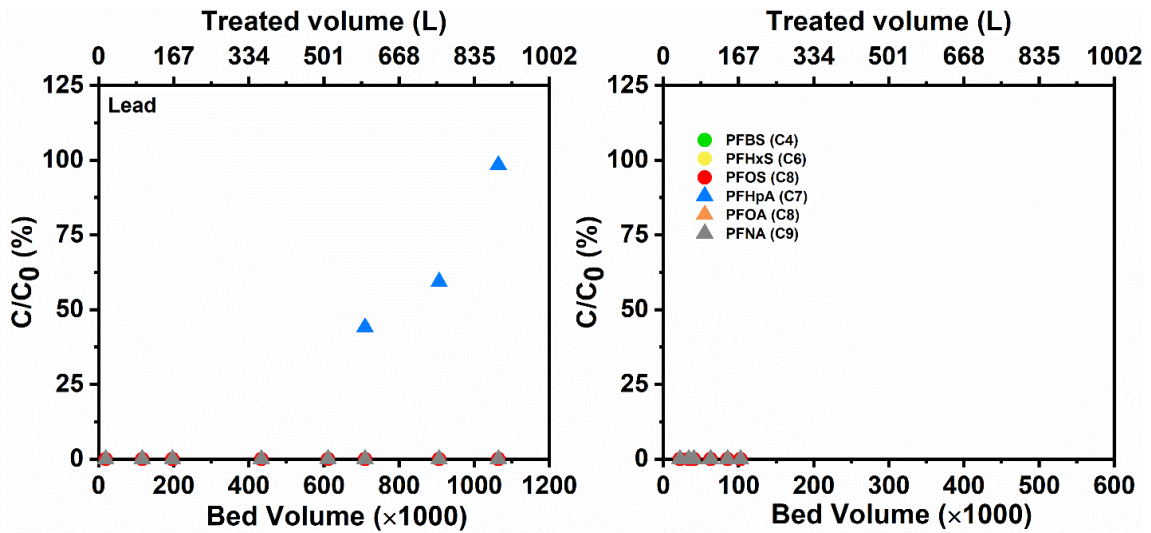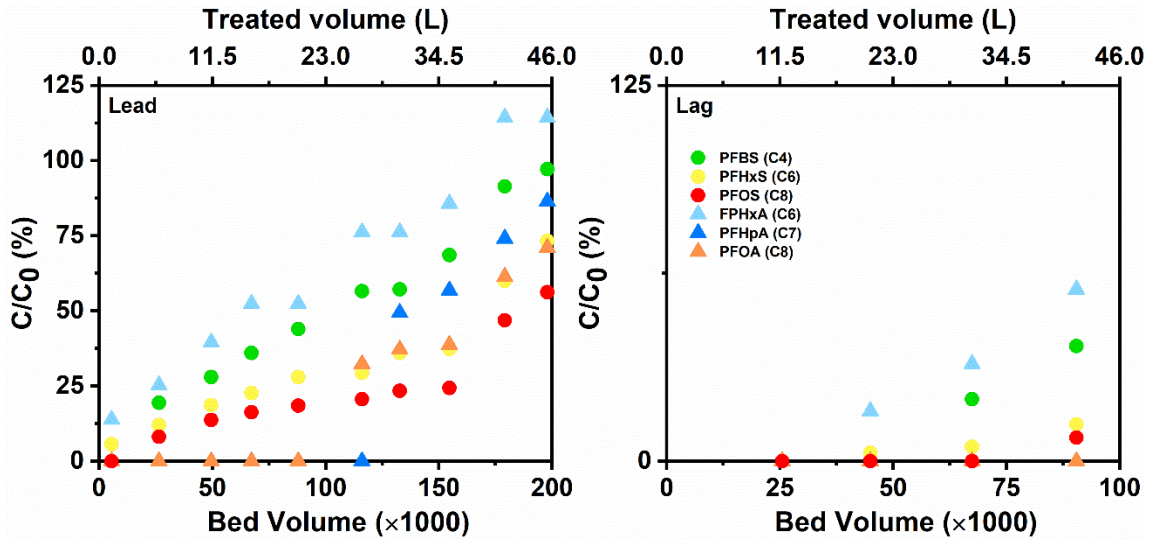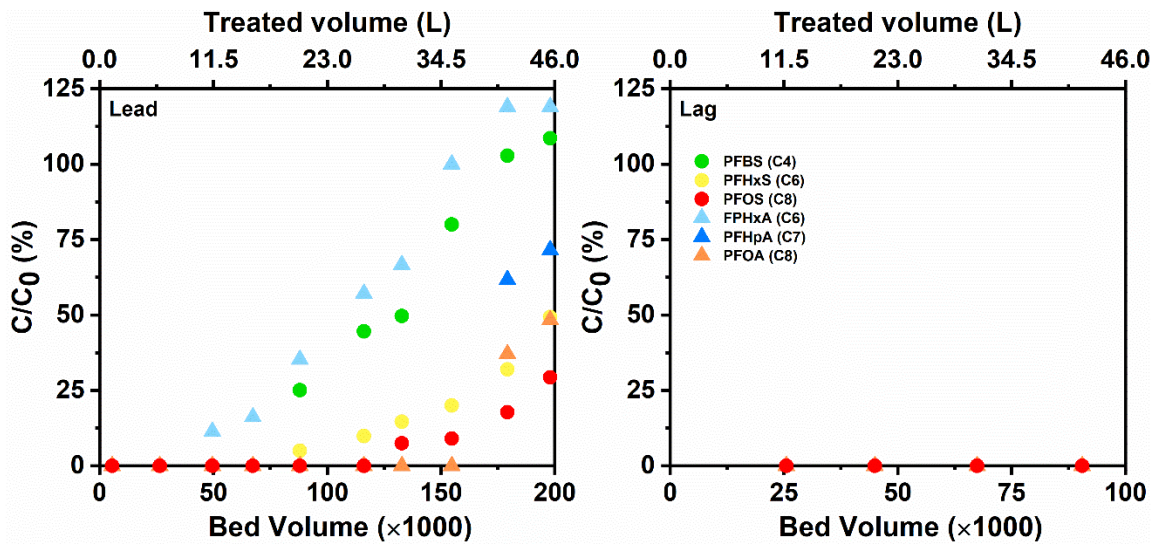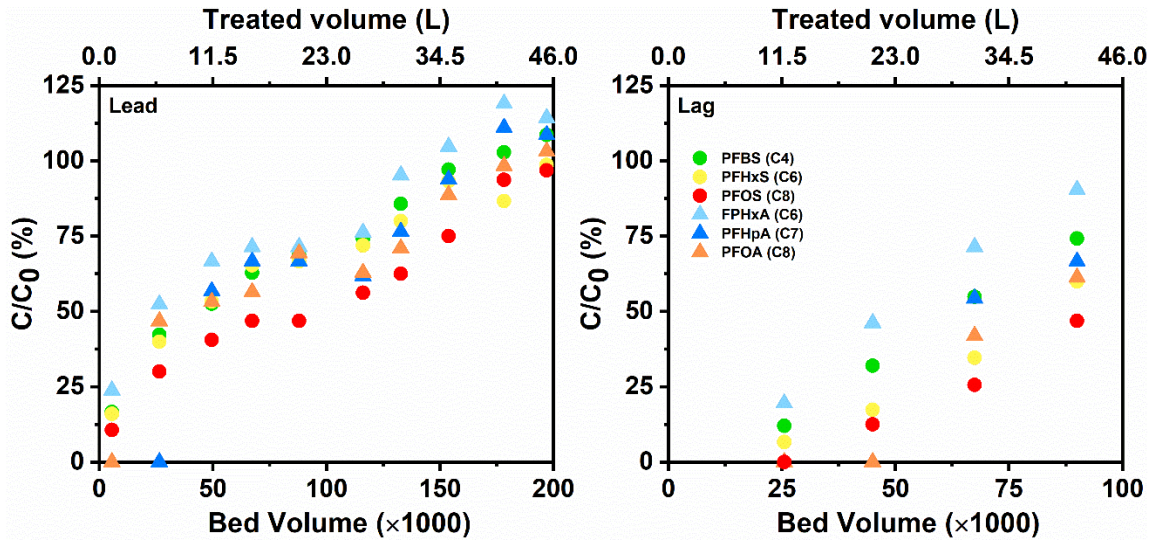Figure S8. PFAS breakthrough curve for RSSCT-4 (feed water: GW-1; packing material: IX1).

Figure S9. PFAS breakthrough curve for RSSCT-5 (feed water: GW-2; packing material: Coal1).

Figure S10. PFAS breakthrough curve for RSSCT-6 (feed water: GW-2; packing material: IX1).

Figure S11. PFAS breakthrough curve for RSSCT-7 (feed water: GW-3; packing material: Coal1).

Figure S12. PFAS breakthrough curve for RSSCT-8 (feed water: GW-3; packing material: Coal2).

117

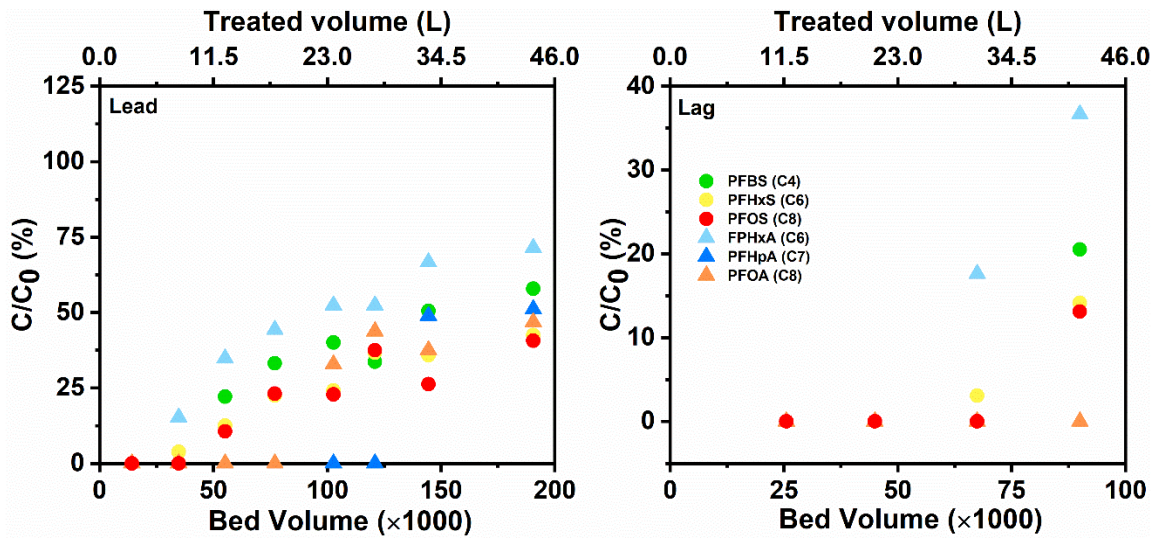Figure S13. PFAS breakthrough curve for RSSCT-9 (feed water: GW-3; packing material: Coco2).

Figure S14. PFAS breakthrough curve for RSSCT-10 (feed water: GW-3; packing material: Coal3).
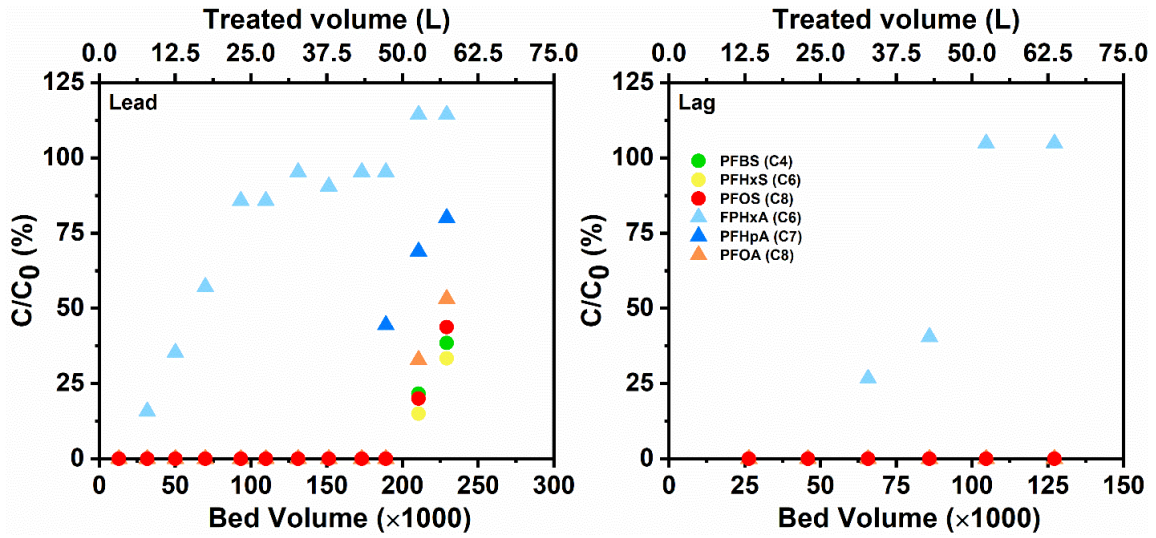
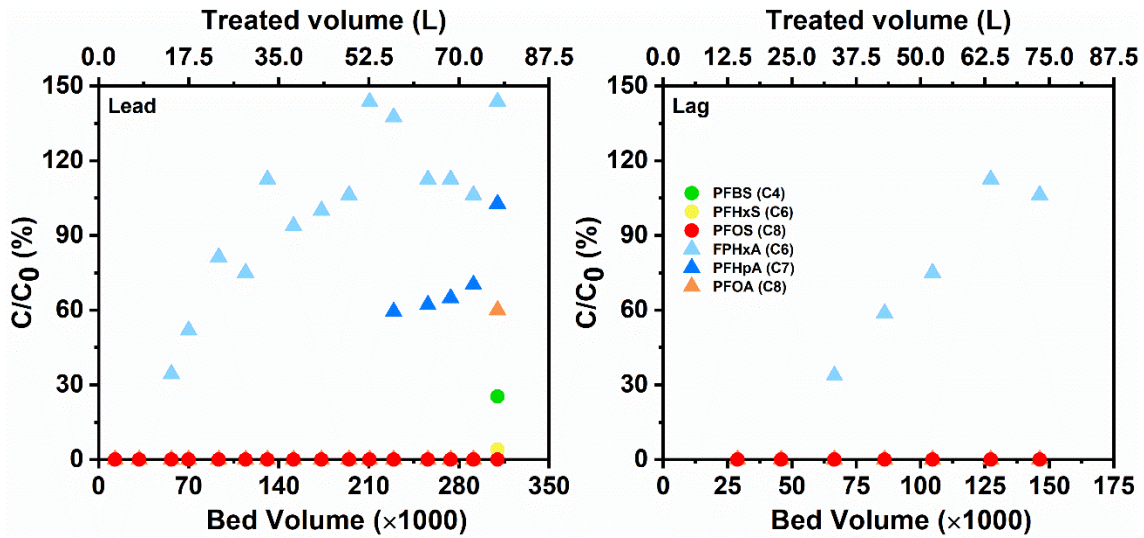Figure S15. PFAS breakthrough curve for RSSCT-11 (feed water: GW-3; packing material: IX1).

Figure S16. PFAS breakthrough curve for RSSCT-12 (feed water: GW-4; packing material: IX1).
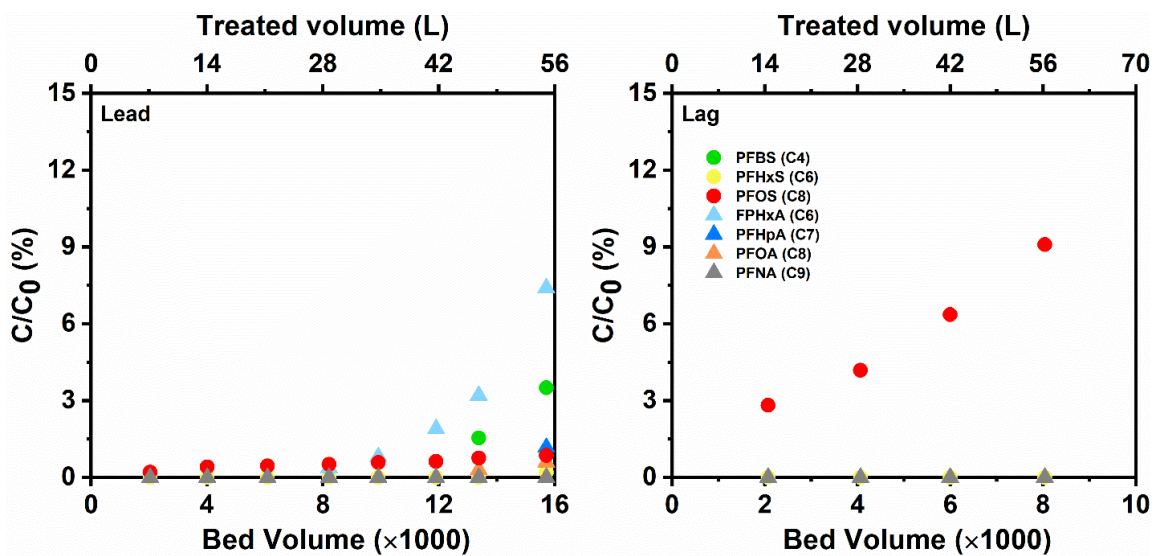
Figure S17. PFAS breakthrough curve for RSSCT-13 (feed water: GW-5; packing material: Coal4).
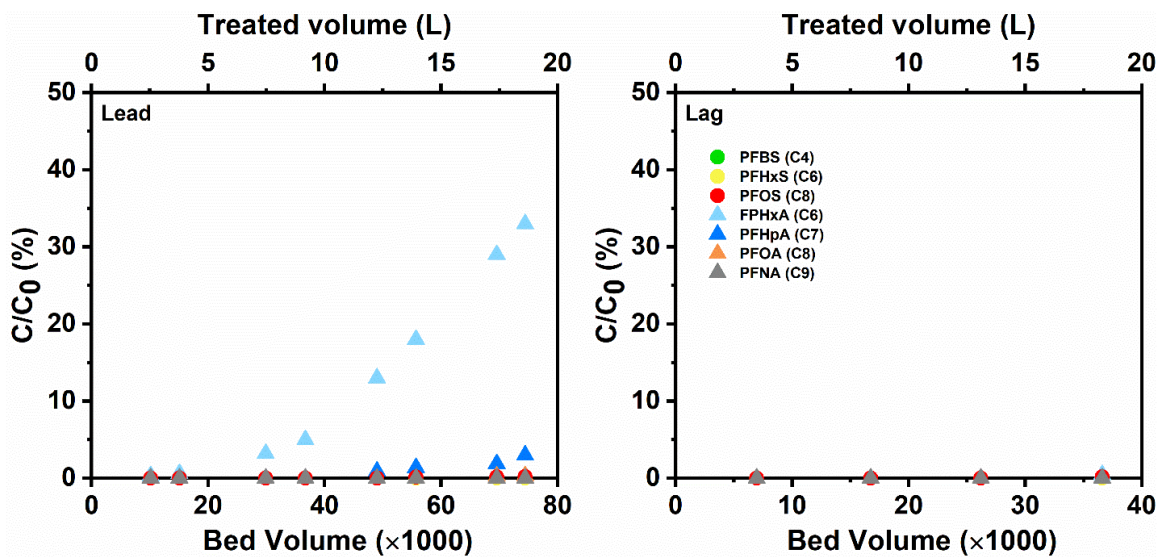

Figure S18. PFAS breakthrough curve for RSSCT-14 (feed water: GW-5; packing material: IX1).
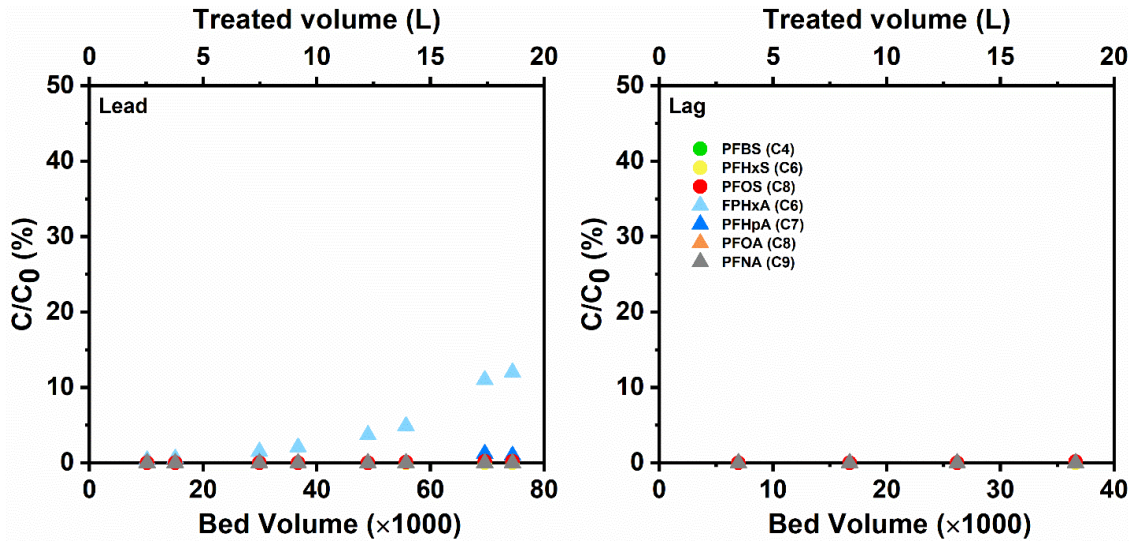
Figure S19. PFAS breakthrough curve for RSSCT-15 (feed water: GW-5; packing material: IX2).
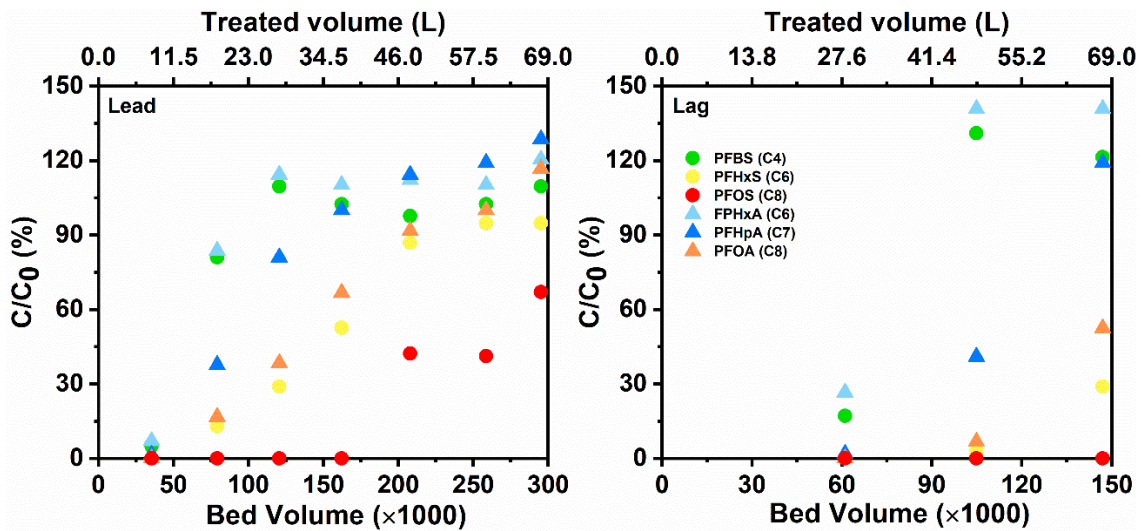

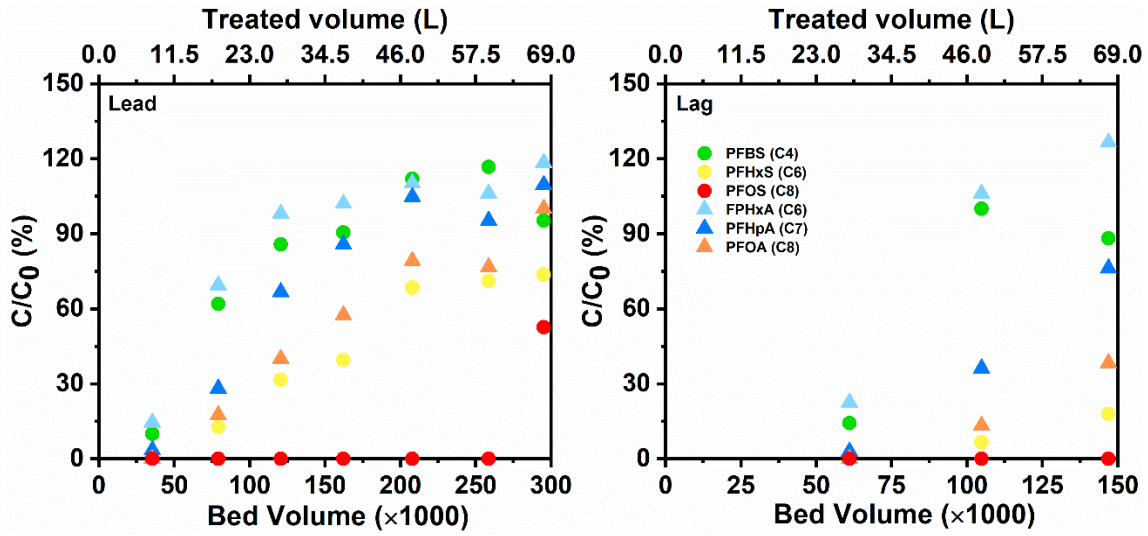Figure S20. PFAS breakthrough curve for RSSCT-16 (feed water: GW-6; packing material: Coal4).

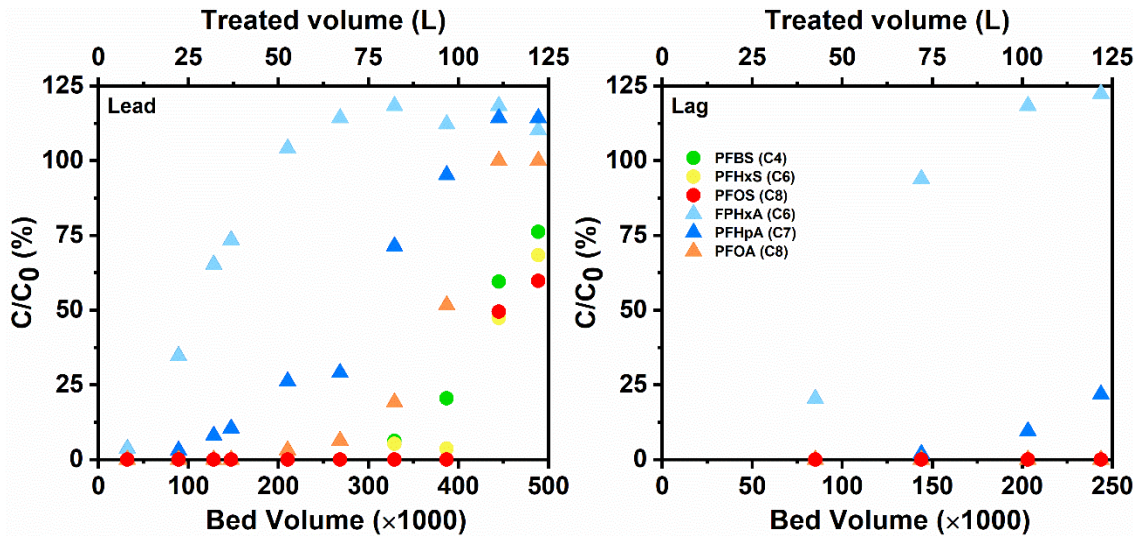Figure S21. PFAS breakthrough curve for RSSCT-17 (feed water: GW-6; packing material: Coal2).

Figure S22. PFAS breakthrough curve for RSSCT-18 (feed water: GW-6; packing material: IX1).

122

Selective adsorption of PFAS
A statistical analysis was conducted to demonstrate the selective adsorpton described. Data

acquired from all BV treated in lead columns and lag columns were consdered, with the

exceptions when all the PFCAs or PFSAs were below the detection limit or when ΣPFAS

breakthrough was <1% (eliminate errors come from detection) or >99% (eliminate errors

due to PFAS desorption). Breakthrough sequence was compared normaizing each species

to its influent concentration (C/C_0). The results are shown in Tables S10 and S11.

Table S9. Number of cases (N_{True}) where longer-chain PFAS were adsorbed better than shorter-chain ones and number when PFCA is adsorbed better than PFAS (for same chain length). The total number of datapoints in the breakthrough curve is N_{total}.

RSSCT	PFCAs		PFSAs		PFCA vs PFSA (C6)		PFCA vs PFSA (C8)	
	N_{total}	N_{True} [a]	N_{total}	N_{True} [b]	N_{total}	N_{True} [c]	N_{total}	N_{True} [d]
1	7	5	7	3	0	0	7	5
2	7	7	7	7	0	0	7	7
3	7	7	7	7	0	0	7	7
4	1	1	0	0	0	0	0	0
5	3	3	5	5	0	0	2	2
6	3	3	0	0	0	0	0	0
7	13	12	13	11	10	10	9	5
8	8	8	6	6	8	8	4	2
9	14	9	10	8	10	10	10	9
10	9	7	9	6	9	9	8	5
11	15	15	2	0	15	15	2	2
12	19	19	1	1	19	19	1	1
13	1	1	1	0	1	1	1	0
14	4	4	0	0	4	4	3	2
15	2	2	0	0	2	2	0	2
16	7	7	7	7	7	7	5	5
17	10	10	10	10	10	10	8	8
18	14	13	4	4	14	14	6	6
Total	144	133	89	75	109	109	80	68

[a] Number of cases when breakthrough of PFCAs follow the order: PFHxA(C6)>PFHpA(C7) > PFOA(C8) > PFNA (C9), if detected in the groundwaters.
[b] Number of cases when breakthrough of PFSAs follow the order: PFBS(C4) > PFHxS(C6) > PFOS(C8).
[c] Number of cases when PFHxA (C6) breakthrough earlier than PFHxS (C6).
[d] Number of cases when PFOA (C8) breakthrough earlier than PFOS (C8).

Table S10. Correlation between PFAS physicochemical properties and their removal efficiency. (^{a} Data at all BV were used, with the exceptions when one or more PFAS species had concentration below the detection limit. PFNA was excluded for RSSCT-2 and RSSCT-3 as no breakthrough was observed in the experiment after ~200,000 BV. ^{b} All correlation coefficients were tested for statistical significance (2-tailed, degrees of freedom = n - 2). Color coding: no color = $p > 0.05$; grey = $p < 0.05$; black = $p < 0.01$.)

RSSCT[a]	Bed volume	Pearson correlation coefficient (R)[b]		
		Molecular weight	Log Kow	Log D (7.4)
1-Coco1 (n=6)	60253	-0.49	0.05	-0.59
	77180	-0.73	-0.19	-0.82
	101362	0.29	0.54	0.21
2-Coal1 (n=5)	80503	-0.89	-0.68	-0.88
	101056	-0.91	-0.76	-0.88
	124179	-0.91	-0.76	-0.88
	138310	-0.93	-0.71	-0.92
	159721	-0.93	-0.63	-0.93
	180703	-0.90	-0.49	-0.93
	193977	-0.93	-0.73	-0.91
3-Coal2 (n=5)	80503	-0.87	-0.80	-0.83
	101056	-0.93	-0.72	-0.92
	119897	-0.93	-0.78	-0.90
	133172	-0.95	-0.71	-0.94
	154582	-0.96	-0.79	-0.93
	175564	-0.95	-0.74	-0.94
	188838	-0.95	-0.66	-0.95
5-Coal1 (n=5)	142206	-0.94	-0.77	-0.91
7-Coal1 (n=6)	132764	-0.90	-0.48	-0.92
	154726	-0.92	-0.53	-0.93
	179204	-0.89	-0.52	-0.90
	197963	-0.93	-0.54	-0.94
8-Coal2 (n=6)	179204	-0.92	-0.61	-0.91
	197963	-0.94	-0.65	-0.93
9-Coco2 (n=6)	49567	-0.78	-0.22	-0.84
	67335	-0.84	-0.45	-0.86
	88001	-0.82	-0.36	-0.86
	116140	-0.83	-0.77	-0.78
	132764	-0.91	-0.64	-0.90
	153810	-0.93	-0.54	-0.95
	178289	-0.64	-0.06	-0.71

	197048	-0.87	-0.33	-0.91
10-Coal3 (n=6)	144446	-0.89	-0.41	-0.92
	190566	-0.82	-0.41	-0.85
11-IX1 (n=6)	210597	-0.50	0.11	-0.58
	229307	-0.43	0.19	-0.51
16-Coal4 (n=6)	208049	-0.85	-0.30	-0.90
17-Coal2 (n=6)	295176	-0.79	-0.12	-0.87
18-IX1 (n=6)	444871.0	-0.42	0.34	-0.53
	488733.8	-0.51	0.25	-0.62

Central Tendency Based PFAS Breakthrough Prediction Models

All the data points from Lead columns in the RSSCTs were used to fit the model, with the expectation of RSSCT-4, 6, and 13 as they had different designs than other column tests (see Tables S2 and S3). Only data from the lead column (n=126 datapoints for PFAS) was used because lag-column has a limited number of datapoints (n=29 datapoints for PFAS) that were at low PFAS concentrations associated with the longer EBCT. Also excluded were the data prior to the first bed volume where PFAS was detected in the RSSCT column effluent (i.e., non-detects were excluded). Because PFHxA or PFNA was not detected in some of the groundwaters, their initial concentrations in those raw water were set to the half detection limit (1 ng/L). The data were linearized by taking the natural log of both sides in Eq. S1, then fitted by linear regression. Stepwise regression (forward selection with $\alpha = 0.05$) was performed by Minitab®19 to sort out significant terms in the model. For PFAS breakthrough model, bed volume (BV), EBCT [min], and PFAS species concentration [ng/L] (including PFBS, PFHxA, PFHxS, PFHpA, PFOA, PFOS and PFNA), pH, conductivity [µS/cm] and DOC [mg/L] in the raw groundwaters were used as quantitative independents; sorbent type was set as qualitative independent. Using $\alpha = 0.05$ resulted in only a few terms being statistically significant, namely sorbent type, BV treated, DOC, and PFHxS, PFHxA, and PFHpA. Other terms were not statistically significant for our database, and thus they do not emerge as parameters in the final stepwise regression equation. The log regression model obtained from the Minitab analysis is shown in Eq. S1. (n=126, $p < 0.001$, S = 0.60, $R^2 = 87.64\%$, $R^2_{adj} = 86.3\%$):

$$\ln[\Sigma PFAS] = -18.00x_1 - 18.61x_2 - 18.58x_3 - 18.57x_4 - 15.71x_5 - 16.97x_6 - 19.56x_7 -$$

$$20.38x_8 + \quad 1.2284 \ln[BV] + 1.069 \ln[PFHxS] - 0.492[PFHxA] + 0.999 \ln[PFHpA] -$$

$$2.01[DOC] \hspace{9cm} \text{Eq. S1}$$

which can be transformed into a power function model as shown in Equation S2:

$$[\Sigma PFAS] = e^{-18.00x_1 - 18.61x_2 - 18.58x_3 - 18.57x_4 - 15.71x_5 - 16.97x_6 - 19.56x_7 - 20.38x_8} \cdot BV^{1.2284} \cdot [PFHxS]^{1.069} \cdot$$

$$[PFHxA]^{-0.492} \cdot [PFHpA]^{0.999}[DOC]^{-2.01} \hspace{4cm} \text{Eq. S2}$$

where $\Sigma PFAS$ is concentration of all the PFAS detected in the effluent; x_1, x_2, x_3, x_4, x_5, x_6, x_7, and x_8 represents sorbents Coal1, Coal2, Coal3, Coal4, Coco1, Coco2, IX1, and IX2, respectively ($x = 1$, if use the sorbent; $x = 0$, if not); *[PFHxS]*, *[PFHxA]*, and *[PFHpA]* are the concentrations of those PFAS species in the groundwaters. Figure S23 shows the normal probability distribution and residual versus fitted log-transformed ΣPFAS (i.e., *Residual = ln[ΣPFAS]$_{observed}$ - ln[ΣPFAS]$_{predicted}$*).
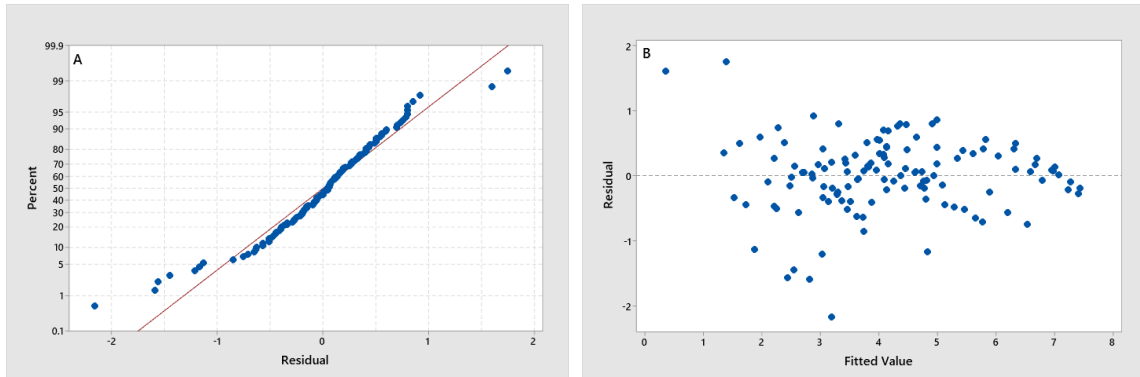

Figure S23. Residual normal probability distribution plot (left panel) and residual versus fitted value plot (right panel) from the model for the breakthrough of the log-transformed ΣPFAS (described in Eq. S1). *Residual = ln[ΣPFAS]$_{observed}$ - ln[ΣPFAS]$_{predicted}$*.

Similar to Equations S1 and S2 that fit ΣPFAS data, models were explored that could differentiate PFAS species. Numerous attempts were made, with mixed levels of success. The inability of central tendency models to achieve good data fits was due to several factors, including: 1) low concentrations of several species, 2) too few a number of

samples in RSSCT effluents that were above detection limits, and 3) fairly low fractional (C/C_0) breakthrough of many PFAS species. Only datasets for PFOA and PFOS emerged as statistically relevant, and those are described below. Because some states currently regulate the sum of PFOA plus PFOS (*[PFOA+PFOS]$_{effluent}$*), the model was developed to predict this summation concentration. Initial attempts to fit all the breakthrough data achieved reasonable fits for GAC but not for IX resins (Figure S24). Therefore, subsequent modeling used only data for PFOA and PFOS breakthrough from GAC columns because PFOA and PFOS had comparatively higher affinity for IX resins than GAC. Thus there were less than 15 suitable datapoints for PFOA and PFOS in IX resin effluent. Fitting and model parameterization were performed for PFOA plus PFOS using only data from GAC breakthrough in lead columns. The regression is shown in Eq. S3 (n= 64, p < 0.001, S = 0.46, $R^2 = 88.0\%$, $R^2_{adj} = 86.0\%$).

$$\ln[PFOA + PFOS]_{effluent} = -19.02x_1 - 19.79x_2 - 18.84x_3 - 19.68x_4 - 16.99x_5 - 17.84x_6 + 0.9586\ln[BV] - 2.82\ln[PFOA] - 2.392\ln[PFOS] + 6.45\ln[PFOA + PFOS]_{influent}$$

Eq. S3

Eq. S3 can be written as power function as shown in Eq. S4:

$$[PFOA + PFOS]_{effluent} = e^{-19.02x_1 - 19.79x_2 - 18.84x_3 - 19.68x_4 - 16.99x_5 - 17.84x_6} \cdot BV^{0.9586} \cdot [PFOA]^{-2.82} \cdot [PFOS]^{-2.392} \cdot [PFOA + PFOS]_{influent}^{6.45}$$

Eq. S4

where *[PFOA+PFOS]$_{in}$* is the combined concentration of PFOA and PFOS in the influent (raw groundwater); x_1, x_2, x_3, x_4, x_5, and x_6 represent sorbents Coal1, Coal2, Coal3, Coal4, Coco1, and Coco2, respectively ($x = 1$, if use the sorbent; $x = 0$, if not). Residual plots are shown in Figure S25. Figure S26 shows the model achieved a reasonable central-

tendency fit of the data: $[PFOA+PFOS]_{predicted} = 1.05 \times [PFOA+PFOS]_{observed} + 3.1$ (R^2=0.83). Figure S26 also shows the capability of the model to the general order of performance for different types of GAC, from worst- to best-performing in terms of capability to remove PFOA+PFOS. As with Equation S1, the model did not simulate well the s-shaped breakthrough curve that typically exemplifies GAC effluent concentrations.
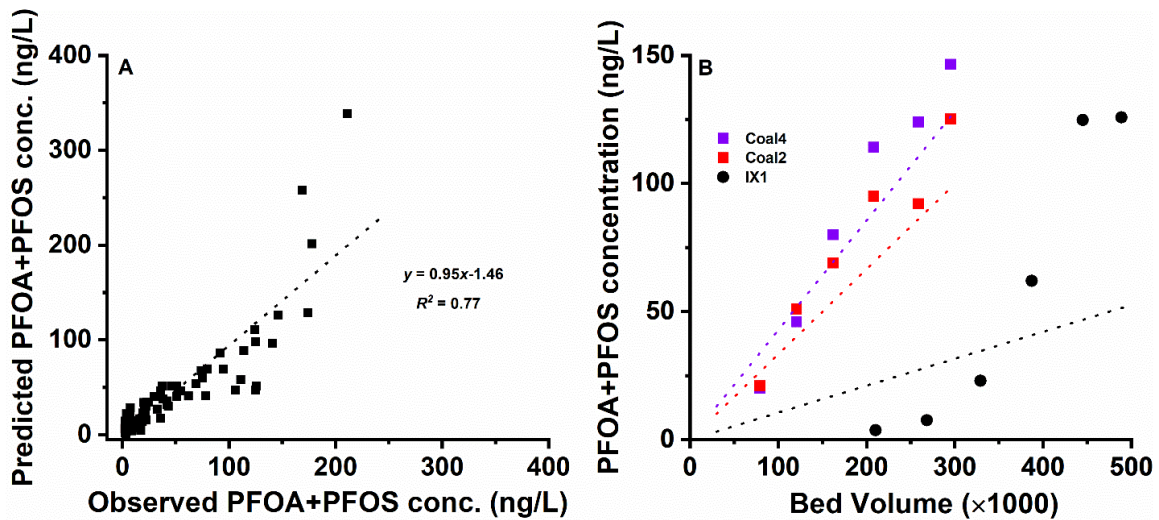

Figure S24. Comparison between observed PFOA+PFOS concentrations and predicted PFOA+PFOS concentrations using all the data acquired from Lead columns in the RSSCTs (panel A). Breakthrough of PFOA+PFOS from Lead columns using GW-6 (ΣPFAS = 1252 ng/L): solid symbols represent observed data, while dotted lines are the predicted breakthrough curves (panel B).
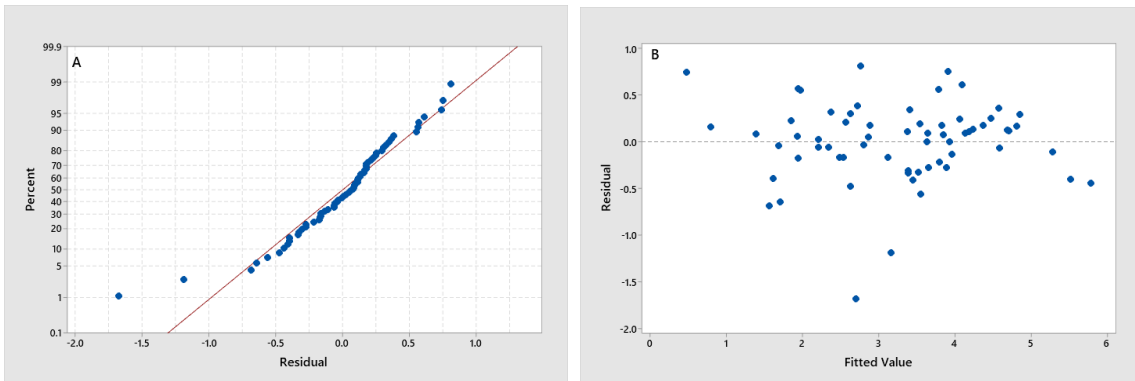
Figure S25. Residual normal probability distribution plot (panel A) and residual versus fitted value plot (panel B) from the model for the breakthrough of combined PFOA+PFOS (described in Eq. S5). *Residual = ln[PFOA+PFOS]$_{observed}$ - ln[PFOA+PFOS]$_{predicted}$*.
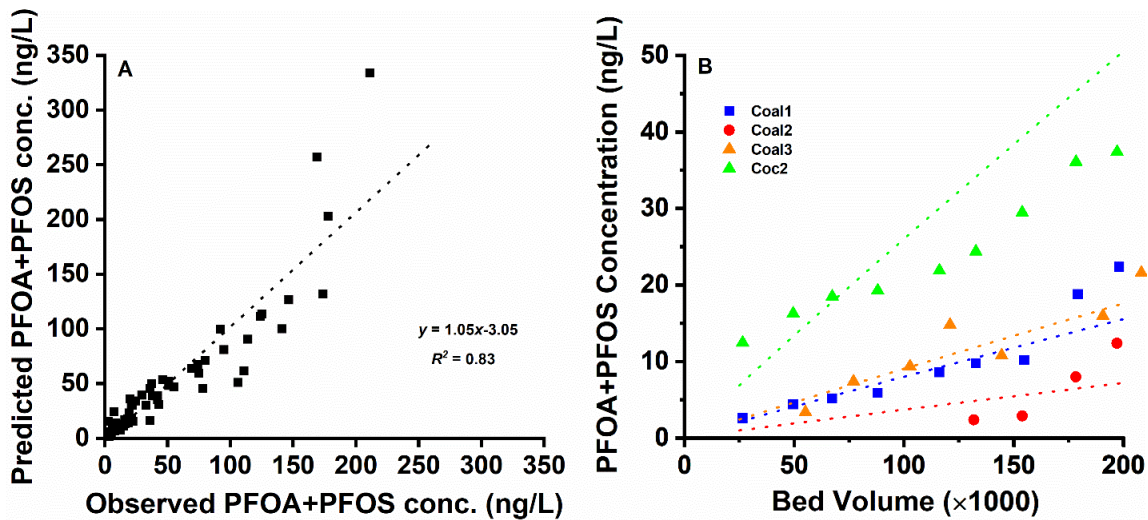

Figure S26. Comparison between observed PFOA+PFOS concentrations and predicted PFOA+PFOS concentrations using data acquired from Lead columns in GAC packed columns (panel A). Breakthrough of PFOA+PFOS from Lead columns using GW-3 (ΣPFAS = 155.8 ng/L): solid symbols represent observed data, while dotted lines are the predicted breakthrough curves (panel B).